University of Windsor
Scholarship at UWindsor

Electronic Theses and Dissertations

2012

Performance and Fuel Economy Analysis of a Mild Hybrid Vehicle Equipped with Belt Starter Generator

Stefano Baldizzone

Follow this and additional works at: http://scholar.uwindsor.ca/etd

Recommended Citation
Baldizzone, Stefano, "Performance and Fuel Economy Analysis of a Mild Hybrid Vehicle Equipped with Belt Starter Generator" (2012). *Electronic Theses and Dissertations*. Paper 4790.

This online database contains the full-text of PhD dissertations and Masters' theses of University of Windsor students from 1954 forward. These documents are made available for personal study and research purposes only, in accordance with the Canadian Copyright Act and the Creative Commons license—CC BY-NC-ND (Attribution, Non-Commercial, No Derivative Works). Under this license, works must always be attributed to the copyright holder (original author), cannot be used for any commercial purposes, and may not be altered. Any other use would require the permission of the copyright holder. Students may inquire about withdrawing their dissertation and/or thesis from this database. For additional inquiries, please contact the repository administrator via email (scholarship@uwindsor.ca) or by telephone at 519-253-3000ext. 3208.

Performance and Fuel Economy Analysis of a Mild Hybrid Vehicle Equipped with Belt Starter Generator

By

Stefano Baldizzone

A Thesis
Submitted to the Faculty of Graduate Studies
through Mechanical, Automotive and Materials Engineering
in Partial Fulfillment of the Requirements for
the Degree of Master of Applied Science
at the University of Windsor

Windsor, Ontario, Canada

2012

© 2012 Stefano Baldizzone

Performance and Fuel Economy Analysis of a Mild Hybrid Vehicle Equipped with Belt Starter Generator

by

Stefano Baldizzone

Approved by:

_____

Dr. Peter Frise, Co-Advisor
Department of Mechanical, Automotive and Materials Engineering

_____

Dr. Narayan Kar, Co-Advisor
Department of Electrical and Computer Engineering

_____

Dr. Bruce Minaker, Program Reader
Department of Mechanical, Automotive and Materials Engineering

_____

Dr. Jill Urbanic, Outside Program Reader
Department of Industrial and Manufacturing Systems Engineering

_____

Dr. Jennifer Johrendt, Chair of Defense
Department of Mechanical, Automotive and Materials Engineering

September 13th, 2012

DECLARATION OF ORIGINALITY

I hereby certify that I am the sole author of this thesis and that no part of this thesis has been published or submitted for publication.

I certify that, to the best of my knowledge, my thesis does not infringe upon anyone's copyright nor violate any proprietary rights and that any ideas, techniques, quotations, or any other material from the work of other people included in my thesis, published or otherwise, are fully acknowledged in accordance with the standard referencing practices. Furthermore, to the extent that I have included copyrighted material that surpasses the bounds of fair dealing within the meaning of the Canada Copyright Act, I certify that I have obtained a written permission from the copyright owner(s) to include such material(s) in my thesis and have included copies of such copyright clearances to my appendix.

I declare that this is a true copy of my thesis, including any final revisions, as approved by my thesis committee and the Graduate Studies office, and that this thesis has not been submitted for a higher degree to any other University or Institution.

ABSTRACT

This thesis focused on the study of a hybrid electric vehicle equipped with a belt starter generator, or BSG. With this system, the conventional starter and the alternator are replaced by one electric machine only, capable of cranking the engine, charging the batteries and supplying the on-board electric loads. These characteristics allow the introduction of new functionalities, including engine stop-start, regenerative braking, and electric assist.

The purposes of the research were two: the assessment of the stop-start performance and the evaluation of the fuel consumption reduction that can be achieved with this system compared to a conventional vehicle. Simulink models of the powertrain were used to obtain the results, which were validated against experimental data from a start cart and a real proof-of-concept vehicle.

The results illustrated the critical factors affecting the stop-start performance, and demonstrated that remarkable fuel savings can be obtained with the BSG, especially for city driving.

DEDICATION

To my parents,

for their unconditional love and support.

ACKNOWLEDGEMENTS

This work is the result of the cooperation of two universities and two companies, and it is thanks to the support and guidance of many people from all these institutions that this thesis was developed.

Firstly, I would like to thank my advisors Dr. Peter Frise and Dr. Narayan Kar from the University of Windsor, for their patience and assistance both during the academic year and during the writing of the thesis. I am particularly grateful also to Jan Stewart and Mike Huston, which were always very helpful throughout the last period spent in Windsor.

Then, I would like to express my deepest gratitude to all the people who assisted me in Chrysler, starting from my tutor Mengyang Zheng and my supervisor Mohammed Malik, for their tremendous help and the efforts they put into getting over the difficulties. Special thanks go also to Antonio Mancina and all the colleagues I worked with, which supported me both professionally and morally: Sachin, Ken, Nadirsh, Witt, Sashi, Tim, Joel, Joseph, Jon, Dale, John, Lucille, Julie, Andrew, Rami, Daniel, Iva, Lucas, Andryas and Ashay.

I would like also to thank the people from Fiat, especially my tutor Ing. Vittorio Ravello, which was always very helpful despite the distance, and Ing. Edoardo Rabino.

Last but not least, I am profoundly grateful to Prof. Giovanni Belingardi from Politecnico di Torino, for his constant commitment to the success of this exchange program, and my two advisors, Prof. Andrea Tonoli and Prof. Alberto Tenconi.

A particular thanks is finally reserved to my girlfriend Mara, my parents and all my friends, who always believed in me during the last year.

TABLE OF CONTENTS

LIST OF TABLES

LIST OF FIGURES

NOMENCLATURE

a	Vehicle acceleration
c_B	Belt damping coefficient
e	Error between reference and actual engine speed
E_{acc}	Accessory Energy
$E_{acc/dec}$	Energy spent to accelerate and decelerate the vehicle according to the driving cycle
$E_{braking}$	Energy required to brake the vehicle according to the driving cycle
$E_{cranking}$	Energy required to crank the engine
$E_{\substack{energy \\ conversion \\ losses}}$	Loss due to energy conversion from mechanical to chemical form
E_{fuel}	Energy of the fuel
E_{fw}	Mechanical energy available at the flywheel
E_{idle}	Energy spent to run the engine at idle
E_{losses}	Total energy dissipated in losses
$E_{\substack{mech \\ losses}}$	Energy lost in the gearbox
E_{regen}	Energy recovered by means of regenerative braking
$E_{\substack{regen \\ losses}}$	Energy losses due to regenerative braking
$E_{road\ loads}$	Energy spent to win the road load resistance
$E_{road\ loads\ (+)}$	Energy spent to win the road load resistance (during constant speed and acceleration)
$E_{road\ loads\ (-)}$	Energy spent to win the road load resistance (during deceleration)
$E_{stop-start}$	Energy saved by the stop-start
$E_{traction}$	Energy spent for the tractive effort
F_0, F_1, F_2	Road load coefficients
$F_{acc/dec}$	Force required to accelerate and decelerate the vehicle according to the drive cycle
F_B	Elastic and damping belt force
F_{cyl}	Force that applies on the piston head due to combustion in the cylinder
F_{decel}	Force required to decelerate the vehicle according to the drive cycle
F_{in}	Inertia force due to reciprocating masses

$F_{road\ loads}$	Road load force
$F_{road\ loads\ (-)}$	Road load force (during deceleration)
$F_{traction}$	Tractive force
$H(s)$	Transfer function between desired and actual motor torque
I	Moment of inertia
k_B	Belt stiffness
k_p, k_1, k_2	Engine friction model coefficients
m_{fuel}	Mass of burned fuel in the drive cycle
m_r	Mass of the reciprocating elements
m_v	Vehicle mass
n_{ev}	Electric drive speed threshold
n_{idle}	Engine speed at idle
n_{fw}	Flywheel speed
p	Pressure
P	Force applied on the piston pin
P_{acc}	Accessory power
P_{accel}	Power required to accelerate the vehicle according to drive cycle
$P_{braking}$	Power required to brake the vehicle according to the drive cycle
p_{cyl}	In-cylinder pressure
P_{decel}	Power required to decelerate the vehicle according to drive cycle
P_{ev}	Electric drive power threshold
P_{extra}	Extra engine power required during vehicle decelerations
$P_{friction}$	Friction brake power
P_{idle}	Engine idle power
P_{regen}	Regenerative braking power
$P_{\substack{regen \\ max}}$	Maximum regenerative braking power
$P_{road\ loads\ (+)}$	Road load power (during constant speed and acceleration)
$P_{road\ loads\ (-)}$	Road load power (during deceleration)
$P_{traction}$	Power for the tractive effort

Q_g	Gross heat released with combustion
Q_w	Heat transferred to the cylinder walls
r_{crank}	Crank radius
r_E	Engine pulley radius
r_M	Motor pulley radius
S	Piston head air
sfc_{idle}	Specific fuel consumption at idle
T_{comb}	Torque produced by combustion
t_{cycle}	Drive cycle duration time
T_E	Engine torque
T_{ev}	Electric drive torque threshold
T_f	Friction torque at the belt-pulley interface
$T_{f\,max}^{k}$	Maximum kinematic friction torque at the belt-pulley interface
$T_{f\,max}^{s}$	Maximum static friction torque at the belt-pulley interface
T_{fr}	Engine friction torque
T_{fr_0}	Static engine friction torque
T_{fw}	Flywheel torque
T_{idle}	Engine torque at idle
T_{in}	Inertia torque due to reciprocating masses
T_M	Motor torque
$T_{M_{CL}}$	Closed-loop motor torque
$T_{M_{OL}}$	Open-loop motor torque
$T_{M_{des}}$	Desired motor torque
T_{pump}	Pumping torque
V	Cylinder volume
v	Vehicle speed
Δx_B	Belt elongation
$\Delta \dot{x}_B$	Difference of the velocities of the belt extremities

Greek symbols

λ	Ratio between crank radius and connecting rod length
γ	Specific heat ratio
θ	Angular position
$\dot{\theta}$	Angular speed
$\ddot{\theta}$	Angular acceleration
η	Efficiency
ρ	Density

Subscripts

amb	Ambient
E	Engine
M	Electric motor
B	Belt
cs	Crankshaft
b	Battery
p	Powertrain
v	Vehicle

Apices

*	Required
s	Static
k	Kinematic

Abbreviations

A/C	Air Conditioning
ABS	Anti-lock Braking System
AC	Alternating current
BMS	Battery Management System
BSG	Belt Starter Generator
CD	Charge-Depletion
CO	Carbon Monoxide
CO_2	Carbon Dioxide
CS	Charge-Sustain
DC	Direct Current
ECM	Electronic Control Module
EIA	Energy Information Administration
EOR	Enhanced Oil Recovery
EPA	Environmental Protection Agency
EV	Electric Vehicle
FTP	Federal Test Procedure
GHG	GreenHouse Gas
HCM	Hybrid Control Module
HEV	Hybrid Electric Vehicle
HHC	Hill Hold Control
HT	Heavy Truck
HVAC	Heating, Ventilation, and Air Conditioning
HWFET	HighWay Fuel Economy Driving Schedule
ICE	Internal Combustion Engine
IEA	International Energy Agency
IGBT	Insulated-Gate Bipolar Transistor
IM	Induction Machine
IPMSM	Interior-mounted Permanent Magnet Synchronous Machine
ISG	Integrated Starter Generator
LCV	Light Commercial Vehicle
LDV	Light-Duty Vehicle

LHV	Lower Heating Value
Li-ion	Lithium ion
MAP	Manifold Air Pressure
MCU	Motor Control Unit
MOSFET	Metal-Oxide-Semiconductor Field-Effect Transistor
mpg	miles per gallons
NEDC	New European Driving Cycle
NGLs	Natural Gas Liquids
NiCd	Nickel Cadmium
NiMH	Nickel Metal Hydride
NO_x	Nitrogen Oxides
NVH	Noise, Vibration, and Harshness
OBD	On-Board Diagnostics
PbA	Lead Acid
PHEV	Plug-in Hybrid Electric Vehicle
PI	Proportional Integral
PM	Particulate Matter
RWD	Real-Wheel Drive
SAE	Society of Automotive Engineers
SOC	State Of Charge
SPMSM	Surface-mounted Permanent Magnet Synchronous Machine
SRM	Switched Reluctance Machine
SUV	Sport Utility Vehicle
TCC	Torque Converter Clutch
TCU	Transmission Control Unit
UDDS	Urban Dynamometer Driving Schedule
VDE	Verband Der Elektrotechnik, elektronik und informationstechnik
VOC	Volatile Organic Compound
VVT	Variable Valve Timing

CHAPTER 1

INTRODUCTION

Sustainable transportation has recently become a key issue in a world facing a continuous growth in the number of vehicles produced and sold. The current personal transportation system model is not sustainable in the long run because it relies heavily on non-renewable supplies. Earth has limited reserves of fossil fuels and oil shortage is a worrying issue that the world will have to face in the future. Moreover, the dependence on these kinds of fuels have introduced great challenges relative to environment and global climate change: the noxious emission from burning fossil fuels are in fact a major cause of air pollution, which ultimately affects human health, and of the production of carbon dioxide (also referred to as greenhouse gas), that is considered one of the main responsible of global temperature increase and dangerous climate instability in many parts of the world.

In addition to the global energy and environmental issues, current standard vehicles are characterized by poor efficiency and high noise emissions, especially during urban driving. These issues indicate that if industry wants to satisfy the increasing demand of personal transportation in a sustainable way, alternative energy sources and carriers must be found and rendered economically feasible.

Many car companies have started to develop and produce electric vehicles (EV) and hybrid electric vehicles (HEV), with the main objective of reducing fuel consumption and emissions of pollutants and carbon dioxide. However, the challenges to be faced are still many, both on the technical and on the economic side, before a complete transition from a fossil fuel-based to an electricity-based transportation system becomes possible.

In this context, this thesis will be focused on HEVs, and in particular on one specific architecture, the so-called Belt Starter-Generator (BSG), in which a relatively small belt-driven electric machine (roughly with the same dimensions a conventional high class conventional alternator) is employed both for engine cranking and for on-board electric energy production, instead of a conventional starter and an alternator respectively. The BSG system, thanks to its features of low cost, low complexity and fuel

economy enhancement, is a cost-effective solution in the vehicle hybridization process, and represents a promising starting point for the transition to a long-term new generation of electric vehicles.

1.1 Objectives

The BSG design involves several modifications in the powertrain components and control strategies. A correct modeling of the system is therefore essential for result prediction and for proper implementation on the vehicle. The first research objective of the thesis is related to this topic, specifically to the modeling of the dynamics of the electric machine-belt-engine assembly, for the determination of the system performance characteristics during engine start events. In fact, one of the main functionalities introduced by the BSG is the so-called stop-start, which allows the engine to be switched off during idle. The number of restarts with a BSG system is then much higher than in a conventional vehicle (at least ten times), as there are many opportunities to switch the engine off, especially during city driving. The quality of such restarts must also be high enough, so that vehicle drivability and passengers' comfort are not compromised. The BSG modeling allows the prediction of how the system will behave during this operation, and represents the starting point for the design of an electric machine controller capable of providing quick and smooth restarts.

The major advantage relative to the BSG implementation, in particular from the customer’s point of view, is the reduction of fuel consumption with respect to a conventional vehicle. The fuel savings are due to the many functionalities that the BSG introduces. However, different components and settings produce different results, so careful system design and calibration is required to obtain the best fuel efficiency for varying conditions.

The second research objective of the thesis is to quantify the impact of BSG components and functionalities on fuel savings. The results are obtained and compared using three different approaches:

- analytical approach: this consists of a simple analytical model for fuel consumption calculation, and is capable of estimating the consumption for different vehicles settings and drive cycles; in particular, it is interesting to assess

how much each of the BSG function contributes to the fuel consumption reduction.

- simulations: this introduces a more complex model, which simulates in detail all the vehicle powertrain, used to evaluate fuel consumption; various study cases are prepared, considering different components and control strategies.
- experimental tests: these are performed directly on a proof-of-concept parallel HEV; specific calibration settings are tested in order to assess, also through tests, the contribution of each BSG function to the fuel consumption reduction, and to validate the simulation results.

1.2 Thesis organization

The thesis is organized in six chapters, which are briefly described below:

Chapter 1 is the introduction, which provides a small preface about hybrid electric vehicles and presents the objectives of the thesis.

Chapter 2 contains a literature survey related to the BSG. Firstly, a background about the current scenario of personal transportation is provided, illustrating the situation with respect to the oil reserves and the environmental issues related to fossil fuels. It is explained why a new model of transportation has become necessary, and how HEVs can help to realize it. Afterwards, HEVs are classified, with focus on the BSG. This system is analyzed in detail, describing possible architectures, various components and sizing criteria. The chapter also addresses the BSG functions and operating principle, explaining how they affect performance and fuel consumption.

Chapter 3, divided in two main sections, covers the modeling, simulation and experimental activities of the thesis research. The first section pertains to the stop-start functionality analysis and modeling. This feature is illustrated through its phases and influencing factors, and subsequently a Simulink model is described, capable of simulating the dynamics of the engine start-up. The second section deals with the fuel consumption simulations and tests, aimed to evaluate the fuel consumption improvements related to the BSG introduction. The three approaches mentioned before (analytical, simulations and tests) are presented, together with the study cases and the vehicle data.

Chapter 4 provides the results of the research and their analysis. It is divided into two sections, as in the previous chapter: in the first one, the results of the engine cranking simulations are shown and analyzed, and the model is validated against experimental test data obtained from a start cart; in the second part, the fuel consumption results for the three approaches are shown singularly and then compared among each other, considering also the effect of different study cases and vehicle calibrations.

Chapter 5 presents the conclusions and the recommendations. The research on BSG modeling and fuel consumption analysis is summarized, and the main outcomes are reported. Future activities are proposed to further develop the research on the basis of these results.

CHAPTER 2

LITERATURE REVIEW

2.1 The current status of personal transportation

Personal transportation has experienced a radical evolution over the last century. Technological progress in all the transportation fields and in the supporting infrastructure has provided people the ability to move rapidly and independently from one place to another. Nowadays, world globalization is also leading people to travel more than in the past, and in the developing countries an increasing portion of the population can afford to buy means of personal transportation.

As a consequence, there has been a continuous growth in the number of automobiles produced and sold worldwide. In 2010, the number of vehicle in operation surpassed the 1 billion-unit mark [1]. In 2011, over 80 million vehicles were produced in a single year (or 220,000 new vehicles produced every day) [2]. Figure 2.1 shows the production trend over the past 15 years.

Except for a 12% decline in 2009 (due to the 2008 global financial crisis), the vehicle production showed on average an increasing trend from 54 million vehicles produced in 1997 to 80 million vehicles produced in 2011.

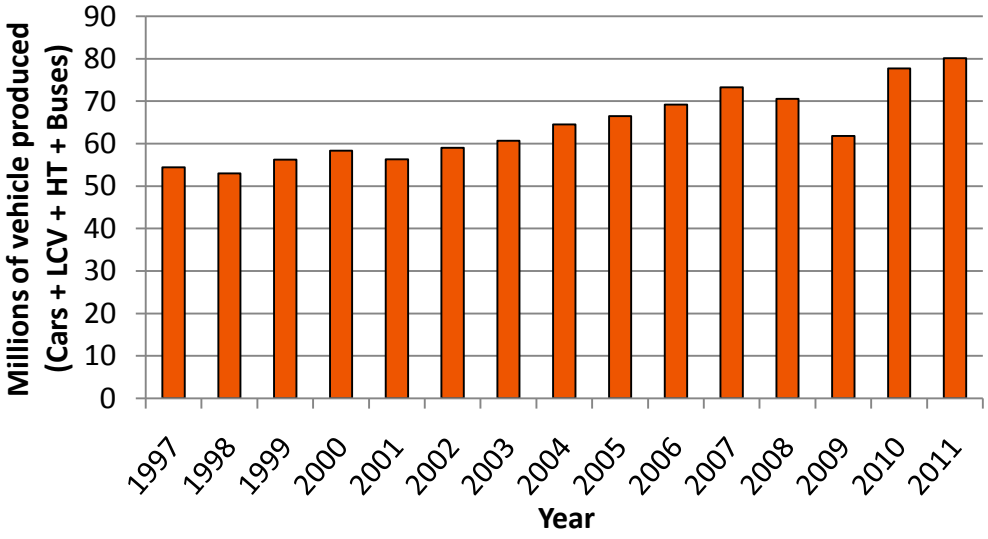

Figure 2.1 - Number of vehicles (cars, light commercial vehicles, heavy trucks and buses) produced between 1997 and 2011 [2].

With further urbanization, industrialization, and globalization, the trend of rapid increase in the number of vehicles worldwide is expected to continue in the future. However, the current personal transportation system has an inherent problem: it relies heavily on oil. Not only are the oil resources on Earth limited, but also the emissions from burning oil products have led to climate change, poor urban air quality, and political conflict. Thus, global energy system and environmental problems have emerged, which can be attributed on a large extent to personal transportation [3].

2.1.1 Oil availability in the future

The status of world oil reserves is a discussion topic that has become of primary interest in the last few decades. The fact that someday oil will not be anymore available, accessible and affordable as in the past will impact not only the transportation system, but the whole current social and economic structure. Many scientists and institutions are trying to predict the status of the world oil reserves for the upcoming years, but often the results are misleading because of the complex nature of the problem. The rest of this section is focused on explaining where the world is heading for with respect to oil availability.

The world liquid fuels come predominantly from reserves of fossil energy. They can be divided into the following types: conventional sources or "crude oil" (usually defined as fields that produce light and medium crude oil), non-conventional sources (heavy oils, tar sands, and shale oil), and natural gas liquids (NGLs) (the liquid component of natural gas) [4]. Conventional oil reserves are the most accessible and least technically challenging to bring into production. In contrast, non-conventional oil resources cease to flow at surface temperatures and pressures and are not readily recovered because production is capital intensive and requires supplementary energy [5]. Presently, more than 85% of the world oil production comes from conventional sources, while the remaining part is predominantly from NGLs [6].

For more than a century, discoveries of new conventional oil fields and the development of new technologies for the production of both conventional and non-conventional oil have ensured ever increasing world oil production [7]. But as liquid fuels are finite non-renewable resources, by definition they cannot continue to meet ongoing

demand. The challenge that the oil industry is facing nowadays is how to increase production when existing fields are experiencing depletion rates of 5% or more while annual demand for oil is expected to increase at rates exceeding 1% [6]. Although more oil may be there to be discovered, given sufficient investment and technological advances, the oil industry is being forced to look for conventional oil in locations that are both risky and more expensive, such as offshore sites in deep water and the Arctic [8], and non-conventional sources, like Canada tar sands and Venezuela heavy oils, that are expensive, energy intensive, and damaging to the environment [9].

Figure 2.2, published by the U.S. Energy Information Administration (EIA), shows how liquid fuel demand (expressed in millions of barrels consumed per day) is likely to evolve in the future years, divided by sector. It is expected that consumption will increase and that almost all additional demand will come from China and India [10]. It can be clearly seen that the transportation sector has the biggest share of consumption. Moreover, in the next years, rising prices for liquid fuels will increase the cost competitiveness of other fuels, leading many users of liquids outside the transportation sector to substitute sources of energy when possible. As a result, the transportation share of total liquid fuels consumption will raise [11].

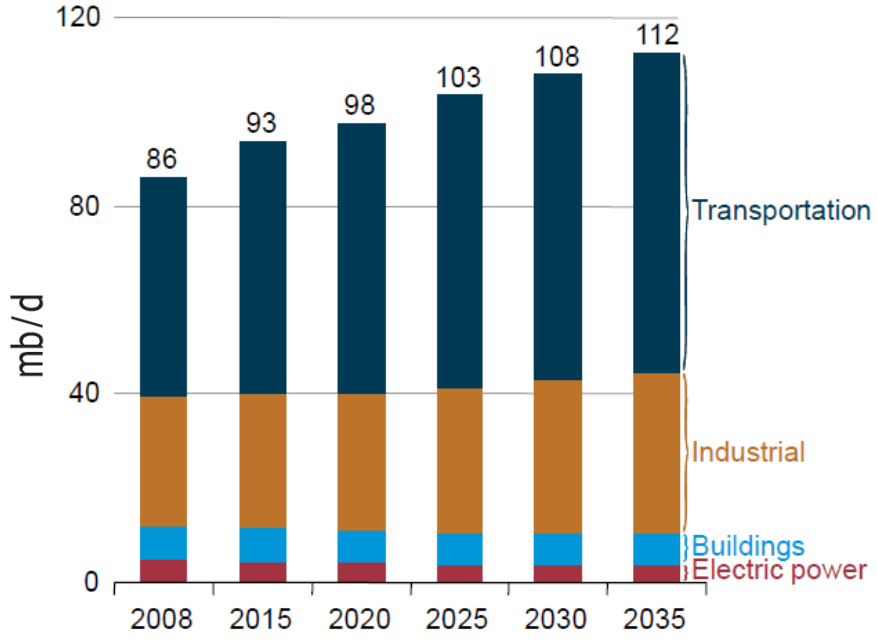

Figure 2.2 - World liquid fuels consumption by sector, 2008-2035 (million barrels per day) [11].

The 2008 International Energy Agency (IEA) projection for world liquid fuel production is shown in Figure 2.3, and is divided into natural gas liquids, non-conventional oil and crude oil. Crude oil is further divided into currently producing fields, fields yet to be developed, fields yet to be found, and additional enhanced oil recovery (EOR). A projection of the liquid fuel consumption growth is showed as well. It was built considering that total liquid fuel consumption in 2008 was 86 Mb/day and that in 2030 consumption is expected to reach 108 Mb/day (Figure 2.2), at an average rate of about 1% per year. Additional demand will be most likely met by non-conventional oil, enhanced oil recovery, and natural gas liquids, which show a steady growth.

Conventional oil production instead will maintain current capacity (it reached the so-called "plateau"), though it is critical to note this is dependent upon the development of known crude oil reserves, the discovery and development of new crude oil fields, and EOR. If these conditions are not met, oil production will start to decline.

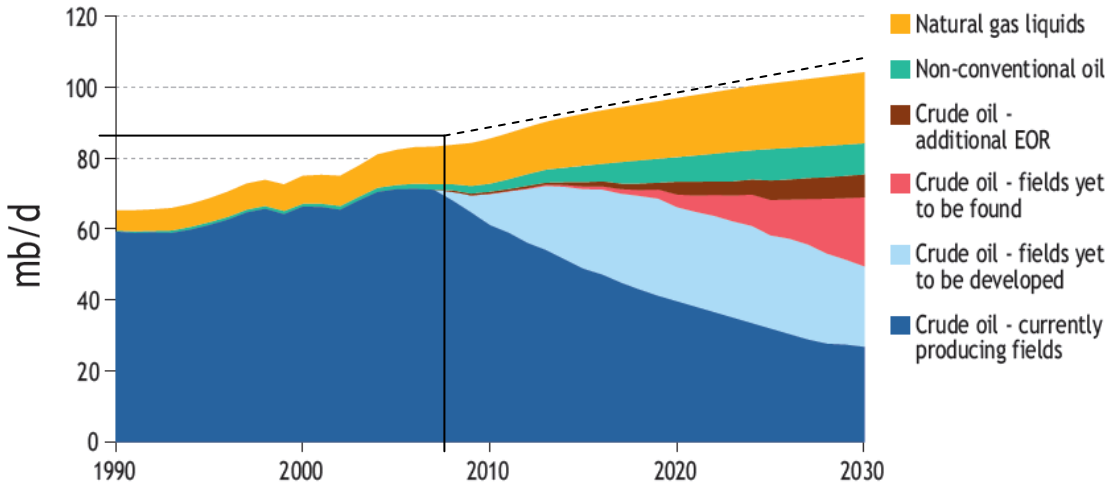

Figure 2.3 - World liquid fuels production by type, 2008-2035 (million barrels per day) [10].

In 2008, conventional oil from producing fields constituted approximately 85% of the global liquid fuel mix, and it is expected to decline at a fast rate in the next years. With this trend, current sources of liquid fuel (crude oil from producing fields, non-conventional oil, natural gas liquids) will only have the capacity to service just over 50% of the demand by 2030. The implication is that the remaining part will have to be met by sources that are not in production today.

The status of world oil reserves and availability remains a contentious issue, split between those who believe oil peak is near (or already surpassed) and production will soon decline, and other institutions such as major oil companies that say there is enough oil to last for decades. This discussion is also stirred up by ambiguity in public data, which mostly arises from:

1) a lack of international standards to report oil reserve volume and grade;
2) the point at which resources may be classified as commercially exploitable reserves;
3) intentional misreporting to favor a financial or political agenda;
4) inherent technical assessment uncertainty [5].

What can be said for certain is that, while there is certainly vast amounts of fossil fuel resources left in the ground, the volume of oil that can be commercially exploited at prices that the global economy has become used to is limited and will soon decline. Supply and demand are likely to diverge in the near future, unless demand falls in parallel with the induced recession. The result is that oil may soon shift from a demand-led market to a supply-constrained market, with obvious social, political and economic consequences. Reducing oil consumption, especially in the personal transportation sector, is therefore essential to achieve energy sustainability.

2.1.2 Environmental issues related to oil

The dependence of the transportation system on oil introduces a great challenge relative to environmental problems and global climate change. The emissions from burning fossil fuels increase the carbon dioxide (CO_2) concentration (also referred to as greenhouse gas or GHG emissions) in the Earth atmosphere. The increase in CO_2 concentration is leading to excessive heat being captured on the Earth surface, which turns into a global temperature increase and dangerous climate instability in many parts of the world.

Figure 2.4 shows global carbon dioxide emissions from fossil fuels in the last two centuries. It can be seen that the most dramatic increase has happened in the last 50 years, in conjunction with the rise in use of petroleum for human activities.

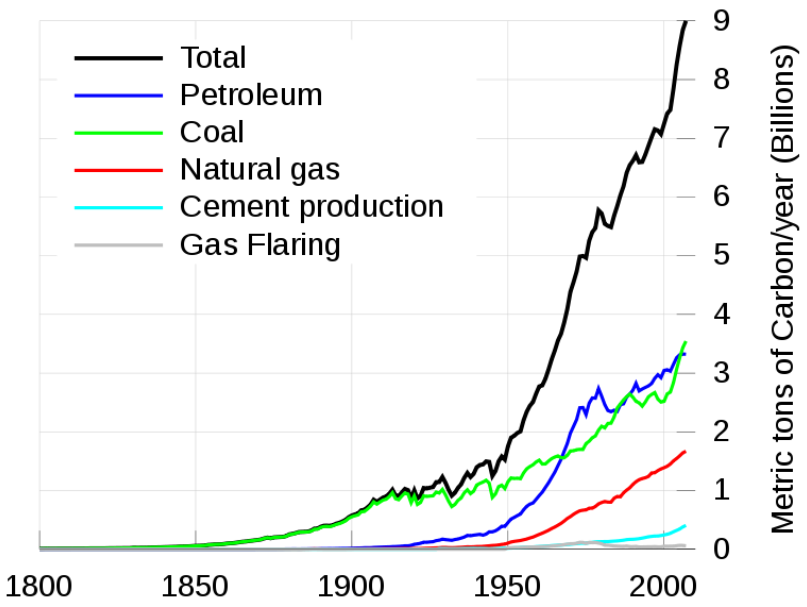

Figure 2.4 - Global carbon emissions produced by human activities [12].

Figure 2.5 illustrates how CO_2 emissions from burning fossil fuels are divided by sector. It can be clearly noticed that transportation sector, and in particular motor vehicles, have the biggest share in the comparison.

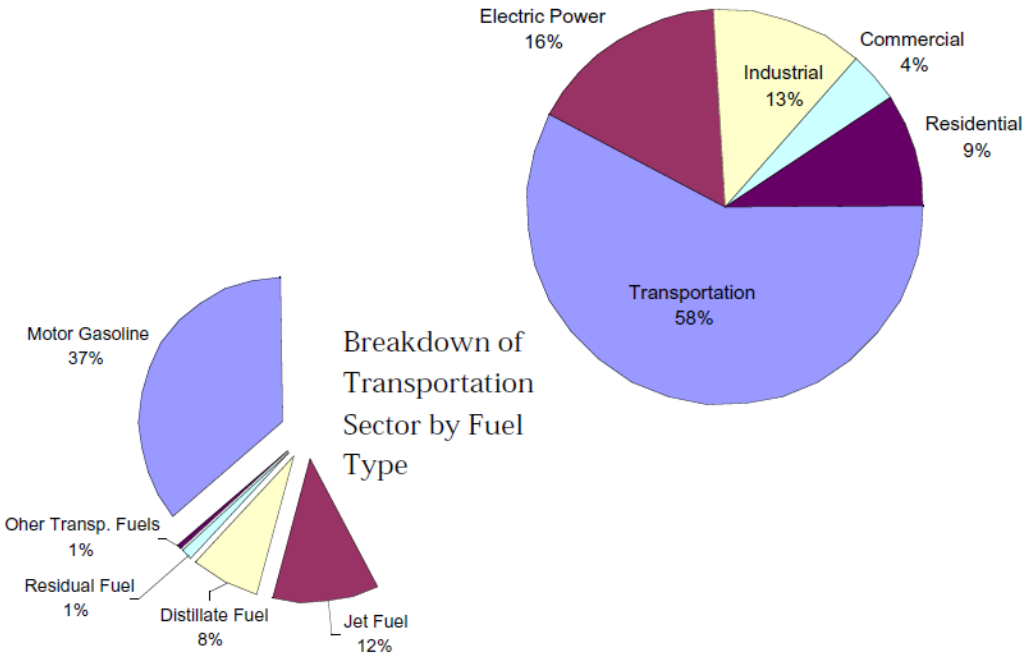

Figure 2.5 - Carbon dioxide emissions from the combustion of fossil fuels by sector for 1999 [13].

The carbon dioxide atmospheric concentration increased from 280 ppm to 397 ppm since the beginning of the Industrial Revolution [14]. This results in a thicker and denser atmosphere due to the action of carbon dioxide and other greenhouse gases, such as water vapor, ozone and methane. Many scientists today agree that the CO_2 concentration increase in the atmosphere is the primary cause for global warming, i.e., the rise in the average temperature of Earth's atmosphere and oceans since the late 19th century. This phenomenon is related to the greenhouse effect, defined as the process by which thermal radiation from the Earth's surface is absorbed by atmospheric greenhouse gases, and is re-radiated in all directions; since part of this re-radiation is back towards the surface and the lower atmosphere, it results in an elevation of the average surface temperature above what it would be in the absence of the gases [15]. Figure 2.6 shows global mean land-ocean temperature change from 1880 to 2011, using the period of 1951-1980 temperature as the basis for comparison [16].

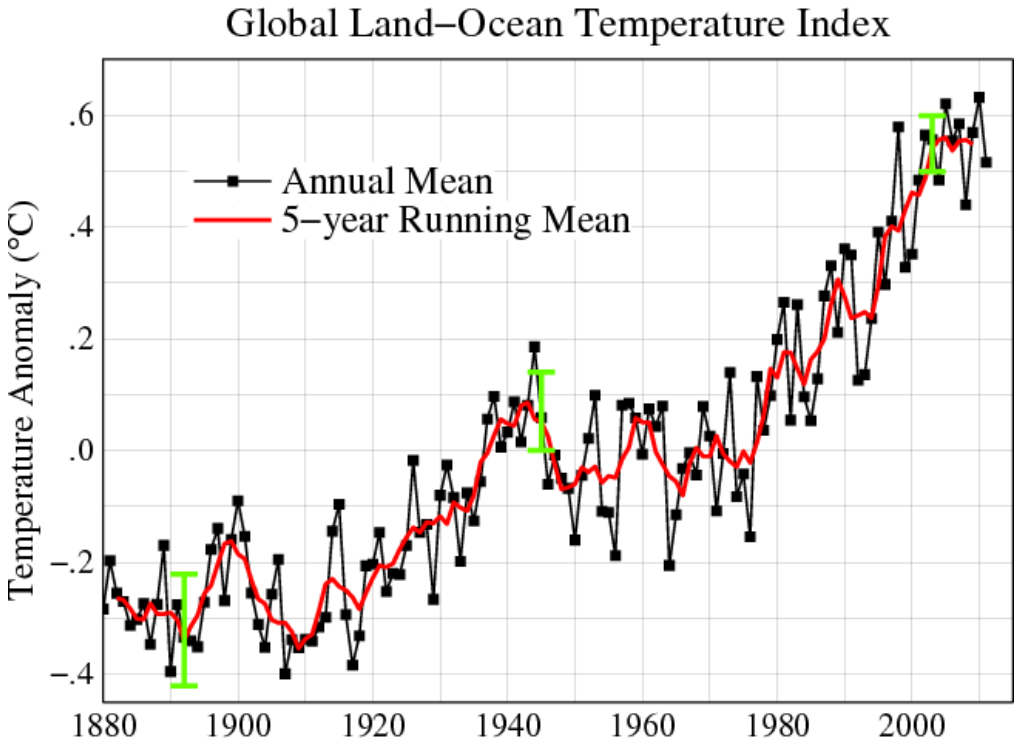

Figure 2.6 - Global mean land-ocean temperature change from 1880–2011, relative to the 1951–1980 mean. The green bars show uncertainty estimates [16].

Over the 21st century, climate change is likely to lead to extreme weather conditions in many parts of the world and ecosystem instability. Hundreds of millions of people will be adversely affected through increased coastal flooding due to sea level rise, reductions in water supplies, increased malnutrition and increased health impacts [17].

Greenhouse gases and global warming are not the only negative outcomes related to oil combustion. The pollutant emissions from conventional fossil fuel-powered vehicles are the major cause of air pollution, and contribute to the creation of smog in large cities, which ultimately affects human health.

Internal combustion engines (ICE) rely on gasoline and diesel combustion during operation. Pollutants are generated during the combustion process inside the engine. In addition, unburned fuel evaporates, and in turn forms the basis for another type of pollution – the volatile organic compounds (VOC).

The emissions from combustion include carbon dioxide, VOC, nitrogen oxides (NO_x), particulate matter (PM) and carbon monoxide (CO). These exhaust emissions can occur in two modes [18]:

- Cold start: during the first couple of minutes after starting the engine of a vehicle that has not been operated for several hours, the amount of emissions is very high. This occurs due to two main reasons:
    - Rich air-fuel ratio requirement in cold engines: right after starting the engine the walls as well as the fuel are cold. Fuel does not vaporize and it is difficult to create a proper combustible gaseous mixture. Therefore very rich fuel ratio is required at the beginning. The excess fuel in the chambers is subsequently burned generating great amounts of hydrocarbons, nitrogen oxides and carbon monoxide.
    - Inefficient catalytic converter under cold conditions: catalytic converters are very inefficient when cold. When the cold engine is started, it takes several minutes for the catalytic converter to reach its proper operating temperature. Before this, gases are emitted directly into the atmosphere.
- Running exhaust emissions: these pollutants are emitted from the vehicle tailpipe during driving and idling after the vehicle is warmed up.

Considering that a substantial number of trips are short, cold start emissions are a major issue in the worsening of air quality. Figure 2.7 shows the emissions of a typical passenger car during cold start. It has been estimated that 70–80% of the total emissions occurs during the first two minutes after a cold start during a standard driving cycle [19].

Since all these pollutants are extremely dangerous for human health, efforts are continuously required to reduce vehicle emissions and improve air quality.

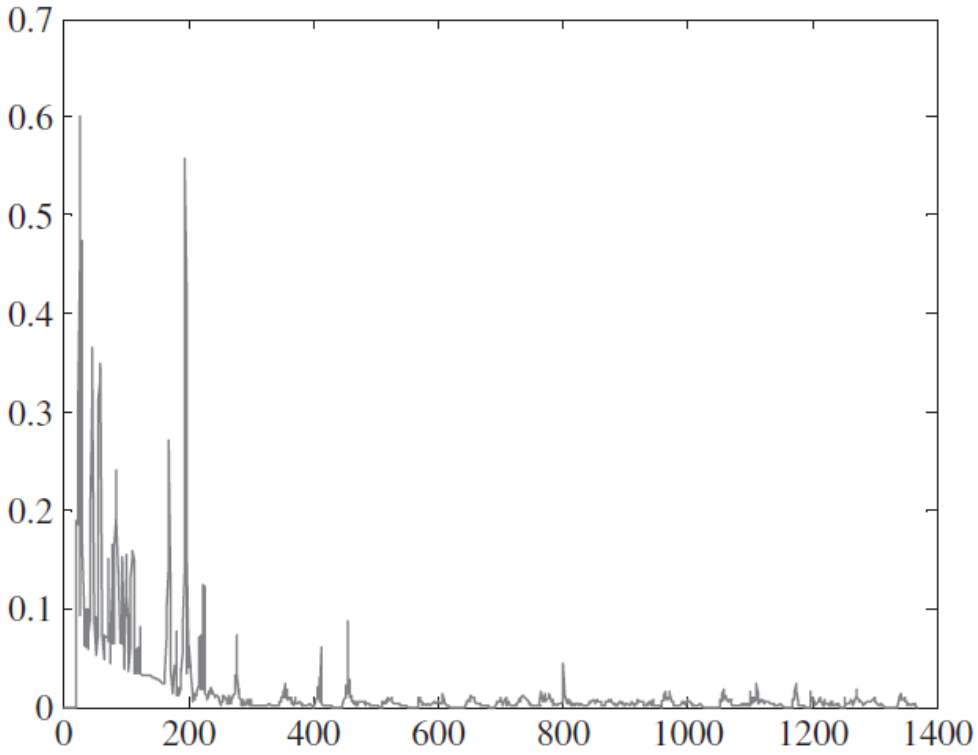

Figure 2.7 - Typical emissions of a mid-size passenger car during cold starting. Shown in figure is the total emissions in grams, which contains VOC, CO, NO_x and PM [3].

2.2 Where road transportation should aim: sustainable transportation

From the explanation in the previous section, it can be inferred that the current personal transportation system model is not sustainable in the long run, due to the global energy and environmental problems associated with the use of fossil fuels. Moreover, standard vehicles are characterized by poor efficiency and high noise emissions. If industry wants to satisfy the increasing demand of personal transportation in a sustainable way, alternative energy sources and carriers must be found and rendered economically feasible.

There are many definitions of sustainable transportation. One of these definitions, from the European Union Council of Ministers of Transport, defines a sustainable transportation system as one that:

- "allows the basic access and development needs of individuals, companies and society to be met safely and in a manner consistent with human and ecosystem health, and promotes equity within and between successive generations;
- is affordable, operates fairly and efficiently, offers a choice of transport mode, and supports a competitive economy, as well as balanced regional development;
- limits emissions and waste within the planet ability to absorb them, uses renewable resources at or below their rates of generation, and uses non-renewable resources at or below the rates of development of renewable substitutes, while minimizing the impact on the use of land and the generation of noise" [19].

However, sustainability extends beyond just the operating efficiency and emissions of the vehicles. For the transportation to be completely sustainable, life-cycle assessments involving production and post-use considerations must be included. Cutting fossil fuel usage and reducing carbon emissions represent only part of the effort to keep human use of natural resources within sustainable limits.

A viable pathway to sustainable transportation is a global transition to vehicles driven by electricity from clean and renewable energy. Electric propulsion is more efficient than the combustion process in a vehicle; well-to-wheel efficiency studies show that, even if the electricity is generated from fossil fuels, fuel consumption of electric vehicles is still less than fuel consumption of conventional internal combustion engine vehicles [20]. But to overcome the problem of fossil energy sources shortage, in the future electricity needs to be produced from renewable sources such as hydroelectric, wind, solar and biomass.

Still, today’s battery-powered electric vehicles have several technological limits, such as reduced driving range and long charging time, as well as high battery cost. Problems are also present for fuel cell-powered electric vehicles, because the technology is not yet mature enough to be competitive.

An intermediate step towards the full electrification of the transportation sector is represented by hybrid electric vehicles (HEV), which use both an ICE and an electric

motor to produce the power required to drive the vehicle. With respect to purely electric vehicles, HEVs reduce the cost and range issues, but are still tied to the ICE and fossil fuels; nevertheless, they have the capability of significantly reducing fuel consumption and pollutant emissions. Moreover, performance usually benefits from the use of electric machines, which in contrast to ICEs are characterized by high torque capability at low speeds.

A further solution is represented by plug-in hybrid electric vehicles (PHEVs), which are equipped with a larger battery pack and usually a larger-sized motor compared to HEVs. PHEVs can be charged from the grid and driven for a limited distance (30-60 km) using electricity only, working in the charge-depletion (CD) mode operation. Once the battery energy has been depleted, PHEVs operate similarly to a regular HEV, working in the charge-sustain (CS) mode operation, or extended range operation. Since most of the personal vehicles are for commuting and 75% of them are driven only 60 km or less daily [21], a significant amount of fossil fuel can be displaced in the tank-to-wheel chain by producing PHEVs capable of a range of 60 km of purely electricity-based propulsion.

Vehicles propelled by electricity also have a reduced carbon footprint (which is the total set of greenhouse gas emissions produced during the vehicle operation). A report published in June 2011, prepared by Ricardo in collaboration with experts from the UK Low Carbon Vehicle Partnership [22, 23], found that hybrid electric cars, plug-in hybrids and all-electric cars, even if they generate more carbon emissions during their production than current conventional vehicles, still have a lower overall carbon footprint over the full life cycle. The study assumed CO_2 emissions in production of 500 g/kWh, which is equal to average UK electricity CO_2 emissions, and a vehicle usage of 150,000 km. Table 2.1 shows the results.

The higher carbon footprint during production of electric drive vehicles is due mainly to the production of batteries. It has been estimated that 43% of the production emissions for a mid-size electric car are generated from the battery production, while for a standard mid-size gasoline internal combustion engine vehicle, around 75% of the embedded carbon emissions during production comes from the steel used in the vehicle glider.

Table 2.1 - Comparison of full life cycle assessment (well-to-wheels) of carbon emissions and carbon footprint during production for four different powertrain technologies [22].

Powertrain technology	Estimated life-cycle emissions (tonnes CO_2)	Estimated emissions in production (tonnes CO_2)	Proportion of emissions in production
Standard gasoline vehicle	24	5.6	23%
Hybrid vehicle	21	6.5	31%
Plug-in hybrid vehicle	19	6.7	35%
Battery-electric vehicle	19	8.8	46%
Based upon a 2015 vehicle in use for 150,000 km full life travel using 10% ethanol blend and 500 g/kWh grid electricity.			

The report highlights the increasing importance of accounting for the whole life-cycle carbon emissions to compare the greenhouse gas emissions of low carbon vehicles. It found that some of the CO_2 savings made during the use of low carbon vehicles is offset by increased emissions created during their production, and to a lesser extent, disposal. However, the overall life cycle CO_2 emissions of vehicles propelled by electricity remain lower than conventional ones, and if the share of renewable sources in the electric power production will increase in the future, the carbon footprint of electric vehicles will further reduce.

In any case, one must remember that hybridization of vehicles is not the ultimate solution for sustainability, though it builds the pathway to a sustainable future. The technology developed along this pathway will allow the necessary transition from fossil fuel-based transportation to the full electrification of the transportation sector. Yet, a parallel effort needs to be made by the electrical power generation industry to increase the renewable and cleaner energy generation [3].

In the most optimistic scenario (i.e., if strong policies for market penetration of electricity-driven vehicles will be achieved), the number of HEV and EV sales is expected to grow steadily and overcome the number of conventional vehicle sales by

2030 [24]. Figure 2.8 shows the predicted trend of light-duty vehicle sales for different powertrain technologies in the next decades.

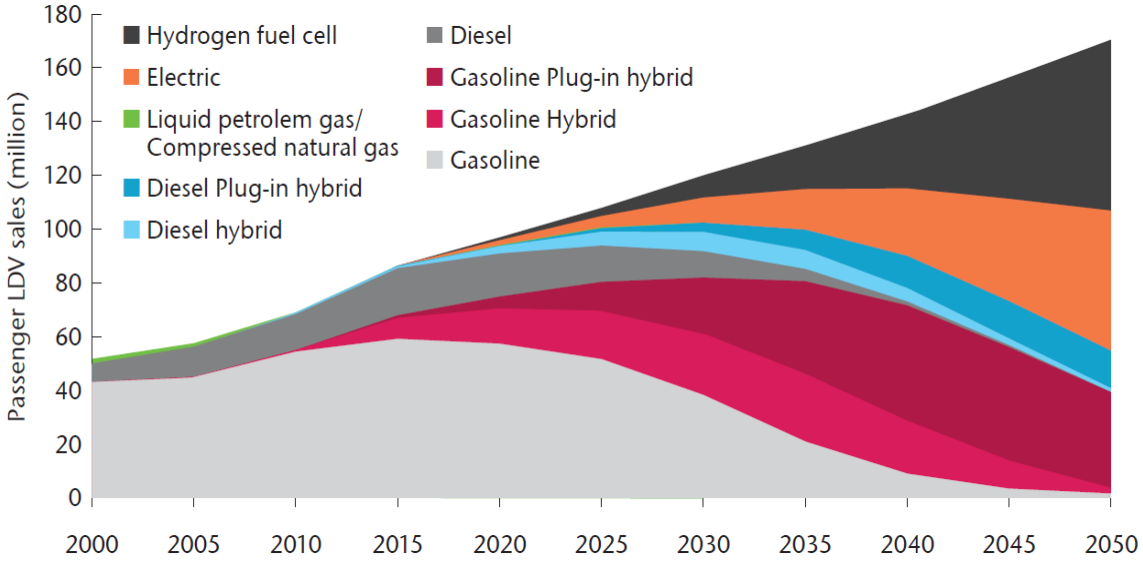

Figure 2.8 - Evolution of light-duty vehicle sales by technology type, in the most optimistic scenario [24].

2.3 Vehicle hybridization: focus on belt starter-generator system

Many types of HEVs exist nowadays. The sizing of the components of the hybrid system can produce various solutions, with different operating performances. Figure 2.9 shows schematically these combinations in relation with the sizing of the constituents of the system. Electric and thermal system "weights" determine the different classification typologies.

In general, HEVs can be classified according to their configuration or to the degree of hybridization. Considering the architecture, the possible solutions are parallel, series and series-parallel HEVs, while when speaking of the degree of hybridization there are micro, mild and full HEVs. Each of them has its own advantages and drawbacks, and the choice of a particular configuration/degree of hybridization depends on many aspects, including the mission assigned to the vehicle.

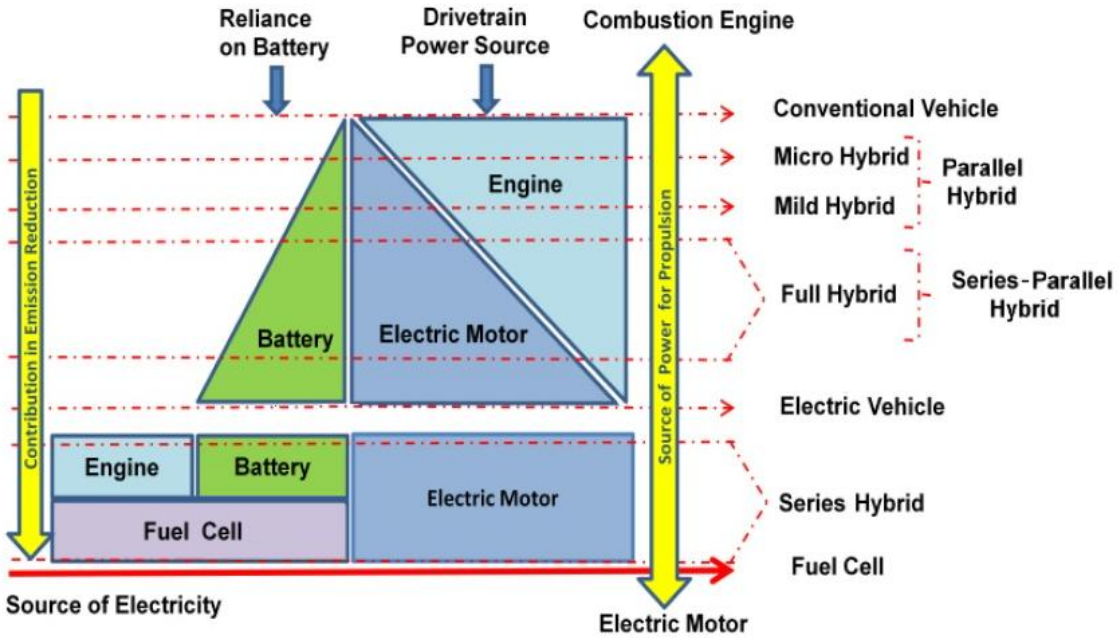

Figure 2.9 - Simplified classification of hybrid vehicles [25].

Giving a detailed description of all the various hybrid systems and of their operating principles is outside the scope of the thesis, and for further information the reader is referred to more specific texts [3, 26, 27]. Generally speaking, mild parallel HEVs represent nowadays an interesting compromise in terms of cost, complexity, fuel consumption reduction and performance enhancement. More specifically, the so-called Belt Starter Generator, or BSG, is a particular architecture of a mild parallel hybrid vehicle that stands out with respect to other solutions (especially those with higher degree of hybridization) for its characteristics of relative ease of implementation on conventional vehicles, limited cost and weight and good fuel economy improvement.

As an example, a current production vehicle equipped with such a system, the Buick LaCrosse eAssist, weights only 6 kg more than the conventional version (this result is also achieved by lightening other components) and obtained an EPA (U.S. Environmental Protection Agency) fuel economy rating of 9.4 l/100km on city cycle, 6.6 l/100km on highway and 8.1 l/100km combined, while the conventional vehicle fuel economy was 12.4/7.8/10.2 city/highway/combined [28]. Comparing the manufacturer suggested retail prices in the U.S. of the two versions (with same 2.4 liter engine), at the time when the hybrid version started to be sold on the market, the BSG entailed a price increase of 2830 US$ [28]. Considering current U.S. gasoline prices and a 45% highway,

55% city driving pattern, the extra cost can be paid back in about 135.000 km. However, it must be noted that other countries such as Italy have much higher gasoline prices, and also that some governments often promote hybrid vehicle sales through money incentives, so the payback distance can be reduced. Finally, also tailpipe CO_2 emissions benefit from the adoption of the BSG, reducing from 240 g/km of the conventional version to 190 g/km [28].

2.4 Description of the Belt Starter Generator

The Belt Starter Generator system, or BSG, is a mild parallel hybrid technology that aroused increasing interest in the last decade for its characteristics of fuel economy improvement, low weight and low delta cost.

With this system, the functions of engine start-up and on-board generation of electric energy are fulfilled by an electric machine alone, instead of the separated conventional starter and alternator. The early preliminary concept of this solution can actually be backdated to almost the same time as the starter was invented in the 1930s [29]. The reciprocal operating principle of electric machines, which can be used both in motoring and generating mode, is in fact long known, but the applications were complicated by the difference of specifications between the motor and the generator and by the system control difficulties when highly developed power electronics was not available. In recent times, with developments in the fields of AC electric machines and power electronics, starter-generator systems became feasible to be implemented in vehicle powertrains.

The BSG and its associated electronics and battery pack form a system that has the ability to perform many functions, including engine stop-start, regenerative braking recuperation, electric power assist-torque boost, early fuel cut-off, higher efficiency electric energy generation and torque smoothing of the driveline.

The BSG represents actually just one of the possible configurations that can be realized for a mild parallel hybrid vehicle using a starter-generator system. The following sections will review the possible architectures and the components that make them up, with particular attention on the solution realized with the belt drive. Then, the BSG

functions and operating principle will be analyzed in detail, explaining also how they affect fuel consumption.

2.4.1 Architectures

When a single electric machine is used to carry out both functions of the starter and the alternator, it is generally called an integrated starter generator (ISG). The configurations that can be implemented for an ISG system depend on the location of the electric machine in the powertrain and its connection to the crankshaft. There are four packaging options with four different drives: direct coupled drive, chain drive, gear drive and belt drive [30].

- Direct coupled drive: in this solution, the electric machine is placed directly on the crankshaft either between the transmission and the engine in the location of the flywheel (Figure 2.10) or on the accessory side (Figure 2.11) [31]. Such a system can provide good torque smoothing capabilities and can also be scaled up in output power level to provide good hybrid propulsion potential. Including the motor on the crankshaft eliminates the need of other mechanical engagement mechanisms and their associated losses, and wear and tear, thus reducing the number of system components and increasing reliability. Depending on the design, the direct coupling may also enable the replacement of the flywheel by the machine rotor, further reducing component requirements. However, the solution on the accessory side necessitates the extension of the shaft external to the engine, thereby posing a problem in the wear of the bearings [31]. Moreover, when powertrain packaging is an important issue, such as in vehicles with transverse engine arrangement, the direct coupling is critical in both the configurations because the powertrain length has to be increased to accommodate the starter-generator. A machine with larger dimensions than present alternators is also required, as the speed ratio of the machine to the crankshaft is 1:1. For this reason, electric motors for direct coupled ISG applications are characterized by a disc shape with big diameter and small thickness, and permanent magnet based machines, which show high torque density, are usually the best solution to meet the engine starting torque requirements [32].

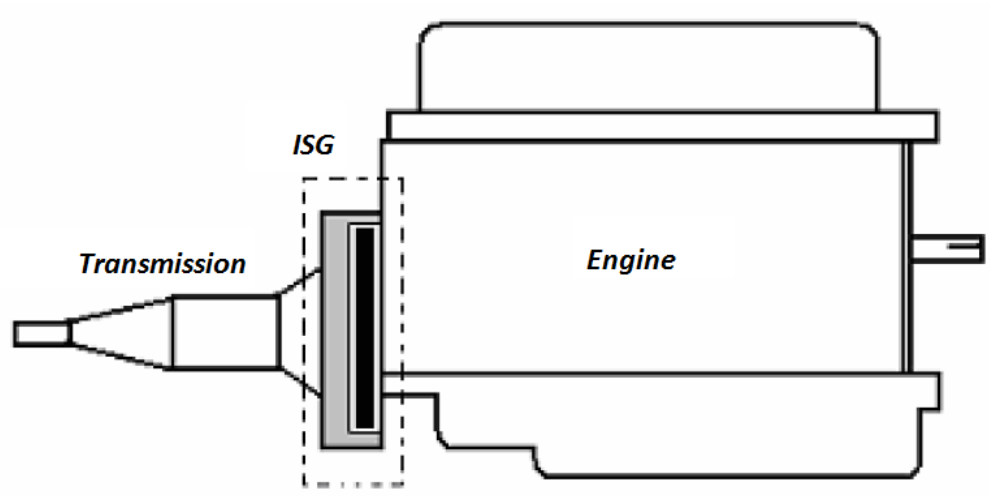

Figure 2.10 - Direct coupled drive - transmission side [31].

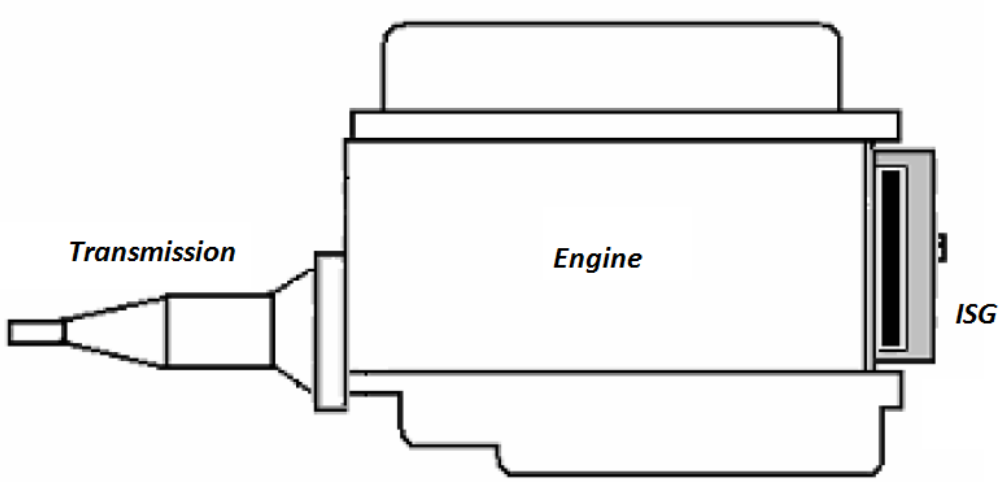

Figure 2.11 - Direct coupled drive - accessory side [31].

- Chain drive: this coupling involves the use of a chain to run over the pulleys. The most logical position for the drive is in the transmission case, in the general location of the conventional starter. The major advantage is possibility to use a smaller chain width compared to the belt solution for the same fatigue life, thanks to higher material tensile strength [30], with evident packaging benefits. The disadvantages are related to the limited space in the transmission case, which has to be redesigned, if the hybrid powertrain was not considered in the original design. Moreover, chains drives have inherent noise issues, which cannot be solved unless more expensive chain, such as silent chains, are used. In general,

this configuration is a viable solution when there is enough packaging space to fit the machine outside and the chain drive inside the transmission case.

- Gear drive: this drive also involves a coupling at the transmission side. The major issue related to such coupling is that at high speeds and not high loads the gear teeth risk to be damaged, or in other words "scoring" can occur [30]. To avoid the problem, a material with elevated hardness should be chosen, increasing the costs. In addition, manufacturing cost is also high, due to the need for ground teeth with high accuracy and surface finish. A multi-stage gear drive would help to reduce the maximum speeds of the teeth, but the packaging constraint would require modifications of the transmission case.
- Belt drive: this coupling, also referred to BSG, is probably the most convenient in terms of packaging, since the connection between electric motor and crankshaft is realized on the accessory side either including the starter-generator in the existing accessory drive or using a separate dedicated belt drive [30]. The former requires an increase in the belt width, and accordingly the pulley widths, in order to accommodate the increased load capacity introduced by the starter-generator. The latter instead does not need any modification in the existing belt drive, reducing the costs, but requires extending the crankshaft in order to install it, occupying extra space and increasing the stresses on the crankshaft bearings due to the overhang [31]. Anyway, the cross-car width of a transverse engine application is essentially unaffected by the BSG. For this solution the electric machine is located in the place of the conventional alternator, where usually more space is available for increased motor type and sizing flexibility [32]. Overall, the BSG has the advantages of low cost, minimal modifications in existing powertrain design, more freedom in packaging, no lubrication required and very low noise. Figure 2.12 shows a schematic architecture of the system. Other components are the battery and the power electronics, which are in charge of powering and controlling the electric machine respectively.

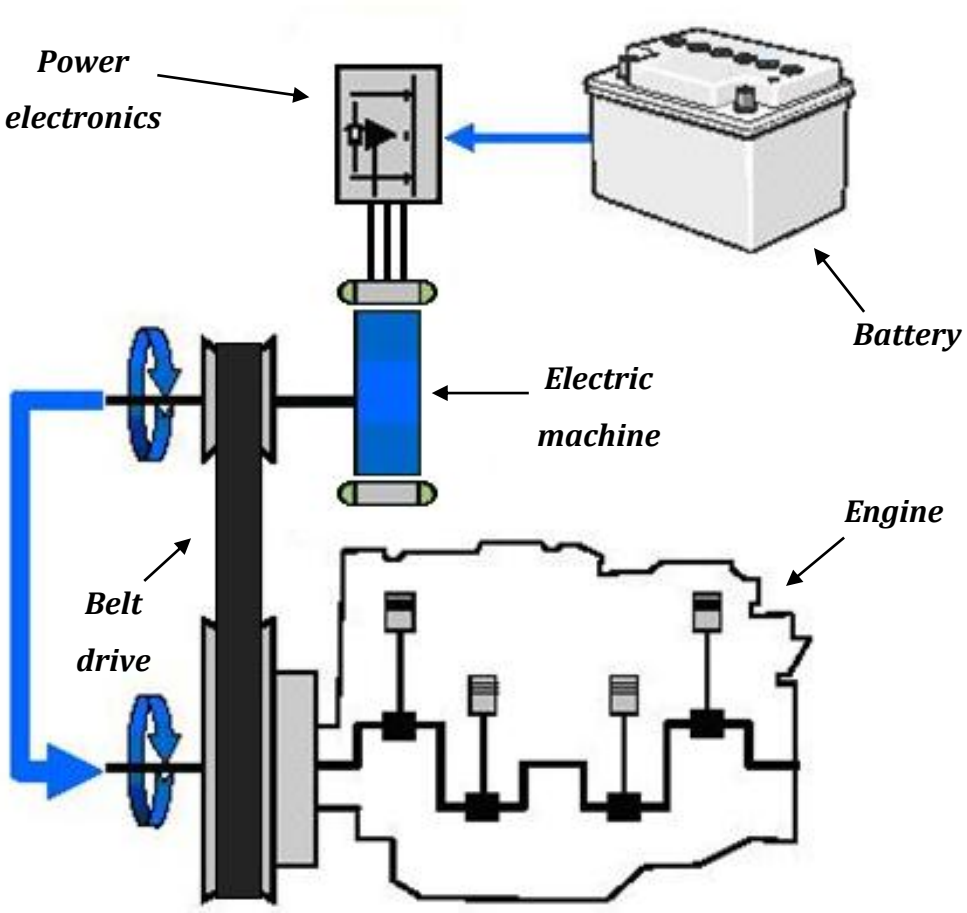

Figure 2.12 - BSG architecture [33].

The BSG, in the configuration which includes the electric machine in the accessory drive, was the chosen architecture for the simulations and the tests which will be presented in the following chapters. As previously stated, the other sections of this chapter will be focused in particular on the this solution.

2.4.2 Powertrain modifications required for the implementation of a BSG

Although the BSG is a relatively simple configuration, it is opportune to describe in more detail the powertrain modifications required for its implementation.

2.4.2.1 Starter-generator support

Starting from the motor side, a new bracket has to be designed to support the electric machine. If it is placed in the same position of the alternator, the bracket has to be fastened on the engine block with the constraint of utilizing the same bolt holes which

were used for the original component [34]. During the design stage, a modal analysis of the new layout is usually required to check for natural frequencies. Resonance during operation must be avoided in order not to compromise the structural integrity of the assembly, so natural frequencies should be moved to values as high as possible, considering constraints in terms of available space and weight.

2.4.2.2 Accessory drive

When the starter-generator is included in the accessory drive, the belt width and accordingly the pulley widths have to be increased in order to accommodate the increased load capacity of the system. If a serpentine belt is used, the redesign process has the following objectives [30]:

- determine the pulley diameters (based on belt fatigue life);
- compute the static tension;
- select the number of ribs;
- predict life;
- predict hub loads (for bearing design).

The selection of the number of ribs is based on loads, duty cycles and fatigue life. As the number of ribs increases, the belt becomes capable of pulling larger loads, but its width and weight of the system increase as well. Moreover, the higher centrifugal forces must be included in the belt life calculations for the correct estimation.

Together with the belt modification, the tensioning system also has to be redesigned too. In a conventional accessory drive system, the electric machine solely provides negative generating torque during engine-powered driving, so the belt tensioner is positioned on the slack side of the crank pulley. In the BSG, instead, the starter-generator operates in both directions, as motor and as generator, and during engine start-up, the slack side becomes the one "after" the starter generator. Therefore, a bi-directional tensioning system must be developed, to ensure that sufficient tension is available in both the operating modes while helping to reduce overall belt tension and bearing loads. A solution can be positioning the belt tensioner on the slack side of the starter-generator to support engine start, with extra idler pulleys added to increase belt wrap around the crank and the starter-generator pulleys [30, 34]. Otherwise, a more complex system can consist

in a dual tensioning design with independent or mechanically linked tensioners on both the slack sides during motoring and generating [35].

2.4.2.3 Transmission

Other powertrain modifications include changes in the transmission hardware and control system, in the case where an automatic transmission is used. With the stop-start, the BSG allows the engine to shut down after the vehicle decelerates to a stop. If a conventional mechanically-driven transmission oil pump is used, during an engine stop event it would stop as well. The oil pressure in the circuit would fall down, disengaging the first gear thus preventing a quick vehicle response during the following launch. To solve this issue, the first gear hydraulic circuit can be modified by implementing a special exhaust valve able to retain circuit pressure until next launch [34]. Another solution, which is more expensive but conceptually more obvious, consists in replacing the original mechanically-driven oil pump with an electric pump, capable of running during engine stop events [32].

Additional transmission modifications are related to the torque converter. Regenerative braking during decelerations requires mechanical power to follow a path opposite to the conventional, i.e., from the wheels to the starter-generator. In a conventional automatic transmission with torque converter, backdriving the engine can only be done efficiently if the torque converter clutch (TCC) is engaged [34]. However, the dynamic response of a standard TCC is usually not sufficient for smooth operation or TCC durability. This issue can be solved installing a one-way clutch, or freewheeler between the torque converter impeller and turbine. During normal operation (e.g. acceleration), the freewheeler is oriented so that it is freely spinning. Instead, when power flows in the opposite sense (e.g. deceleration), the freewheelers locks up to passively backdrive the engine [34]. Recent transmission versions, like those using clutch-to-clutch shifts as part of their fundamental design, are usually already capable of providing regenerative braking functions without design changes [32].

Finally, transmission control system modifications are also introduced to allow electric downshift synchronization. In order to perform smooth and seamless shifts, the

starter-generator can be used to electrically rev the engine up to synchronize the speed between two subsequent gears [34].

2.4.3 Considerations on BSG components and design parameters

The BSG introduces in the powertrain new components, such as the starter-generator and the battery, and a new electric system configuration. Each component has to be properly sized to achieve the performance requirements dictated by the application.

2.4.3.1 Electric machine

The electric machine for BSG systems, which in this context can also be referred to starter-generator or motor-generator, replaces the current automotive starter and alternator, fulfilling alone both the jobs conventionally carried out by these two components, i.e., engine start and electric energy generation.

2.4.3.1.1 Starter and alternator vs. BSG

The power range of current alternators for passenger cars is up to 2.5 kW in most applications. This limitation is caused by high rotor leakage flux between claw poles with increase of axial lamination length [29]. Moreover, at the present-day battery voltage of 14 V, high currents are difficult to handle and lead to high copper losses. The efficiency map, qualitatively reported in Figure 2.13, shows two other significant disadvantages of current alternators: first, efficiency is overall not very high, degrading to values as low as 30% at high speeds and low loads; second, the current output at low speeds is limited, which leads to problems in the load balance of the vehicle electric system [35].

Current starter motors use a solenoid switch and a pinion-gear drive with a transmission ratio in the range of 1:10~1:20 to apply a high cranking torque to the engine. They are able to rev the engine up to the minimum engine speed for the start of ignition (60~100 rpm for gasoline and 80~200 rpm for diesel engines [37]), but higher speeds during start-up would help to reduce noxious emissions significantly [38]. Moreover, they are characterized by high current draw, noise due to the pinion-gear engagement and relatively long cranking time. Figure 2.14 shows qualitatively some characteristics of a starter motor for normal and cold cranking.

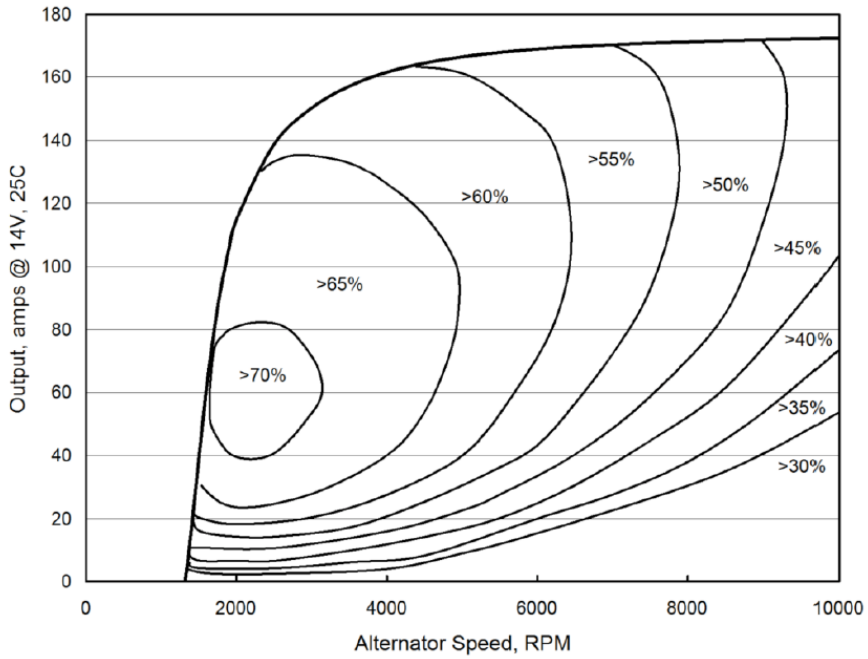

Figure 2.13 - Sample alternator efficiency map [36].

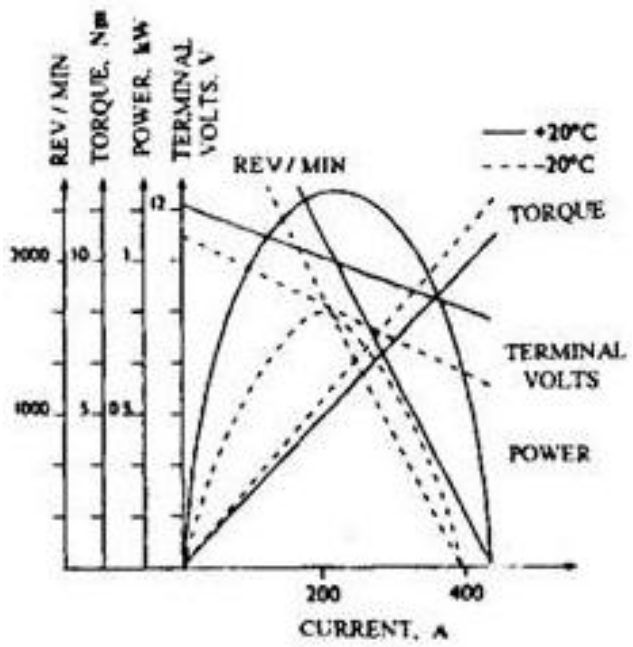

Figure 2.14 - Curves of a 12 V, 0.9 kW starter [39].

The starter-generator unites the functions of the described devices in a single machine, but introduces many other advantages:

- during generation, higher electric outputs can be achieved, even at low speed, and with better efficiency (which however depends on machine typology and material); this allows the overall electric power demand to be increased;

- during motoring, higher power outputs enable higher start-up speeds and short cranking time; due to the speed-torque characteristic of the machine, it can also offer an additional motoring contribution to the engine during acceleration;
- the system architecture and the machine characteristics allow regenerative braking; the amount depends on the torque transmission capability of the belt and the power ratings of electric machine and battery.

BSG systems are intended to reach power outputs over 10 kW and efficiencies over 80% for all speeds and both motoring and generating modes. Peak powers can also be significantly higher [35].

2.4.3.1.2 Design requirements

An important feature of a starter-generator for BSG application is its ability to crank the engine quietly and quickly. When the vehicle operator wants to move the vehicle after an engine off event, the system must respond rapidly and rev the engine up to normal operating speed in a short period of time. Another fundamental task to be performed by the motor-generator is starting the engine under extremely low temperatures. During cold cranking, the breakaway torque the machine has to provide is usually 1.5~1.8 times the nominal cranking torque to overcome engine static friction [29]. These two requirements define the values of peak motoring torque and motoring torque curve of the machine [40]. Figure 2.15 shows the desired motoring torque characteristics.

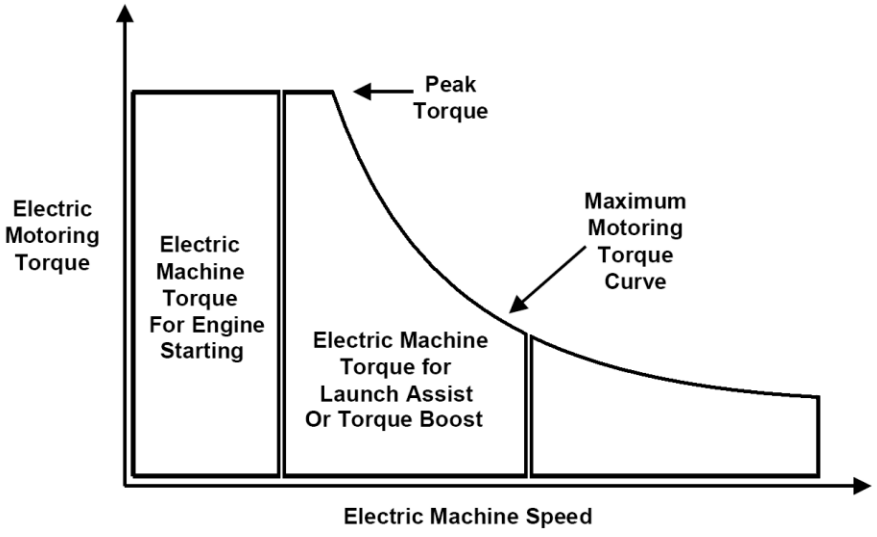

Figure 2.15 - Motoring torque requirements [40].

The cold cranking requirements determines the peak torque value, while the starting time requirement defines the maximum motoring torque curve. A good starting time is in the range of 250~400 ms depending on the application [40]. If a fast start is required, a machine with high power rating must be employed. Moreover, an extended constant torque speed range is important for cold cranking; in fact, electric motoring up to the idle speed can help to smooth the engine speed profile, stabilizes the first cycles of combustion [34] and reduces emissions.

The other important feature of the motor-generator is the regenerative braking capability. It has to convert mechanical power during decelerations to electrical power to charge the battery. More generally, the electric machine can operate in the generating mode from idle speed up to the red line speed of the engine, but three principal areas are more common [40], as illustrated in Figure 2.16.

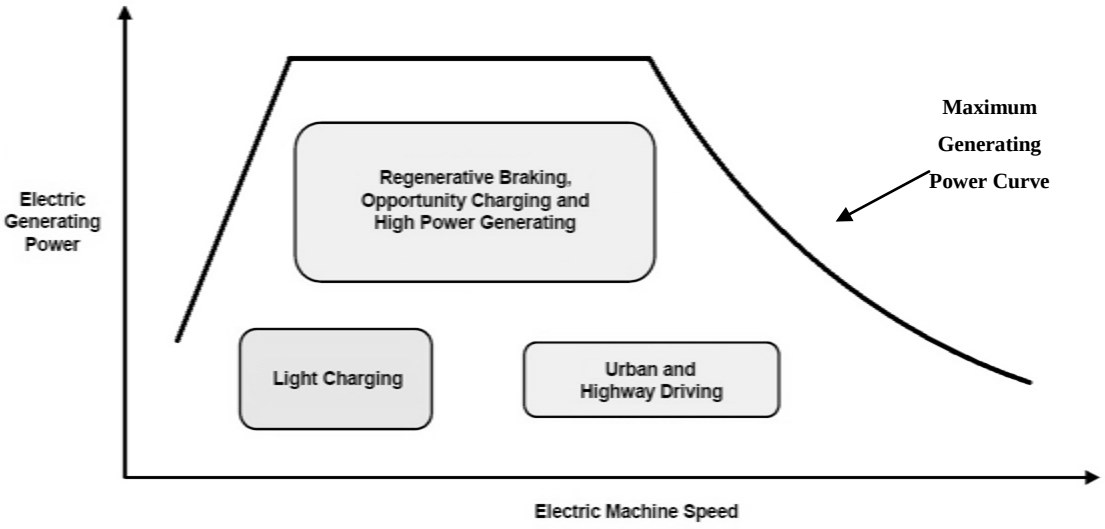

Figure 2.16 - Principal generating areas [40].

This figure shows the speed and power ranges of the main operating modes. Very low and very high engine speed areas are usually not extensively used because of technical limits (power decreases at low rpms and a bigger machine would be needed to have high generating power at high rpms). During the design, the generating performances of the machine are critical specifications since all the electric power required by the electric loads is provided by the motor-generator, so they must be carefully studied.

The motor-generator can also offer an extra torque contribution on top of the engine torque during the so-called electric assist, which can improve the performance of the vehicle and fuel economy. The torque value for performing electric assist are usually determined from customer requirements. It can be limited to engine speed values where the engine cannot develop high torque (i.e., from idle speed to usually 2000~2500 rpm for a gasoline engine), or even up to engine red line (i.e., 5000~6000 rpm) if applicable.

Logically, the reduction ratio between crank and motor-generator pulleys is an important design parameter, because torque and speed ranges of the electric machine depend on it. Since the motor-generator is mechanically linked to the crankshaft, the reduction ratio is usually chosen in order to avoid that the machine runs at dangerous speeds above the maximum speeds limit. For a gasoline engine with 6000 rpm maximum speed, the current reduction ratios are in the range of 2.3~3.2, depending on the maximum allowed speed of the electric machine [29]. A lower reduction ratio means lower motor-generator speeds but also lower torque available at the crankshaft. Therefore the ratio must also be chosen considering the torque specifications of the motor and its capability to overcome the engine static friction torque during start-up, especially for cold cranking.

2.4.3.1.3 Starter-generator machine typologies

With the development of power electronics and microprocessors, multiphase alternating current brushless machines have become the dominating starter-generator typologies for BSG applications. The most common are Induction Machines (IM), Surface and Interior Permanent Magnet Synchronous Machines (SPMSM and IPMSM) and Switched Reluctance Machines (SRM).

An induction machine consists of a normal three-phase stator and an aluminum squirrel cage rotor. It is a well-developed technology, characterized by rugged rotor configuration, wide speed range and low maintenance features. Its major drawbacks are the relatively low specific torque and the fact that at high speeds, which correspond to high stator current frequencies, the maximum torque is inversely proportional to the square of the current frequency, so the power capability decreases with speed increase. This prevents the machine from providing wide constant power operation [29]. The issue

can be overcome by oversizing the machine and converter ratings or using special control techniques [31].

A permanent magnet machine is made up of classic three-phase stator and a rotor with permanent magnets, that can be mounted either on the surface or in the interior. Surface permanent magnet machines are simpler in construction but have problems at very high speeds, due to the high centrifugal forces that compromise the rotor mechanical integrity. This is particularly true for BSG applications, where machine speeds can be as high as 20,000 rpm. Moreover, the electromagnetic characteristics make it difficult to achieve an extended constant power operation, and at high speeds there is a safety issue due to the potential existence of high voltage, which render packaging more problematic. On the other hand, interior permanent magnet machines have a more robust rotor construction, since the magnets are embedded inside the rotor, and therefore they can reach higher speeds. The permanent magnets are also protected against iron dregs in the air gap and corrosion. However, the manufacturing and magnetization processes are more difficult and expensive. Besides that, they can provide a constant power over a wider speed range, and since the torque is available from both magnets and iron saliencies, there is the option to use less magnet (which is made of a very expensive material) in comparison to surface permanent magnet machines for the same power rating [31]. In general, the main advantage of PMSMs is their high efficiency due to the absence of field coil losses, leading to the higher torque and power density among all the machine typologies considered in this analysis. They represent a good choice when packaging and weight are main issues.

Finally, a switched reluctance motor has wound field coils for the stator windings and an iron structure with salient poles for the rotor. The latter does not carry any windings or magnets, being made up of just iron laminations, making the structure very robust and the machine cost very low. In addition, the low rotor moment of inertia and its simple construction benefit high speed operation, and the salient poles produce a fan effect in the air gap so that extra rotor fan can be avoided. Efficiency is similar to highly efficient induction machines [29]. The main disadvantages of SRMs are high torque ripples, vibrations and acoustic noise, caused by the non-sinusoidal excitation. This problem can be addressed by using improved converter designs with an increased number

of pair poles and better control on the current waveform and the switching angles (which however reduces specific torque) [31].

Overall characteristics of the described machines are shown in Table 2.2.

Figure 2.17 shows the qualitative results of a cost analysis comparison. Interior permanent magnet machines have the highest machine cost, due to the expensive material and manufacturing process. Induction machines show the lowest cost thanks to the mature manufacturing technology. It has also been estimated that the converter to machine cost ratio is around 10:1 [31], but it is expected that the converter cost will drop significantly year by year, making low cost machines like switched reluctance motors economically feasible to be adopted in automotive applications.

Table 2.2 - Comparison of different machine typologies for BSG application [29].

Electric machine type	IM	SPMSM	IPMSM	SRM
Peak efficiency and compactness		✓	✓	
Low torque ripple and noise	✓	✓	✓	
Easy close loop control	✓	✓	✓	✓
Fewer control sensors	✓			
Wide speed range	✓		✓	✓

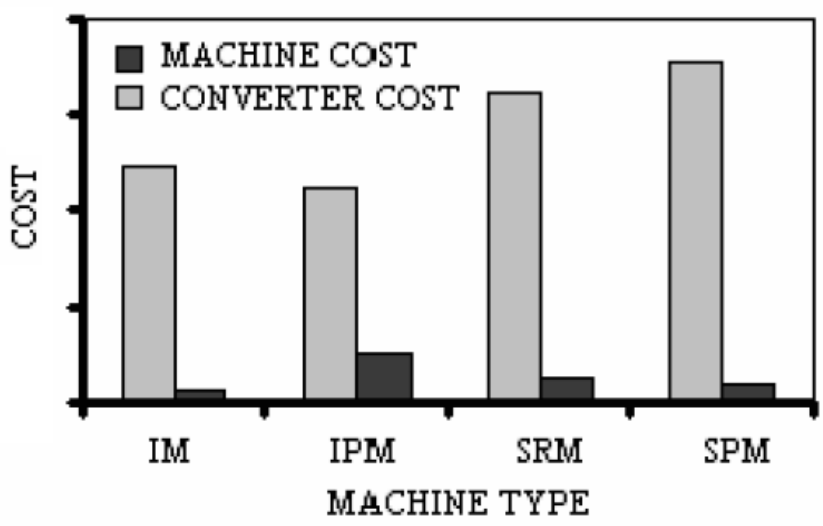

Figure 2.17 - Cost comparison of different machine topologies [31].

2.4.3.1.4 Hints about machine controller design

The different functions of the BSG define which are the appropriate variables to control in each operating mode. At low speeds, i.e., during engine cranking or engine switching off, there are usually desired speed profiles to be followed, so the controller has to be speed-based in order to achieve this functionality [40], and it can be structured to have an outer speed loop with an inner torque control. Concerning electric power assist, torque-based commands are involved, since the driver request during fast and deep acceleration pedal depression is translated in a torque command to be added from the electric machine to the driveline. Generating instead, both during engine-driven charging and regenerative braking, is more suitable to have power-based commands, but since machine speed is determined by engine speed it can be controlled indirectly through torque [40].

Ideally, the machine contribution should be instantaneous, up to the its capability, and as efficient as possible. However, many variables influence machine performance and capability, among which are available terminal voltage, temperature of the machine and speed of operation. The available voltage varies considerably between motoring and generating phases, and temperature ranges from values as low as -40°C in cold environmental conditions to values as high as 150°C during heavy duty machine operations [40]. Machine speed is set by the engine, so it is subject to all the ripples characteristic of the engine (such as compression pulses) which are also worsened by the play in the tensioners. Moreover, the reduction ratio between engine and machine pulleys impose very high acceleration rates to the motor-generator.

A compensation for the fluctuations of these variables must be made for a successful system implementation and to improve efficiency and performance. In the low speed constant torque region, a current controller will be able to naturally compensate for oscillations in terminal voltage and engine speed [40]. Above this region, however, current commands must be adjusted depending on voltage and temperature fluctuations, which also influence the torque capability of the machine at each speed.

2.4.3.2 Battery

The choice of the battery for a BSG application is of primary importance, since its characteristics determine the vehicle strategy and influence the performance of the whole system.

2.4.3.2.1 Design requirements

While for electric vehicles the interest to maximize the driving range defines the energy capability requirements and guides the sizing of the battery packs, for hybrid vehicles the dominant concern is instead the required peak power [41]. The power rating is determined by the necessity to handle peak demands both in discharge, during motoring phases, and in charge, for regenerative braking. The power requirements are further defined by expected cold temperature cranking performance. Power ratings in current BSG vehicles usually range from 10 kW to 20 kW depending on battery voltage and typology.

Voltage is another important parameter to consider during the design. The new capabilities introduced by the BSG, consisting in higher electric machine contribution both in terms of power and duration, render conventional 14 V systems (using 12 V batteries) not suitable for hybrid applications. In recent years, a new, 42 V standard has been proposed, in order to satisfy the raise in on-board electric power demand and to increment the power handling capability of conventional vehicles [42]. With this system, referred to as 42 V PowerNet [43], many degrees of hybridization become possible, including BSG. To realize it, a 36 V battery is required.

But the 42 V PowerNet is not the only solution. Higher voltage systems can also be implemented, as for hybrid vehicles with higher degree of hybridization. There are advantages and drawbacks of using a high voltage system instead of a 42 V system (also referred as "low voltage" system).

First, for a fixed battery power level, a low voltage system requires higher currents. The connections between the battery and the machine terminals present a finite resistance. Even if the wires can be made larger to reduce their resistance, other connectors can only be minimally improved at a reasonable cost [42]. Therefore, the low voltage system is characterized by higher ohmic power losses than the high voltage

system, if the same connectors and wires are used. Equivalently, if the two systems are compared with the same amount of power losses, the high voltage system offers the opportunity to use cheaper connectors and wires. The battery volume for a high voltage system can also be reduced, since less current is drawn and less capacity is required [41].

Second, the voltage level impacts the rating of the inverter. The power devices best suited for low voltage applications are power MOSFETs, but these devices cannot withstand too high current levels, which ultimately affects the ability of the machine to produce power at high speed and leads to performance deterioration [42]. The necessity to have higher current limits imposes the use of particular power MOSFETs that are limited in availability and expensive [42], or the implementation of a greater number of standard MOSFETS in parallel. For high voltage applications (higher than 200 V [44]), IGBTs are more suitable, having the capability to efficiently handle high voltage levels. They are also produced in large quantities, so they are cheaper and more available.

Third, the control algorithm of the electric machine and its efficiency are also affected by the voltage level. In theory, the electric machine can operate with similar performance at difference voltage levels, if the stator winding is proportionally modified in the cross section and turn number to allow for different levels of current and back-emf. However, if the voltage is too low, very aggressive flux weakening is necessary, which results in low torque/ampere ratios and poor machine efficiency [42]. As a result, the higher voltage system permits larger constant power speed range and more efficient high speed operation.

From what has been explained, high voltage systems seem to be a better solution than low voltage systems. Nevertheless, the safety requirements must be also taken into account in the balance. In 1988, the SAE have investigated the effects of higher voltage electrical systems for automotive applications on human body. Their recommendations, presented in SAE J2232 concluded that if the system voltage were kept below 65 V_{DC}, including periodic ripple, it would not be necessary to prevent direct electrical contact between people and circuits. On the basis of this research, the German VDE standards determined in VDE 0100/410 that the peak bus voltage should not exceed 60 V_{DC} without protection [43]. As a consequence, systems with voltage higher than 60 V have the major drawback of requiring, at the design stage, to electrically insulate wires and any other

circuit component that might come in contact with people (battery, inverter, DC/DC converter). This results in increased complexity and, most of all, cost, and may also more than offset the performance advantages previously described.

2.4.3.2.2 Battery typologies

For BSG applications (but more in general for hybrid applications), lithium ion (Li-ion) and nickel metal hydride (NiMH) technologies are the best choices in terms of energy density and power density. Compared to other battery technologies, such as lead acid (PbA) and nickel cadmium (NiCd), this results in a much lighter and less voluminous battery pack for a given set of specifications. At the same time, higher specific power allows high peak power levels associated with regenerative braking and electric assist, for the same weight of the pack [41].

Specific energy and power characteristics of different battery technologies are often summarized in the Ragone plot, reported in Figure 2.18. As mentioned, Li-ion and NiMH technologies have the best performance, and both of them can easily satisfy HEV requirements.

However, while the Ragone plot captures the performance map of various batteries, other criteria need to be considered, including cost, cycle and calendar life, and safety. Moreover, these factors are connected to each other [45].

Table 2.3 reports more detailed information about the main energy storage technologies. Non-electrochemical energy storage systems such as ultracapacitors and flywheels are shown as well for the sake of completeness. However, they are not usually employed in hybrid applications because of their low energy density, which would involve a high weight of the energy storage device.

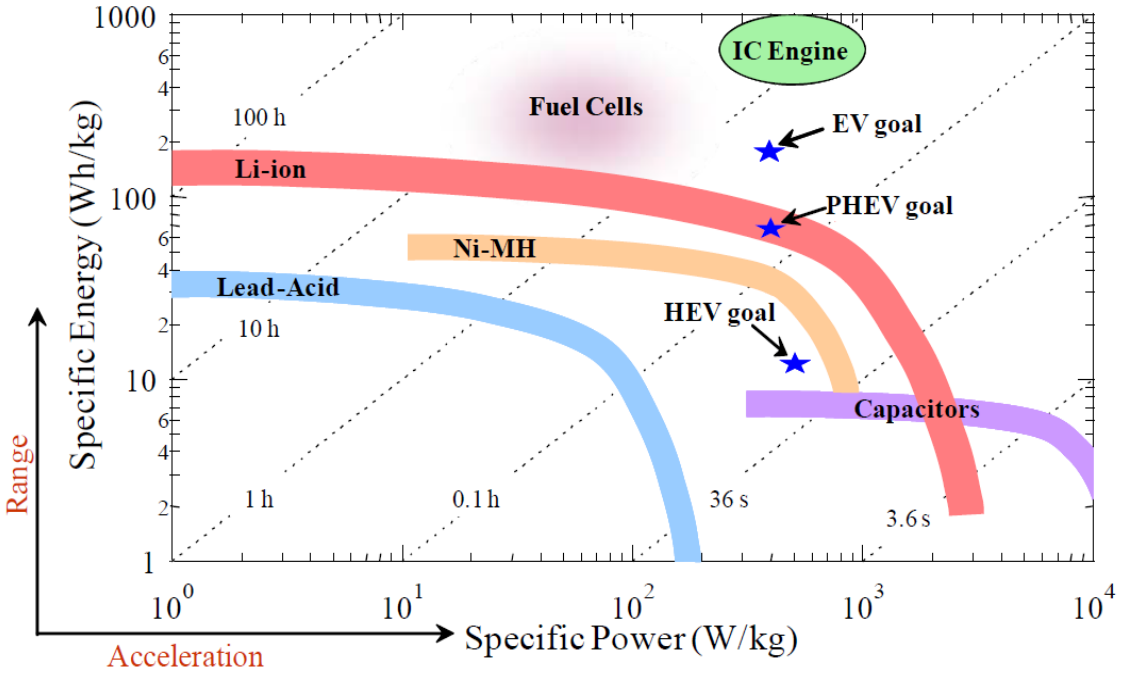

Figure 2.18 - Ragone plot (specific power density in W/kg vs. specific energy density in Wh/kg) of various electrochemical energy storage and conversion devices [45].

Table 2.3 - Characteristics of energy storage technologies [46].

energy storage technology		*characteristics*						
		energy [Wh/kg]	[Wh/l]	power [W/kg]	number of cycles @ 80% DoD	efficiency [%]	temperature range [°C]	cost [€/kWh]
PbAC	flooded	25 - 40	60 - 100	140 - 350	200 - 1500	70 - 75	20 - 40	100 - 190
	VRLA	30 - 40	80 - 100	140 - 300	300 - 1000	80 - 85	20 - 40	100 - 190
	compressed	40 - 50	100	140 - 250	800 - 1500	70 - 85	20 - 40	35 - 50
alkaline	NiCd							
	power	25 - 40	130	500	800 - 1500	70 - 75	-40 - 50	400 - 1000
	energy	40 - 50	130	120 - 350	800 - 1500	70 - 75	-40 - 50	400 - 1000
	NiZn	60 - 80	200 - 300	500 - 1000	200 - 1000	60 - 65	0 - 40	500 - 800
	NiMH							
	power	40 - 55	80 - 200	500 - 1400	500 - 2000	70 - 80	0 - 45	400 - 2000
	energy	60 - 80	200 - 350	200 - 600	500 - 2000	70 - 80	0 - 45	200 - 700
lithium based	LiIon							
	power	70 - 130	150 - 450	600 - 3000	800 - 1500	85 - 90	-20 - 60	700 - 2000
	energy	110 - 220	150 - 450	200 - 600	800 - 1500	85 - 90	-20 - 60	150 - 600
	LiPolymer	100 - 180	100	300 - 500	300 - 1000	90 - 95	-110	300 - 500
	ultracap							
	power	3 - 5	3 - 10	2000 - 10000	500k - 1M	95 - 100	-20 - 90	1700 - 2300
	energy	12 - 20	3 - 6	2000 - 10000	500k - 1M	95 - 100	-20 - 90	1700 - 2300
	flywheel							
	power	1.8 - 3.7	7 - 17	100 - 1000	10k - 50k	90 - 95	-20 - 50	200 - 660 [€/kW]
	life	1 - 10	3.7 - 5.7	100 - 1000	10k - 100k	90 - 95	-20 - 50	300 - 400 [€/kW]

In a BSG application, the battery is characterized by numerous and wide state of charge (SOC) cycles. This aspect represents a drawback because this kind of operation limits the cycle life [45]. In addition, the SOC should be kept between 40 to 80% so that good charge acceptance and efficiency during regenerative braking can be realized [34]. Li-ion and NiMH technologies have the characteristic of acceptable power output at low state of charge [41], while for standard PbA batteries low SOC operation can compromise reliability and long term battery life. In this case, the battery must be kept closer to high charge values, with the drawback of decreasing system efficiency [34].

In the battery design and implementation, thermal and functional management and control must not be overlooked. Li-ion requires more control monitoring than NiMH due to undesirable overcharge and overtemperature characteristics [41]. Cooling systems for this kind of applications could be either air or liquid.

From the cost point of view, Li-ion and NiMH batteries are generally much more expensive than lead acid. Li-ion however is viewed as having the potential to become cost competitive in high volumes over time [41].

While complicated, the interplay between all the various factors to be considered in the choice of the battery suggests that, even if NiMH batteries are more common in current hybrid vehicles, Li-ion batteries are the most promising candidate for use in vehicular applications. The three main reasons for this conclusion are the higher energy, higher power, and the potential for lower cost of Li-ion batteries when compared to NiMH batteries. This conclusion has been the reason why significant research efforts have been directed toward Li-ion batteries [45].

2.4.3.3 Electric system configuration

The introduction of the new battery on the vehicle, in the 36 V or in the high voltage configuration, requires a redesign of the electric system layout. In fact, many electrical components and systems may be shared with other vehicles and be powered at 14 V, so to maximize economies of scale and reduce the investment cost of changing all systems to the new voltage level, a "dual" voltage architecture is preferred [43].

With such an architecture, shown in Figure 2.19, the higher voltage bus supplies the main battery and the electrical loads that would directly benefit from that voltage level,

while the 14 V loads are powered through a voltage conversion operated by a DC/DC converter, which supplies also a 12 V battery. It can be advantageous to have a bi-directional converter, capable of switching the input and output sides depending on the necessity. For example, in the case of a jump start it would be required to transfer energy from the 12 V battery to the high voltage battery, and with a buck converter this would not be possible [43]. For a system with a voltage higher than 60 V, the DC/DC converter must be galvanically insulated for safety reasons.

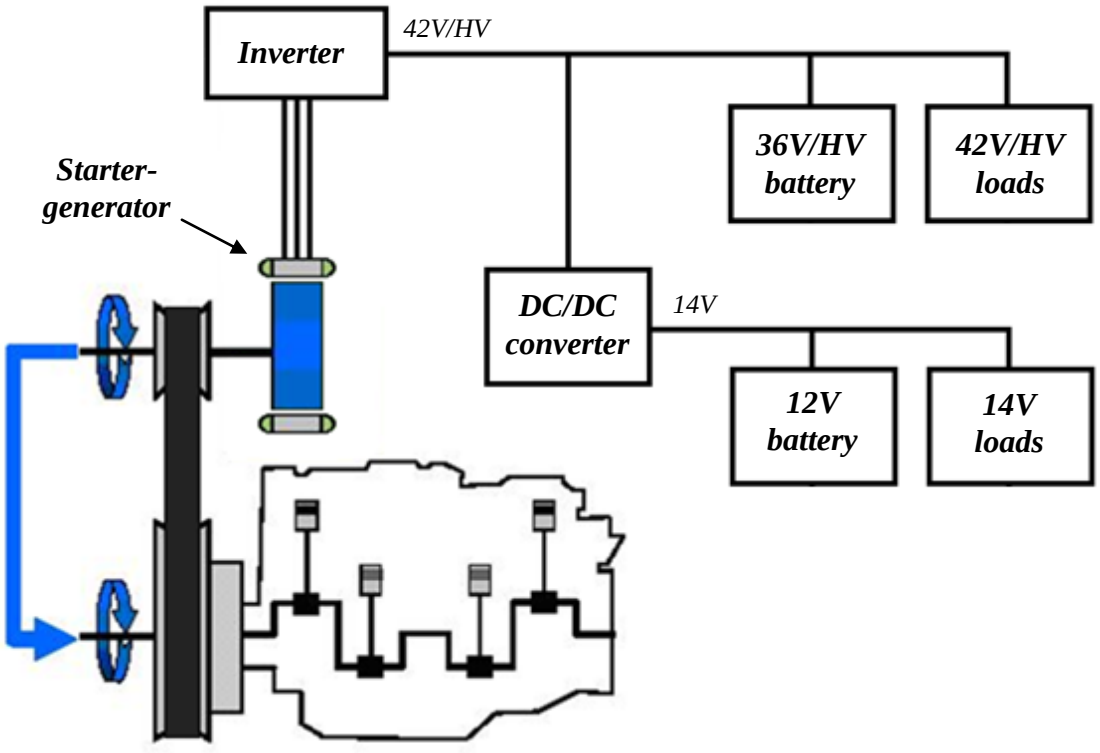

Figure 2.19 - DC/DC converter dual voltage architecture [43].

There are many other ways to implement dual voltage systems, for example using distributed DC/DC converters throughout the vehicle which supply different voltages to different loads, or implementing a single DC/DC converter without the 12 V battery. In both these cases, the converters have to be capable to handle peak power demands versus sizing them to handle average power [43]. The final architecture will be defined after a comparison of the different configurations, finding a tradeoff in terms of performance, complexity and cost.

2.4.4 BSG functions and operating principle

Information on the main function introduced by the BSG has already been provided in the course of this chapter. This section is aimed to summarize them and to give a structured description of how they affect the vehicle drivability.

In general, the most important features realized by the BSG are:

- engine stop/start;
- regenerative braking;
- electric power assist - torque boost.

Secondary functions can be summarized in:

- engine torque smoothing;
- early fuel cut-off during deceleration;
- opportunity battery charging and discharging;
- electrically motored creep (for automatic and automated-manual transmissions).

2.4.4.1 Engine stop-start

The main objective of the BSG is to reduce fuel consumption by cutting the fuel to the engine when it is not being used to propel the vehicle. This can happen in two situations: when the vehicle is stopped (for example at a traffic light during urban driving), the fuel is cut and the motor-generator brings the engine to rest, switching it off; in addition, when the vehicle is coasting or decelerating the fuel can be cut as well, and the engine is back-driven by the transmission [47].

However, there are many conditions that have to be checked by the hybrid controller to enable fuel cut off and engine stop, and the parameters usually differ from vehicle to vehicle. Among the most important are battery SOC and engine temperature.

The SOC is usually kept between specific limits to avoid early battery ageing. When the SOC of the battery is low from previous discharge phases, the engine must be prevented from switching off, because during the following cranking it may drop below the lower limit.

Concerning engine temperature, the engine must not be switched off until its temperature reaches a certain threshold, below which the catalytic converter cannot work properly and emissions are remarkably high. This is particularly important when air

temperature is very low: not only would emissions be excessive and prolonged, but also if low air temperature is combined with low SOC, the power may not be enough to crank the engine. Furthermore, if during an engine stop phase the temperature drops below the value required for correct converter operation, the controller must disable stop/start and switch the engine on.

In any case, the motor-generator needs to have the ability to stop and start the engine smoothly and quickly, also maximizing coast and deceleration fuel cut opportunities [47].

2.4.4.2 Regenerative braking

Another important function provided by the BSG is regenerative braking, activated during decelerations in association with fuel cut off. The electric machine, used in this case as a generator, provides part of the braking effect and recaptures a portion of the kinetic energy (which otherwise would be dissipated as heat in the friction brakes) transforming it into electric energy to recharge the batteries. The recaptured energy is then used to carry out all the functions which require electric energy, such as to provide electric power assist or to feed the electric loads during idle stop. By optimizing the regenerative braking control, the charging of the battery during fuel on cruising can be minimized, thus reducing the amount of fuel consumed.

Due to the BSG architecture, during regenerative braking the engine keeps spinning, although being in fuel cut off. In order to reduce the losses in the powertrain and allow more power to reach the generator, during deceleration fuel cut off the engine control system can open the throttle valve and command the valvetrain (if a Variable Valve Timing (VVT) system is present) to reduce pumping losses.

In order to exploit all the potential of regenerative braking, the control system should prevent the friction brakes from being activated until the limit of regenerative braking power is overcome. Figure 2.20 shows this logic.

For low deceleration power requests, the brake power is completely realized by the motor generator. As the driver depresses the brake pedal beyond the point corresponding to $P_{\underset{max}{regen}}$, the maximum regenerative power is exceeded and the friction brakes enter in action. As previously mentioned, current BSG systems can reach regenerative power

peaks of more than 10 kW at the generator side. This logic, however, requires the brake system to be commanded by the hybrid controller: the brake pedal position must be monitored by a sensor and the brake hydraulic system has to be activated by a dedicated actuator. In other words, the traditional braking system has to be replaced by a brake-by-wire system, with increased costs and safety issues that need to be managed.

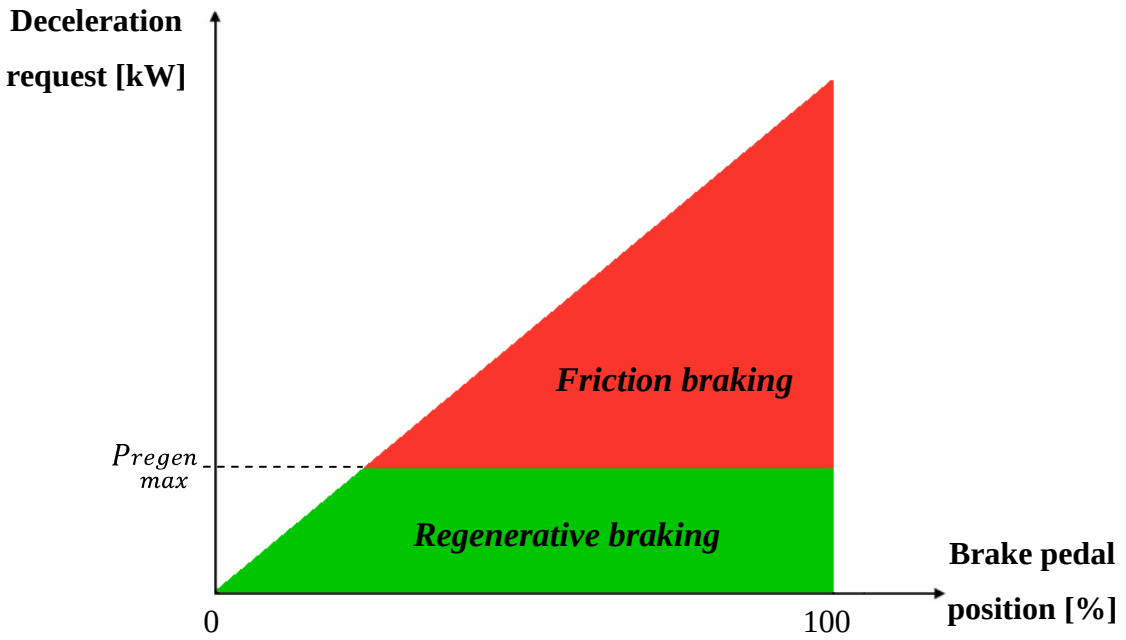

Figure 2.20 - Regenerative braking logic.

Furthermore, during the design, considerations about the dynamic behavior of the vehicle must be made: since the regenerative braking applies on the driving wheels, when the driver requires high deceleration, the driving wheels risk reaching the brake limit earlier than usual, with bad consequences on handling and comfort. Regenerative braking can be disabled for high deceleration requests, or the brake balance has to be reorganized, considering also the coexistence of the anti-lock braking system (ABS).

2.4.4.3 Electric power assist - torque boost

With electric power assist - torque boost, the motor-generator provides a torque aid on the top of the engine torque, to improve throttle response during vehicle starts and during fast acceleration requests. The quick dynamic behavior of the electric machine can partially make up for the slow engine transients and improve vehicle acceleration performance. The amount and duration of electric assist intuitively depends on the battery

capability of providing electric energy to the motor, so on maximum discharge power and SOC, and on the motor power rating.

Electric assists helps also to improve vehicle drivability. During sudden pedal requests by the driver, it can happen that in the available gear the engine is not capable of meeting the desired torque, so a downshift is necessary. With electric assist, the motor-generator can compensate for the extra torque request until the engine revs up and is capable to provide more torque: in this way the downshift can be avoided.

2.4.4.4 Other functions

The BSG can provide some other secondary functions that improve fuel consumption and drivability.

Both open- and closed-loop speed controls can be implemented on the motor-generator to smooth engine torque especially during cranking. Torque irregularities are mainly originated by engine compression pulses when fueling has not been initiated yet. Chapter 3 will go deeper into this topic.

Fuel cut-off during deceleration has been already mentioned in the previous sections. It is important to highlight that to further reduce fuel consumption and to promptly enable regenerative braking, early fuel cut-off is preferable. A significant advantage of having the engine spinning during decelerations is that a responsive redelivery of tractive power can be ensured upon driver request [47].

Opportunity battery charging and discharging refers to the practice of using the BSG in particular situations to produce electric energy or consume it in order to modify the battery SOC and keep it within the safety limits. For instance, if the SOC is low, the engine is extra fueled to drive the electric machine, used as a generator, and charge the battery (opportunity charging). Similarly, if the SOC is sufficiently high, the control system selects the engine operating conditions so that part of the requested power is provided by the motor which discharges the battery (opportunity discharging) [47]. The advantage of this function is that through multiple and wide charge-discharge battery cycles, the hybrid control system can select the engine operating conditions where it is more efficient, reducing fuel consumption. This technique is also referred to as "load shift".

Finally, electrically motored creep applies when the BSG is matched with an automatic or an automated-manual transmission. When the vehicle is exiting an idle stop with the first gear engaged, the motor-generator can provide low-speed electrically motored creep to improve the start response [47]. Electric machine contribution and engine parameters must be blended to compensate for torque spikes and provide smooth fuel on-off transitions.

2.4.5 Impact of the BSG on fuel consumption

All the described functions contribute both to fuel consumption and CO_2 emissions reduction. The most important contribution are represented by the stop-start functionality and the regenerative braking (which is particularly effective on drive cycle with many brake opportunities and for vehicles with a heavy weight). Electric assist helps to reduce fuel consumption thanks to the "load shift", but its effect is usually lower compared to the two other functions.

Battery and motor power ratings affect fuel consumption as well. Higher power capabilities allow to have more benefits in term regenerative braking and electric assist, but with increased cost, weight and system integration issues. The choice of the battery voltage (and consequently of the power capabilities) depends on these aspects, but neither of the two proposed solutions (42 V vs. high voltage) is the best in absolute value. The decision will be also based on other factors, such as vehicle segment and mission or company know-how.

The BSG can also indirectly contribute to fuel reduction, because its characteristics offer the possibility of downsizing the ICE or to use longer gear ratios (downspeeding). Both these solutions reduce fuel consumption, since they force the engine to run in higher efficiency areas. Besides that, the torque reserve that can be readily released by the BSG in the case of necessity (especially during accelerations at low speed), can overcome the loss in performance associated with downsizing, or avoid frequent downshifting if longer gear ratios are used [48, 49].

However, it must be remembered that in actual vehicles, some fuel economy is compromised to obtain better drivability. For instance, the practice of keeping the engine speed at low values during braking with automatic transmissions would often force the

electric machine to run in the constant torque region, where power capability is limited compared to higher speeds. This implies that the regenerative braking potential can't be entirely exploited. Likewise, fuel can't be cut immediately after the accelerator pedal is released, particularly for low speed driving in lower gears [34], because the torque spikes related to fuel on-off transitions would produce excessive drivetrain lash.

Summarizing, fuel consumption reduction for a vehicle equipped with a BSG can reach 15-20% [31, 32, 35, 47, 48, 50, 51], depending on power capabilities of the components, drive patterns, vehicle dimensions and weight, control strategies and powertrain calibration.

CHAPTER 3

DESIGN AND METHODOLOGY

In this chapter, the description of the modeling, simulation and experimental activities of the thesis research is presented. It is divided into two main sections, corresponding to the two research topics of the thesis.

The first section covers the stop-start functionality analysis and modeling. This feature will be illustrated through its phases and influencing factors, and subsequently a Simulink model will be described, capable of simulating the dynamics of the engine start-up.

The second section deals with the fuel consumption simulations and tests, aimed to evaluate the fuel consumption improvements related to the BSG introduction. Three approaches are followed (analytical, simulations and tests), which will be described in detail, together with the study cases and the vehicle data.

3.1 Stop-start performance evaluation and modeling of the belt starter generator system

One of the most important functions introduced by the BSG is the stop-start strategy, which allows one to switch off the engine during vehicle idle and to save a remarkable amount of fuel. A key factor in the successful implementation of the starter-alternator technology is the ability to start and stop the engine quickly and smoothly, without issues related to noise, vibration and harshness (NVH), that have negative effects on vehicle drivability.

The starter-alternator torque and power characteristics compared to a conventional starter allow contributions of the electric machine over a broader range of speeds. This helps to better control engine speed, for instance during the transition between motoring and firing phases, provided that a suitable control strategy is implemented.

Modeling of the engine and BSG dynamics is essential to predict how the system behaves and to design a control system capable of starting and stopping the engine rapidly with no or little unwanted vibrations.

In this section, the stop-start functionality will be analyzed in detail, considering its implementation on the vehicle and examining its operating principle. After that, a Simulink model will be shown, which simulates engine, electric machine and belt dynamics for engine motoring conditions. This model is capable of predicting instantaneous engine speed starting from motor torque values as a function of time. The results can be validated against experimental data collected from a start cart, made up of a BSG system connected to the engine.

3.1.1 Engine stop-start with the BSG

Engine stop-start is a rather complex function, with a sphere of influence which extends much beyond the simple benefits on fuel economy. Many aspects and features of the vehicle influence and are influenced by the stop-start.

3.1.1.1 Implementation of the function

It has already been mentioned that stop-start is constrained by battery SOC (the function is disabled when SOC is low to prevent depletion) and by engine temperature (cold starts produce high amount of pollutant emissions and consume much battery energy, so stop-start is avoided for engine temperatures below a certain threshold). Besides these, it is also important that the hybrid controller checks the data from the on-board diagnostics (OBD) system regarding correct functioning of the powertrain components. For instance, the operating temperatures of the engine, transmission, auxiliaries, electric machine, power electronics and battery must stay within a safe range during the operation.

Then, the BSG may introduce issues related to NVH. The main sources of vibration during stop-start are related to the torque spikes coming from air compression in the cylinders and fuel on-off transitions. Vibrations generally propagate through the engine mounts to the vehicle body and to the seat track. If the engine is started in drive mode (for automatic transmissions), engine speed oscillations can also propagate through the driveline to the wheels. Moreover, noise could also be caused by the cooling system of the battery and power electronics if air from the vehicle cabin is used. To avoid a negative impact on the customer, all these sources must be contained. Regarding the

torque spikes, the electric machine can include both an open- and closed-loop controller capable of compensating for the spikes, limiting engine oscillations to acceptable values. The cooling system noise issue instead is usually handled using component design expedients that minimize noise without reducing air flow.

A further problem is associated to heating, ventilation and air conditioning (HVAC). If the air conditioning (A/C) compressor is belt-driven as in a conventional vehicle and is not substituted by an electric version, the HVAC is compromised during engine off phases. A tradeoff must be found between passengers' comfort and stop-start frequency and duration. For instance, a selectable A/C mode can be provided, which allows the driver to choose between uncompromised comfort mode (by disabling stop-start functionality when the HVAC system cannot maintain the desired cabin conditions) or improved fuel consumption mode (which maximize stop-start frequency and duration by allowing the cabin comfort to degrade slightly) [32].

Lastly, another issue is related to engine cranking and vehicle launch on roads with moderate and steep grades. On these kinds of roads, when the engine is still off, the driver must keep the brake pedal depressed to hold the vehicle on the grade. However, during the brake-release event, there is a phase where the brake pressure is no longer sufficient to hold the vehicle, while the engine restart has not been triggered yet. In this situation, the vehicle may to roll back. A solution to this problem is to implement a hill hold control (HHC) system, which traps the brake pressure in the hydraulic system for a limited time to let the engine start. The brake pressure can be then ramped out gradually to improve smoothness of the vehicle launch [32].

3.1.1.2 Engine start

The engine start phase can be divided in five sub-phases, as illustrated in Figure 3.1, corresponding to specific operating conditions:

1. Engine off: the car is at rest and the engine is switched off; during this phase, the driver lifts his foot from the accelerator pedal and triggers engine restart.
2. Initial spin up: the hybrid controller, passed all the checks, commands the electric machine to build-up the torque to crank the engine; at the beginning, the motor has to overcome static friction, so as soon the torque reaches the breakaway value the engine starts spinning.

3. Spin up: the electric machine continues to accelerate the engine according to a predetermined acceleration profile, studied to crank the engine quickly and smoothly, with limited vibrations; at the same time, the intake air throttle valve is kept closed, and the manifold air pressure (MAP) starts to reduce from ambient pressure because of the air suction in the cylinders during the intake phase.
4. Combustion ramping: when the MAP is low enough and reaches a threshold value, the combustion can be initiated; low intake pressure allows the introduction of small amounts of fuel, which combined with spark retard produce low torque (and limited vibrations). Engine torque is gradually increased, while motor torque is correspondingly decreased; they are managed to produce together the reference acceleration. Engine speed usually overshoots slightly over idle speed, a characteristic associated with engine firing and idle speed controller performance [52].
5. Engine on: when engine stabilizes to idle speed, and motor torque has been completely ramped out, the start-up is completed and the engine is on.

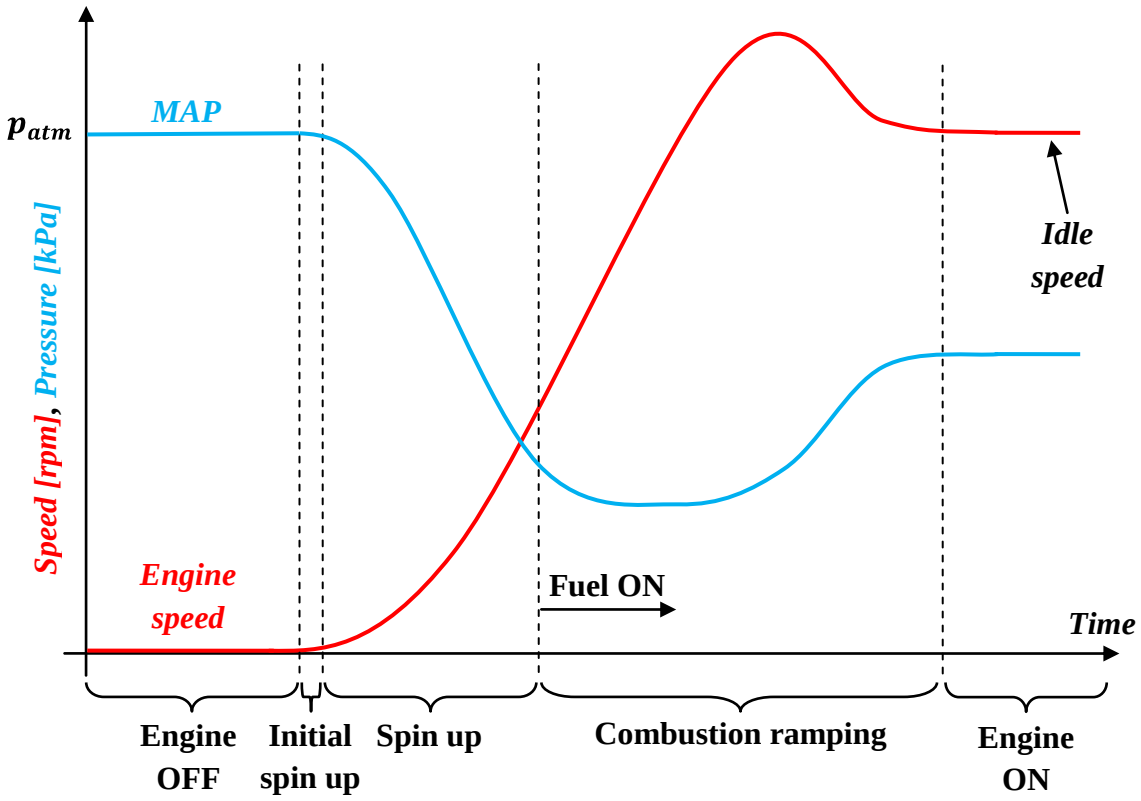

Figure 3.1 - Engine speed and MAP trends during engine start event.

As previously mentioned, the engine is required to follow a reference acceleration profile, which in turn determines the speed profile. The choice of the profile is the result of tradeoff among the driver's request, motor and battery capabilities and the passengers' feeling. The starting time can be adaptive on the basis of how rapidly the driver releases the brake pedal and depresses the accelerator, meaning that he wants a more or less prompt restart. However, a quicker cranking involves higher battery and motor power request and more vibrations transmitted to chassis and driveline. Therefore, starting time has a lower limit coming from either of the two issues. Common cranking times are in the range of 250~400 ms [40].

3.1.1.3 Engine stop

The engine stop phase is conceptually similar to the engine start phase, except for the fact that is reversed. It can be divided in four sub-phases, as illustrated in Figure 3.2:

1. Engine on: the engine is at idle speed, while the driver brakes the car bringing it to rest and triggering engine stop;
2. Combustion ramping out: the hybrid controller has to check that all the vehicle functionalities are ok, and then it can start to ramp the combustion out. The intake air throttle valve is closed (so that MAP reduces) and the spark is gradually retarded to lower the torque from the engine. At the same time, the electric machine increase its contribution controlling that the engine follows the reference deceleration profile;
3. Spin down: at this point the fuel is cut off and the engine is spun down by the electric machine;
4. Engine off: engine is at rest, having reached zero speed, while MAP returns to ambient pressure.

In contrast with the start time, the stop time can be a little bit longer, since usually there are no particular time requirements on this phase. This helps to improve the smoothness of the event, provided a suitable machine control.

In case of the so-called "change of mind" of the driver, meaning that he decides to restart the engine while it is shutting down, combustion can be reinitiated following the sequence of engine start.

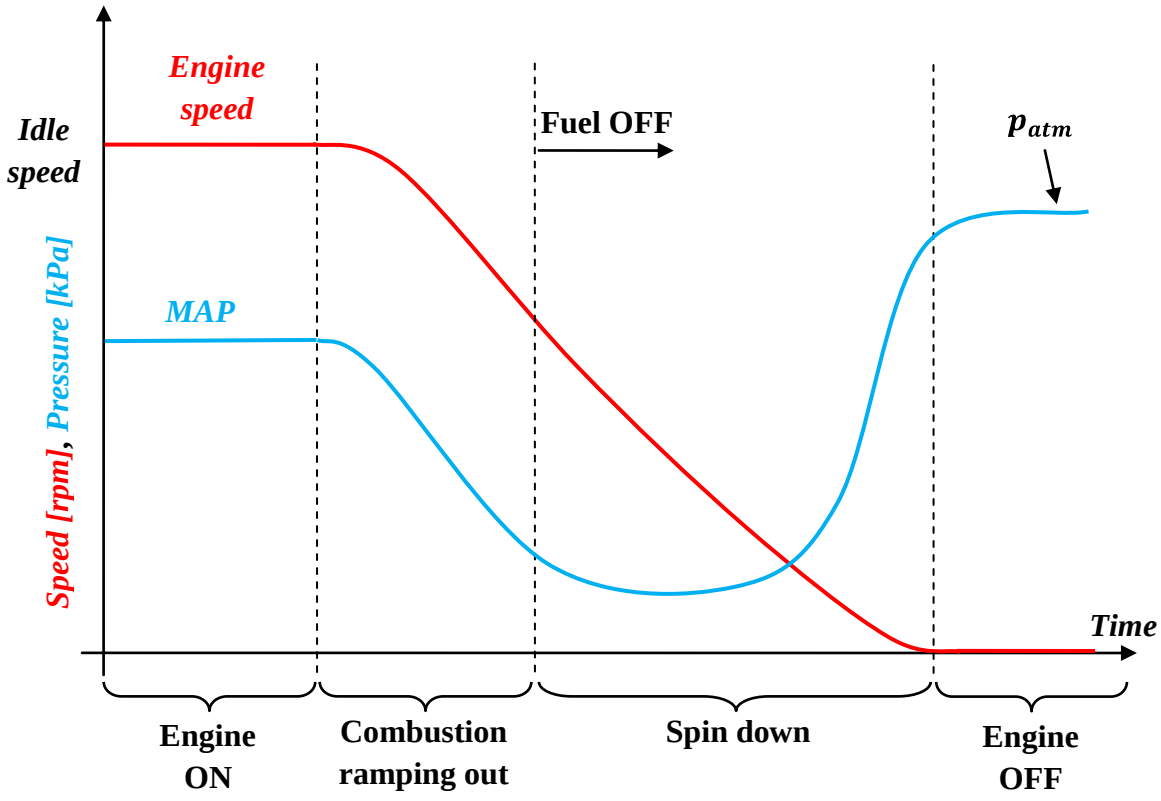

Figure 3.2 - Engine speed and MAP trends during engine stop event.

3.1.1.4 Controller design for the stop-start

The objective of the controller is to quickly start the engine smoothly and reliably. The stop-start procedure however is characterized by some disturbance factors, and one of the most important is represented by air compression pulses. When air is compressed in the cylinders, in fact, it works as a spring, producing a negative crankshaft torque (in the opposite direction of the rotation). In the same way, when the engine is still in the motored phase, air expansion produces a positive torque. Intuitively, this torque is a function of the crankshaft position. Figure 3.3 shows its trend for a motored six cylinder engine. It can be noticed in particular that the first three torque oscillations are irregular compared to the following ones. The reason is that after the engine stops, the air in the cylinders which valves are open gets to ambient pressure, and when the engine restarts the air exchange process for those cylinders is different from steady state. Therefore, it takes some time before the exchange process gets equal for all cylinders.

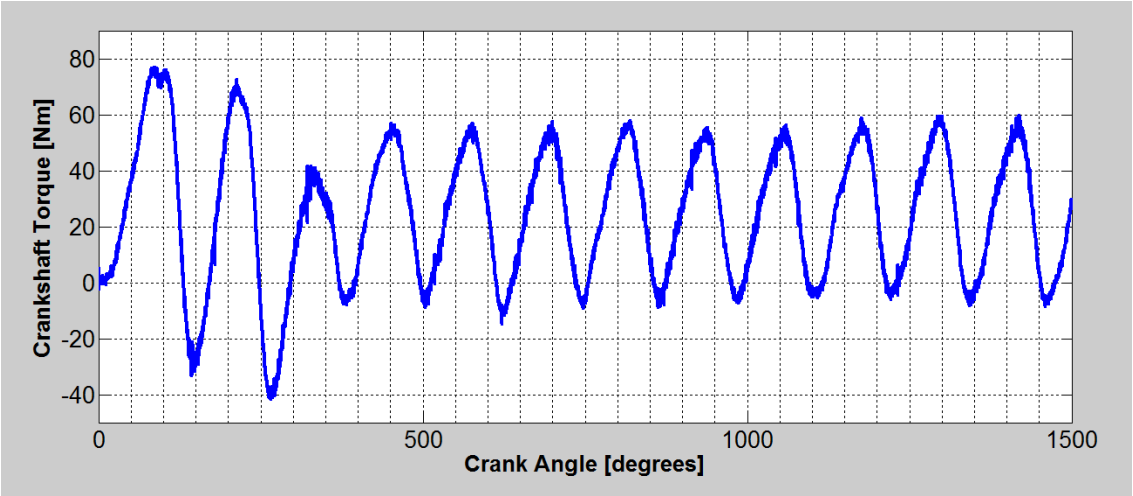

Figure 3.3 - Engine speed and MAP trends during engine stop event.

Despite the flywheel, which thanks to its inertia reduces the effect of the torque spikes, still some engine speed oscillations are present, which are transmitted as vibrations to the driveline and to the engine mounts. The controller should then be capable of performing two functions: rev the engine up or down according to the reference profile, and compensate as much as possible for engine speed oscillations caused by disturbance factors. In order to perform these tasks, the controller must include both a closed-loop path and an open-loop path.

The closed-loop portion of the controller attempts to match engine speed to the predetermined profile, and is usually realized through a proportional-integral (PI) controller structure that compensates for the error between the reference and the actual speed [52]. The open-loop portion is required mainly because the closed-loop control would not be fast enough to compensate for the engine torque fluctuations. The open-loop correction term uses the engine crankshaft position signal and other variables to calculate the torque ripple generated by the disturbance factors (among which is air compression). Its objective is to use the electric machine to reduce the effects of such torque ripple on engine speed, which could potentially result in quicker start and stop operations as well as little or no vibrations perceived by the passengers during engine cranking and idle [53]. In reality, because of the maximum torque capability of the machine, it often happens that this control objective can be only partially achieved, limiting the potential improvements [52].

Anyways, in order to implement this control logic, the structure is usually characterized by an outer speed loop with an inner torque control. Two possible configurations are shown in Figures 3.4 and 3.5.

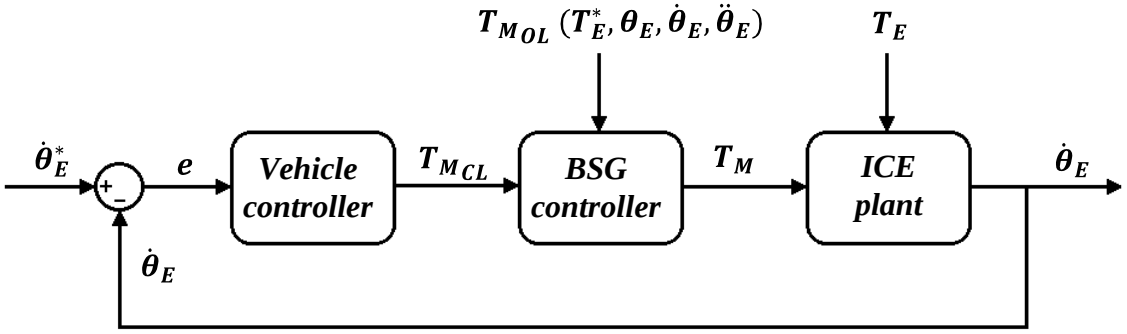

Figure 3.4 - Stop-start controller structure with ECM involvement.

In the first configurations, the error e between reference engine speed $\dot{\theta}_E^*$ and actual engine speed $\dot{\theta}_E$ is fed to vehicle electronic control module (ECM), that through an algorithm evaluates the closed-loop electric machine torque $T_{M_{CL}}$. This is in turn supplied to the BSG controller, which combines it with the open-loop torque $T_{M_{OL}}$. As previously said, the task of $T_{M_{OL}}$ is to compensate for engine speed fluctuation, and it is a usually a function of required engine torque (T_E^*), actual engine position, speed and acceleration (θ_E, $\dot{\theta}_E$ and $\ddot{\theta}_E$). The output of the BSG controller is the actual torque T_M that the machine has to produce. Such torque and that provided by the engine itself (T_E) contribute to accelerate or decelerate the engine and to change its speed.

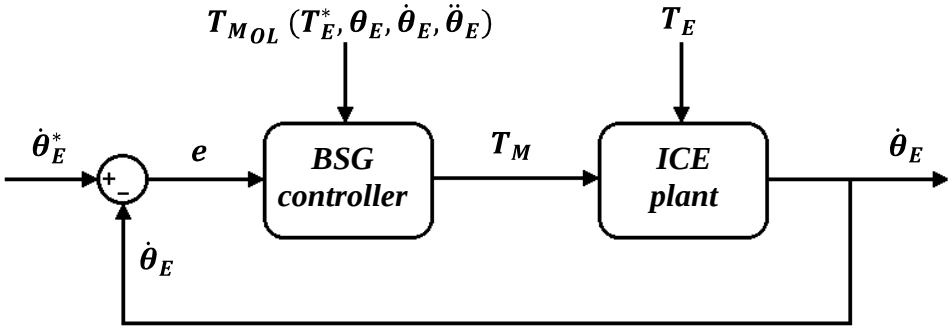

Figure 3.5 - Stop-start controller structure without ECM involvement.

The second configuration is simpler, because there is no involvement of the ECM in the loop. The error e is fed directly to the BSG controller, that combines it with the open-loop machine torque $T_{M_{OL}}$ to produce the actual torque T_M.

The advantage of the second configuration compared to the first one is that there is only one stage of calculations instead of two and the communication system of the car is busy for less time. This translates in a faster response of the controller to engine speed fluctuations. However, there is a risk to lose control on the BSG torque: when the ECM is involved in the calculations, it is possible to take into account additional vehicle parameters (for example from the engine) that can limit the torque for unsafe conditions; the BSG controller does not have this capability, so in the second configuration torque commands may induce dangerous situations unless a more complex algorithm is used.

3.1.2 Engine and BSG dynamics modeling

This section presents a Simulink model of engine and BSG dynamics, capable of simulating the system behavior when the engine is motored by the electric machine (the effects of fuel injection and combustion were not considered). It was intended to represent a real existing BSG system, made up of a commercial starter-generator and a V6 engine, running on a start cart. Figures 3.6 and 3.7 illustrate a CAD model and a picture of the assembly, while Table 3.1 shows component specifications. In a second step, the Simulink model could be the starting point for the design of the starter-generator controller.

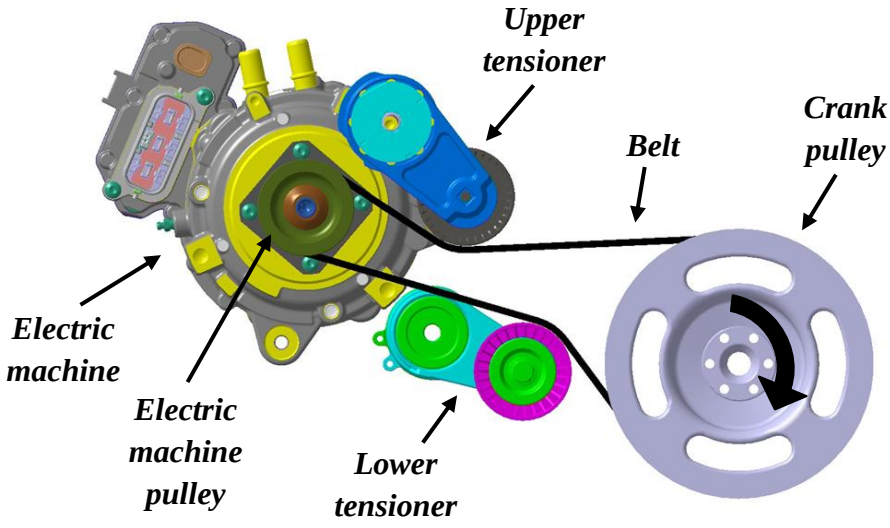

Figure 3.6 - CAD model of the start cart BSG system.

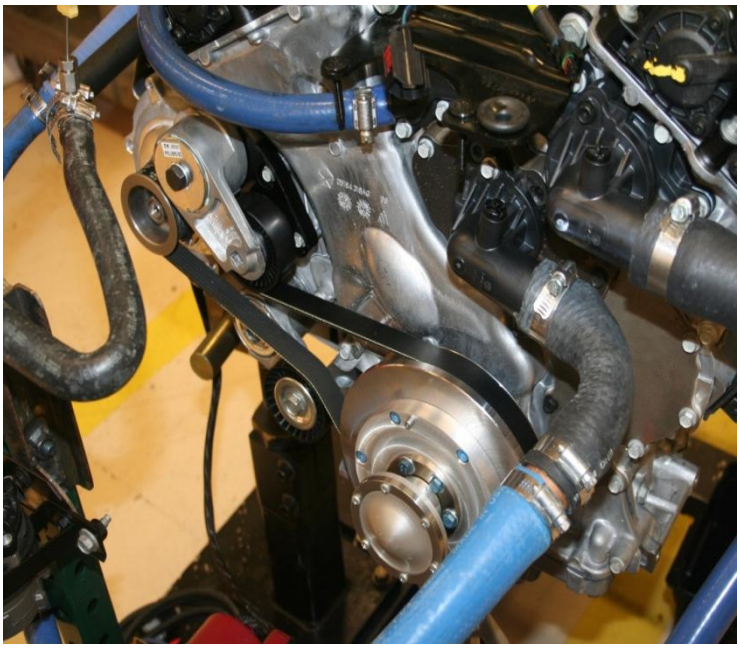

Figure 3.7 - Picture of the start cart BSG system.

Table 3.1 - Start cart engine specifications.

Engine				
Displacement	**Layout**	**Type**	**Maximum torque**	**Maximum power**
3.6 L	V6	Aspirated	353 Nm @ 4800 rpm	211 kW @ 6400 rpm

Table 3.2 - Start cart electric machine specifications.

Electric machine				
Type	**Rated power**	**Max. motoring torque**	**Max. generating torque**	**Maximum speed**
Induction	18 kW	57 Nm	- 57 Nm	17400 rpm

Table 3.3 - Start cart belt transmission specifications.

Belt transmission					
Belt type	**Belt material**	**No. of ribs**	**Motor pulley diameter**	**Engine pulley diameter**	**Reduction ratio**
Serpentine	Aramid	6	63 mm	179 mm	2.84

3.1.2.1 Model structure and equations of motion

The model simplified structure is shown in Figure 3.8. The dynamics of the system is a consequence of the interaction between electric machine and engine, which are mechanically linked by the belt. Electric machine, belt and engine torque models calculate the torques and forces in play (T_M, T_E, F_B), having as inputs engine and motor angular positions and rotational speeds of the previous time step ($\theta_M, \dot{\theta}_M$ and $\theta_E, \dot{\theta}_E$). These torques and forces are fed to the electric machine and engine dynamics blocks, which outputs are the new positions and speeds.

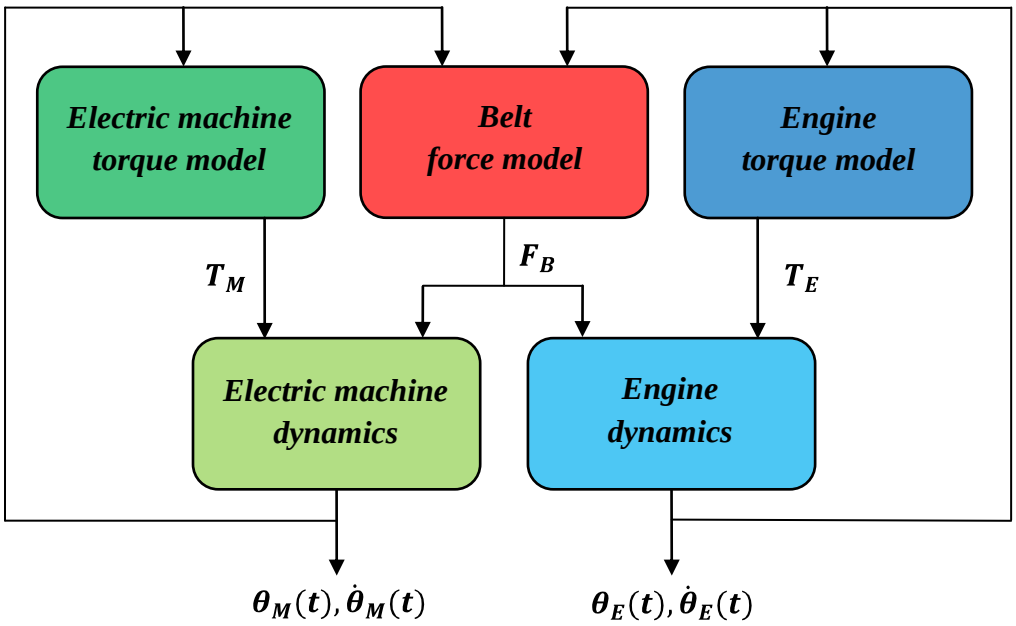

Figure 3.8 - Simplified structure of the model for BSG simulation.

The approach adopted for the solution of the problem is based on Newton's dynamics laws. Figure 3.9 shows the free body diagram of the system. For simplicity, the tensioners have not been considered in the model, so the belt branches between the pulleys were assumed to be straight. Since the belt moves the driven pulley by "pulling" it instead of "pushing", it was sufficient to write the equations of motion on the tight side only, i.e., the side where the motor "pulls" the engine.

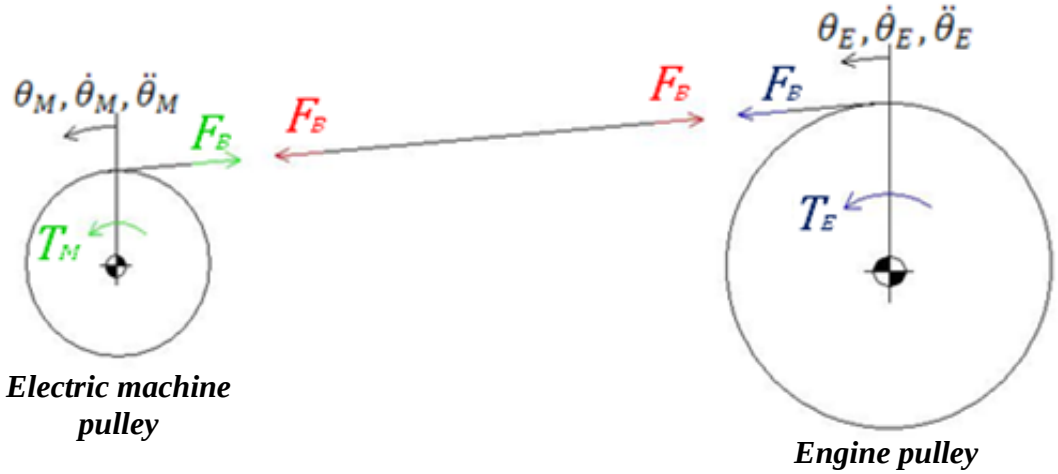

Figure 3.9 - Free body diagram of electric machine-belt-engine assembly.

The equations of motion (contained in the electric machine and engine dynamics blocks) are written in the form of coupled differential equations for motor and engine pulleys respectively:

$$T_M - F_B r_M = I_M \ddot{\theta}_M \tag{3.1}$$

$$T_E + F_B r_E = I_E \ddot{\theta}_E \tag{3.2}$$

where: T_M and T_E are motor and engine torques;

F_B is the force which account for belt elasticity and damping;

r_M and r_E are motor and engine pulley radii;

I_M and I_E are motor and engine moments of inertia;

$\ddot{\theta}_M$ and $\ddot{\theta}_E$ are motor and engine angular accelerations.

By integrating the acceleration, it is possible to obtain angular speeds ($\dot{\theta}_M, \dot{\theta}_E$) and positions ($\theta_M, \theta_E$).

3.1.2.2 Modeling of the components

In the following, it will be shown how motor-generator, engine and belt can be modeled, or equivalently how T_M, T_E and F_B were obtained.

3.1.2.2.1 Motor-generator

The motor-generator can be represented by means of a transfer function $H(s)$ that takes into account the internal dynamics of the component (due for example to inverter delays, torque buildup time in the machine, etc) [52]:

$$T_M(s) = H(s) \cdot T_{M_{des}}(s) \tag{3.3}$$

where $T_{M_{des}}$ and T_M are desired (input) torque and machine actual torque. As previously described, the BSG controller usually calculates the desired torque combining an open- and a closed-loop command. In general, $H(s)$ is a function of voltage and speed of the motor-generator; however, the inner dynamics of the machine are usually much faster than those of the engine, especially at low speeds [52], so the transfer function can be approximated with the unit:

$$H(s) \cong 1 \quad \rightarrow \quad T_M \cong T_{M_{des}} \tag{3.4}$$

In the simulations, the problem was further simplified. The values of T_M were either assumed or imported from experimental data obtained with tests on the start cart. The model is capable of calculating the engine speed profile versus time in motored conditions, when a certain motor starter-generator is provided as input. Using experimental torque values, it is possible to validate the model by comparing the engine speed profiles of simulations and tests.

3.1.2.2.2 Engine

T_E is a complex non-linear function of engine speed and position. It includes the effects of gas pumping, fuel combustion, inertia of the reciprocating masses and friction:

$$T_E = T_{pump} + T_{comb} + T_{in} + T_{fr} \tag{3.5}$$

Using analytical calculations, T_{pump} and T_{comb} can be lumped together starting from the in-cylinder pressure p_{cyl}, which can be obtained through a simplified single-zone, thermodynamic model [54]:

$$\frac{dp_{cyl}}{d\theta_E} = -\gamma \frac{p_{cyl}}{V} \frac{dV}{d\theta_E} + \frac{\gamma - 1}{V} \left(\frac{dQ_g}{d\theta_E} - \frac{dQ_w}{d\theta_E} \right) \tag{3.6}$$

where: γ is the specific heat ratio;

V is the cylinder volume;

Q_g is the combustion gross heat release;

Q_w is the heat transferred to the cylinder walls.

This model considers only the portion of engine cycle between intake valve closing and exhaust valve opening, so the gas exchange processes are assumed to be at ambient pressure (which is reasonable for engine speeds corresponding to idle or lower).

Otherwise, the in-cylinder pressure can be obtained from experimental results, instrumenting the combustion chamber with a pressure sensor.

The in-cylinder pressure is then used to calculate the force acting on the piston. The crankcase is usually kept at ambient pressure, so the effective force that is transmitted to the connecting rod is:

$$F_{cyl} = S \cdot (p_{cyl} - p_{amb}) \tag{3.7}$$

where S is the piston head surface.

The inertia torque due to reciprocating masses deals with the motion of piston and connecting rod, and is a complex function of geometry and crank position. The engine moment of inertia I_E used in Equation 3.2 is considered a constant term, accounting only for the rotating mass inertia of the engine (crankshaft, flywheel, crank pulley, etc). In this way, the equation of motion remain linear, as the non-linear inertia of the reciprocating masses is approximated as "external" torque. The approach to calculate the inertia torque starts from the evaluation of the inertia force for a single cylinder, approximated as:

$$F_{in} \cong -m_r r_{crank} \left[\ddot{\theta}_E \left(sin\,\theta_E + \frac{\lambda}{2} sin\,2\theta_E \right) + \dot{\theta}_E^2 (cos\,\theta_E + \lambda\, cos\,2\theta_E) \right] \tag{3.8}$$

where: m_r is the mass of the reciprocating elements

r_{crank} is the crank radius

λ is the ratio between crank radius and connecting rod length

The minus sign in the equation takes into account the fact that the inertia force is opposed to the motion of the crankshaft.

Given the geometry of the crank-slider mechanism shown in Figure 3.10, F_{cyl} and F_{in} can be lumped together in a single force P applied on the piston pin.

$$P = F_{cyl} + F_{in} \tag{3.9}$$

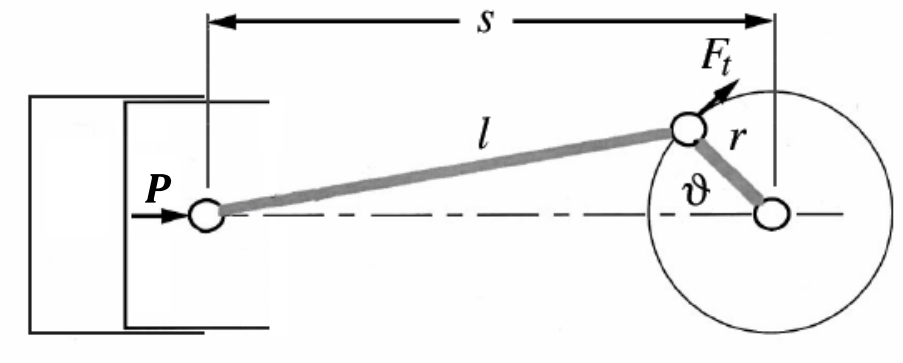

Figure 3.10 - Schematic diagram of the crank-slider mechanism.

The crankshaft torque is the product of the crank radius and the component of *P* perpendicular to the crank arm:

$$\left(T_{pump} + T_{comb} + T_{in}\right) = r_{crank} P \left(sin\theta_E + \frac{\lambda sin2\theta_E}{\sqrt{1 - \lambda^2 sin^2\theta_E}} \right) \tag{3.10}$$

This calculation is relative to one cylinder only, so for a multi-cylinder engine the corresponding torques have to be summed up, taking into account the phase differences among them.

Lastly, the friction torque T_{fr} is non-linear function of engine speed, load and temperature. In the literature there are simplified [55] and more detailed [56] friction models. For example, the following approach calculates T_{fr} as a function of in-cylinder pressure and engine speed [55]:

$$T_{fr} = T_{fr_0} + k_p p_{cyl} + k_1 \dot{\theta}_E + k_2 \dot{\theta}_E^2 \tag{3.11}$$

The k_i coefficients depend in turn on engine block and oil temperatures, so tests on the engine are usually needed to estimate how temperature varies and to properly adapt the parameters [54].

However, if friction torque experimental data of the engine under analysis are directly available, the implementation in the BSG model is more straightforward, with the drawback of needing another data set if a different engine has to be simulated.

Summarizing, in the Simulink model some assumptions and simplifications were made. Since the engine is considered to be motored, no combustion occurs. p_{cyl} was obtained from tests on the motored engine, and accounts only for air compression, expansion and exchange processes. The inertia torque due to reciprocating masses was assumed to be negligible compared to the other terms, so it was not considered in the

analysis. Finally, experimental data were used for the friction torque, provided in form of tables with torque as a function of engine speed, load and temperature. However, the load was fixed by the study case, i.e., motored engine (corresponding no load), so the number of variables was reduced to two.

3.1.2.2.3 Belt

The belt transmission was modeled to account for its stiffness and damping characteristics. Referring to Figure 3.9, they are included in the following equation for the evaluation of the elastic and damping belt force:

$$F_B = k_B \Delta x_B + c_B \Delta \dot{x}_B \tag{3.12}$$

where: k_B is the belt stiffness;

c_B is the belt damping coefficient;

Δx_B is the belt elongation;

$\Delta \dot{x}_B$ is the difference of the velocities of the belt extremities.

The model included also a logic capable of simulating belt slip. If slip occurs, it was assumed to happen at the motor pulley, where the belt wrap is lower. The operating principle can be explained by the transition between two modes:

1. no-slip: belt and motor pulley move together;
2. slip: belt and motor pulley have differing angular velocities.

Handling the transition between these two modes presents a modeling challenge: as the system gains a degree of freedom upon slip, the transmitted torque goes through a step discontinuity.

To correctly solve the problem, the belt must be provided with a mass, which is assumed concentrated on the motor pulley. According to Figure 3.11, the state equations for the coupled system are derived as follows:

$$T_M - T_f = I_M \ddot{\theta}_M \tag{3.13}$$

$$T_f - F_B r_M = I_B \ddot{\theta}_B \tag{3.14}$$

where: T_f is torque transmitted at the belt-pulley interface;

$\ddot{\theta}_B$ is the belt angular acceleration calculated at the motor pulley;

I_B is the is the belt moment of inertia calculated at the motor pulley, and equal to

$$I_B = m_B r_M^2 \tag{3.15}$$

in which m_B is the belt mass.

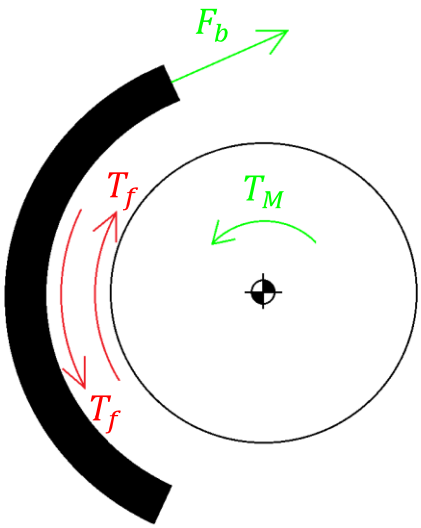

Figure 3.11 - Free body diagram of belt and electric motor pulley.

During the no-slip operation, belt and pulley share the same kinematics, so the systems acts as a single unit with combined inertia. So Equations 3.13 and 3.14 are joined into a single equation as follows:

$$\dot{\theta}_B = \dot{\theta}_M = \dot{\theta} \quad ; \quad \ddot{\theta}_B = \ddot{\theta}_M = \ddot{\theta} \tag{3.16}$$

$$T_M - F_B r_M = (I_M + I_B)\ddot{\theta} \tag{3.17}$$

Combining Equations 3.13, 3.14 and 3.17 with the constraint of equal angular accelerations, the torque transmitted at the belt-pulley interface can be calculated:

$$T_f = \frac{I_B T_M + I_M F_B r_M}{I_M + I_B} \tag{3.18}$$

The system remains in the no-slip condition unless the magnitude of T_f exceeds the static friction capacity $T_{f\,max}^{s}$, which depends on system geometry, static friction coefficient and belt tension. At this point, the belt starts to slip, and the new equations of motion become:

$$T_M - T_{f\,max}^{k}\, sgn(\dot{\theta}_M - \dot{\theta}_B) = I_M \ddot{\theta}_M \tag{3.19}$$

$$T_{f\,max}^{k}\, sgn(\dot{\theta}_M - \dot{\theta}_B) - F_B r_M = I_B \ddot{\theta}_B \tag{3.20}$$

where $T_{f\,max}^{k}$ is the maximum kinematic friction torque, and $sgn(\dot{\theta}_M - \dot{\theta}_B)$ takes into account the fact that slip can occur in both directions. In this state, belt and motor are uncoupled and move at different speeds.

In order to exit the slip mode, two conditions must be satisfied, i.e., belt and motor speeds have to return equal and the torque transmitted at the interface must be lower or equal than the static friction capacity:

$$\dot{\theta}_M = \dot{\theta}_B \quad \text{and} \quad T_f \leq T_{f\,max}^{s} \tag{3.21}$$

Figure 3.12 summarizes the system behavior in a state diagram.

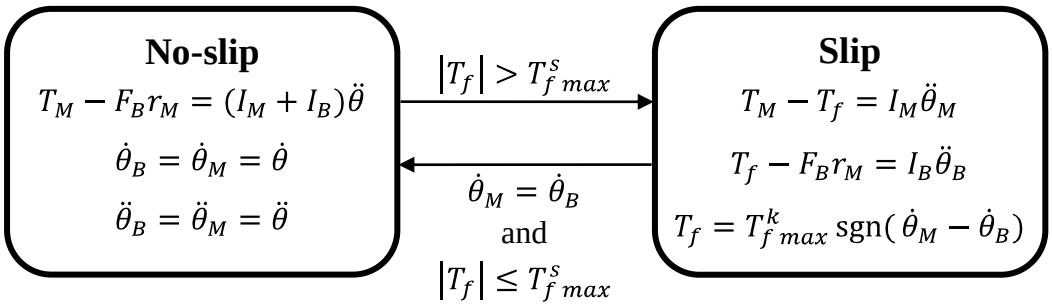

Figure 3.12 - State diagram describing no-slip/slip transition.

In the calculations it must be ensured that, when switching between two dynamic modes, the initial conditions of the new mode match the state values immediately prior to the switch. In Simulink, slip was implemented using enabled subsystems, which modeled the system dynamics in either no-slip or slip condition, and a logic block, in charge of checking the system state and switching from one mode to the other.

3.2 Fuel consumption analysis

This section describes the simulations and tests aimed to evaluate the fuel consumption improvements of a vehicle equipped with a Belt Starter Generator with respect to a conventional vehicle.

As discussed in Chapter 2, the BSG enables to introduce three main features:

- engine stop-start;
- electric power assist;
- regenerative braking.

Each of them contributes to reduce fuel consumption in a different way. Engine stop-start cuts the fuel to the engine when it is not being used to propel the vehicle. Thus, when the vehicle is stopped, the fuel is cut and the engine is stopped as well. Electric assist decreases fuel consumption indirectly: through multiple and wider charge-discharge battery cycles, the hybrid control system selects the engine operating conditions where it is more efficient. This technique is also referred as "load shift". Regenerative braking is activated during coast and decelerations to recapture a portion of the kinetic energy to recharge the battery. By optimizing the regenerative braking control, the charging of the battery during fuel-on cruising can be minimized, thus reducing the amount of fuel consumed.

The main objective of the simulations and tests was to estimate the saving in fuel consumption that can be obtained with these features. In particular, as it will be better described in the following sections, they have been set up in order to introduce one feature at a time, i.e., starting from a vehicle engine stop-start only and adding electric assist in a second step and regenerative braking in a third step.

Another set of simulations is focused instead on the evaluation of the fuel consumption of a vehicle equipped with BSG with modifications in component characteristics and sizes. In other words, a sensitivity analysis of the fuel consumption will be performed considering different vehicles, engines, electric motors and batteries.

Three main approaches were considered:

- Analytical approach;
- Simulations through an already existing model for fuel consumption evaluation;
- Tests on a proof-of-concept hybrid vehicle.

This section introduces these approaches, describes the logic behind them, presents study cases and drive cycles and lists the required data, which were either obtained or assumed. A preliminary analysis of the outcomes will be also shown. The main results about fuel consumption, along with their comparison and discussion, are instead presented in Chapter 4.

3.2.1 Analytical approach

This approach consists in estimating fuel consumption starting from simple data, such as vehicle main characteristics and drive cycle profiles, and making some assumptions on efficiencies in the powertrain. The logic behind the method is based on the losses that occur during a drive cycle: of the total fuel energy consumed, a portion is used to overcome the road loads and drive the car through the cycle, while another portion is dissipated in losses of various nature.

Figure 3.13 shows graphically this energy flow.

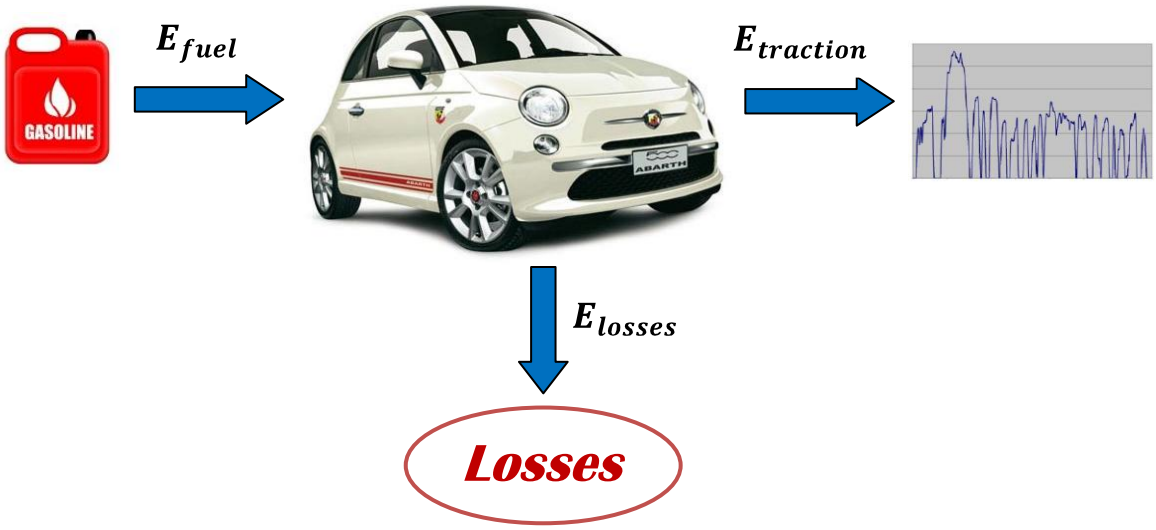

Figure 3.13 - Simplified diagram of the energy flow occurring in a vehicle. The energy of the fuel (E_{fuel}) is partially transformed by the car into energy for the tractive effort ($E_{traction}$) and partially dissipated in losses (E_{losses}).

The energy balance equation is simply:

$$E_{fuel} = E_{traction} + E_{losses} \tag{3.22}$$

Once $E_{traction}$ and E_{losses} are calculated or assumed, the value of E_{fuel} can be found, and from it the fuel consumption value is obtained (in l/100 km or mpg).

3.2.1.1 Tractive energy

The tractive energy is the energy required by the vehicle to run through the cycle. It can be expressed as the sum of two terms: the energy necessary to overcome the road loads E_{rl} and the energy needed to accelerate and decelerate the vehicle according to the speed profile set out by the cycle $E_{acc/dec}$:

$$E_{traction} = E_{road\ loads} + E_{acc/dec} \tag{3.23}$$

This equation can also be expressed in terms of forces, which vary along the cycle:

$$F_{traction} = F_{road\ loads} + F_{acc/dec} \tag{3.23}$$

The road loads are external resistances acting on the vehicle during motion. For both urban and highway driving, the road loads consist of aerodynamic drag (F_{aero}), rolling resistance (F_{roll}) and climbing resistance (F_{climb}). The aerodynamic drag, produced by the motion of the vehicle in the air, escalates with a square law with vehicle speed, so it consumes relatively more energy during highway driving. In comparison, the energy losses from rolling resistance (produced by the hysteresis of the tire at the surface with the roadway) are mainly a function of miles traveled: vehicle speed has a limited effect on rolling resistance except at the highest speeds reached on occasion during highway driving. Climbing resistance applies only when road grade is different from zero. Standard drive cycles are usually run on flat road, so this term is not present in the analysis. In general, the total road load force can be therefore written as:

$$F_{road\ loads} = F_{aero} + F_{roll} + F_{climb} \tag{3.25}$$

$F_{acc/dec}$ is the force needed to accelerate and decelerate the vehicle according to the cycle, and is governed by Newton's second law. This force provides the linear acceleration of the vehicle:

$$F_{acc/dec} = m_v a = m_v \frac{dv}{dt} \tag{3.26}$$

where m_v is the vehicle mass and a is the acceleration set out by the drive cycle.

Figure 3.14 illustrates a free body diagram of a vehicle during motion with the associated forces (for simplicity the road is assumed flat, i.e., no climbing resistance is applied).

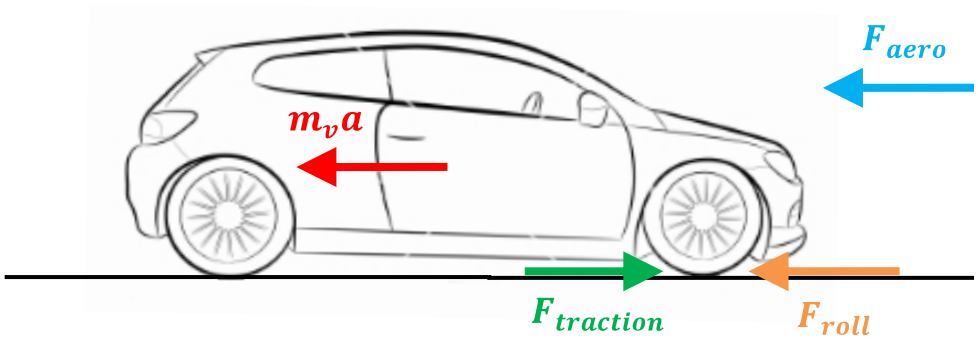

Figure 3.14 - Free body diagram of a vehicle.

The road load resistance can actually be calculated in two ways: the individual components (aerodynamic, rolling and climbing) can be computed at each time instant and summed, or, if the vehicle road load coefficients F_0, F_1 and F_2 of the vehicle are known, the road load resistance at a specific speed can be easily calculated using the following equation:

$$F_{road\ loads} = F_0 + F_1 v + F_3 v^2 \tag{3.25}$$

The road load coefficients are obtained from coast-down tests on real vehicle, and represent the coefficients of the quadratic interpolation of the road load curve. They take into account aerodynamic drag, rolling resistance, resistance in the driveline downstream of the gearbox and resistance due to possible remaining torques of the braking system, but not road grade.

For instance, considering a vehicle with the road load coefficients listed in Table 3.4:

Table 3.4 - Road load coefficients of a sample vehicle.

$F_0\ [N]$	$F_1\ \left[\frac{N}{km/h}\right]$	$F_2\ \left[\frac{N}{(km/h)^2}\right]$
205.863	0.074	0.124

the road load resistance profile on a flat road has the trend shown in Figure 3.15.

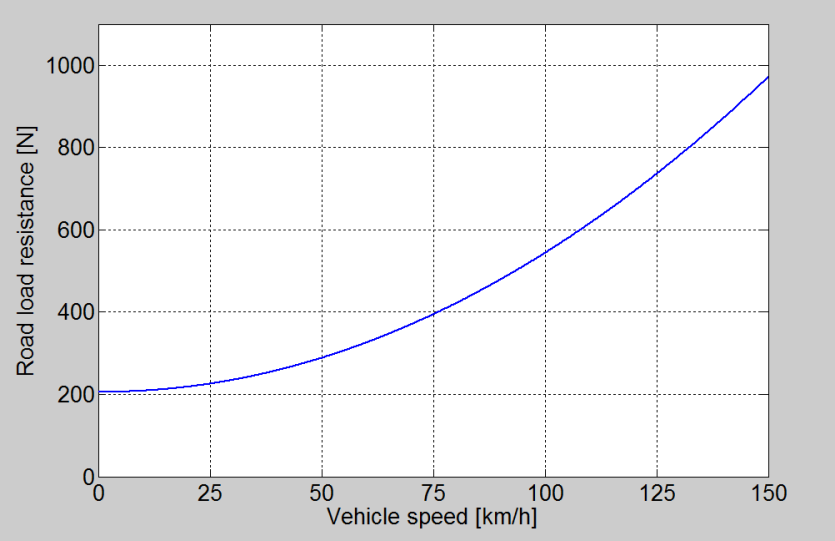

Figure 3.15 - Road load resistance curve of the sample vehicle.

Therefore, the tractive force can be written as:

$$F_{traction} = F_{road\ loads} + F_{acc/dec} = F_0 + F_1 v + F_3 v^2 + m_v \frac{dv}{dt} \tag{3.28}$$

The tractive power can be simply calculated multiplying the tractive force by the cycle speed:

$$P_{traction} = F_{traction} \cdot v = F_0 v + F_1 v^2 + F_3 v^3 + m_v \frac{dv}{dt} v \tag{3.29}$$

Finally, the tractive energy is obtained by integrating the tractive power over cycle:

$$E_{traction} = \int_{cycle} (F_0 + F_1 v + F_3 v^2)\, dt + \int_{cycle} m_v \frac{dv}{dt}\, dt \tag{3.30}$$

It can be proved that the second integral, calculated over the whole cycle, is equal to zero. In fact:

$$\int_{cycle} m_v \frac{dv}{dt}\, dt = m_v \int_{t=t_i}^{t=t_f} v\, dv = \frac{1}{2} m_v (v_f^2 - v_i^2) = 0 \tag{3.31}$$

because $v_i = v_f = 0$, since the car is at rest both at the beginning and at the end of the cycle. This integral can be also seen as the difference in kinetic energy of the car between end and beginning of the cycle, which has to be null.

As a consequence, $E_{traction}$ is calculated only through the road load power integral:

$$E_{traction} = E_{road\ loads} = \int_{cycle} (F_0 + F_1 v + F_3 v^2)\, dt \tag{3.32}$$

3.2.1.2 Energy losses

The amount of fuel consumed by a motor vehicle over a distance is affected by the efficiency of the vehicle in converting the chemical energy in the fuel into mechanical energy and transmitting it to the axles to drive the wheels.

The losses in this system have different origins. They can be summarized as:

- engine losses: only a relatively small portion of the fuel energy is transformed in mechanical energy available at the flywheel; some energy is dissipated because of pumping losses, friction, heat rejection and combustion losses;
- mechanical losses: some losses occur in the driveline, i.e., in the torque converter or clutch (depending on which of the two is present) and in the gearbox; the mechanical losses downstream the gearbox have been already taken into account inside the vehicle road load coefficients; when regenerative braking is active, another mechanical loss affects the energy balance: while the regenerative power goes upstream the powertrain chain, it drags the engine which is usually in fuel cut off, so the friction of the engine must be accounted as a loss to be subtracted from the instantaneous regenerative power; instead, when the power flows back from the battery to the wheels, it is supposed that engine is on (assisted by the electric motor), so losses due to engine friction can be considered already accounted inside the engine losses;
- energy conversion losses: these losses are particularly important for hybrid vehicles, where a remarkable quantity of energy is subjected to multiple form conversions; a part of the mechanical energy available at the crankshaft can be transformed in electrical energy through the generator to run the electrical loads, or to be stored in the battery, where it is in turn subjected to another transformation (from electrical to chemical). The hybrid vehicles which are capable of providing electric power assist are characterized also by a reverse path of the energy (from the battery to the electric motor to the crankshaft), with further losses. Summarizing, these losses take into account the efficiency of electric machine, inverter, battery and their links (mechanical and electrical);
- accessory power consumption: part of engine brake power is used to run the accessories; this value can be assumed constant throughout the cycle;

- losses due to friction brake: when the drive cycle profile requires a deceleration which the vehicle can't follow just coasting down, an action on the brake pedal is required; therefore, the brakes dissipate to the environment part of the kinetic energy of the car;
- losses at idle: during idle, some fuel is burned but no power at the wheels is produced, so the corresponding fuel energy is considered as a loss.

All the energy loss components will be better defined by equations in the following sections.

Figure 3.16 depicts the energy flows and sinks for a conventional gasoline-powered mid-size passenger car. As previously stated, most of the energy available in the fuel tank (about two thirds) is lost in converting heat into mechanical work at the engine, much of it unavoidably. For urban trips consisting of stop-and-go driving, a significant percentage (about 15 to 20%) is also lost in standby operations during coasting, braking, and idling in traffic. For urban driving, only 10 to 15% of the fuel energy is ultimately transmitted as power to the wheels. Because standby losses are lower during highway driving and because the engine is operating more efficiently, a higher percentage of fuel energy - about 20% - makes its way to the wheels. While the specific percentages vary by vehicle type and trip, the flows shown in Figure 3.16 are generally representative of current passenger vehicles.

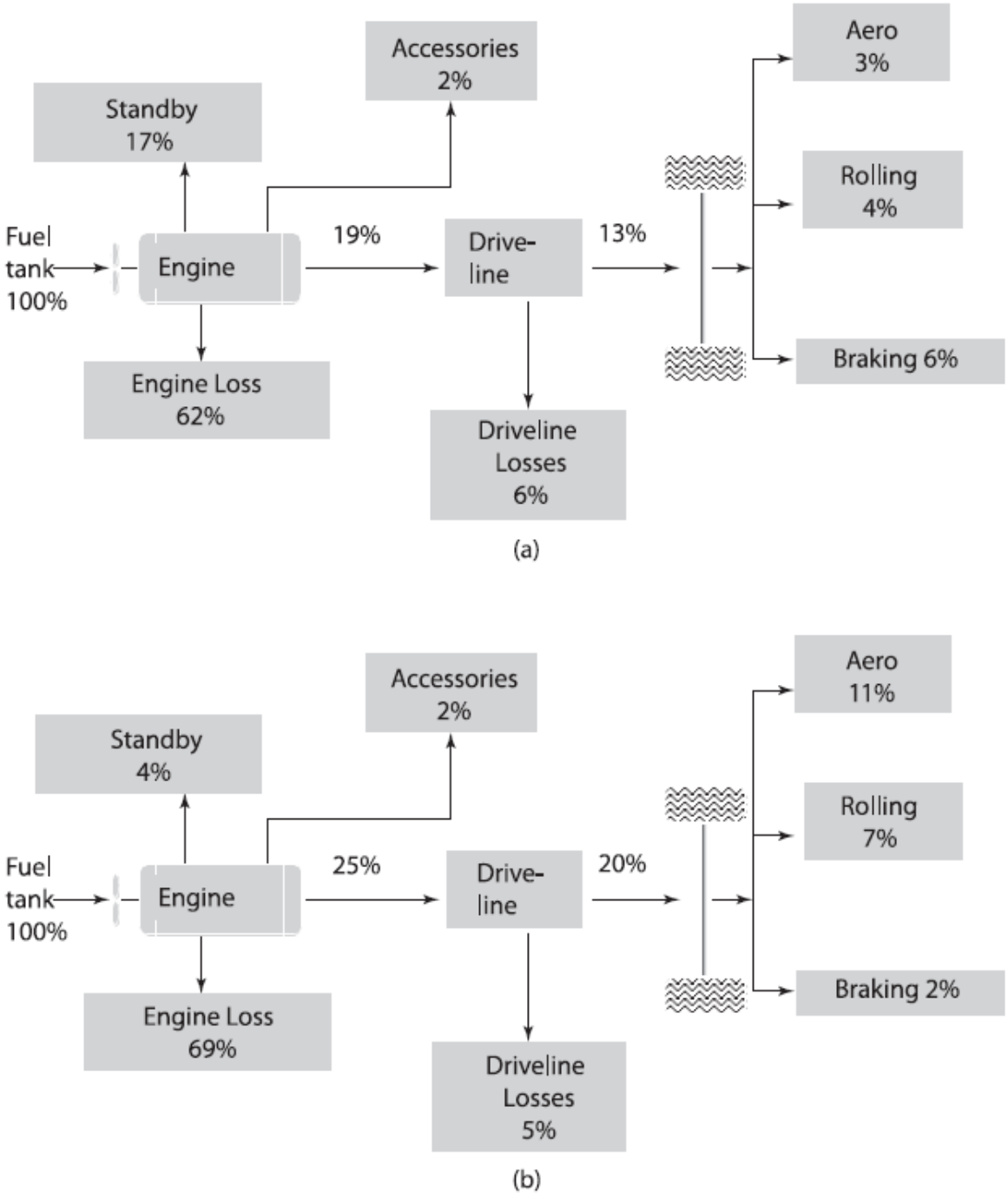

Figure 3.16 - Example energy flows for a late-model midsize passenger car:
(a) urban driving; (b) highway driving [57].

3.2.1.3 Efficiency of the system

The accessory power consumption can actually be considered as necessary for the vehicle correct functioning. As a consequence, two different types of efficiency can be defined, the vehicle and the powertrain efficiency:

$$Vehicle\ efficiency \quad \eta_v = \frac{E_{traction}}{E_{fuel}} \tag{3.33}$$

$$Powertrain\ efficiency \quad \eta_p = \frac{E_{traction} + E_{acc}}{E_{fuel}} \tag{3.34}$$

where E_{acc} is the energy absorbed by the accessories. $E_{traction}$ is also called vehicle energy demand, while $E_{traction} + E_{acc}$ is called "total" vehicle energy demand. These efficiencies express how much of the fuel energy is effectively used to overcome the road loads and run the vehicle through the cycle.

As an example, Figures 3.17 and 3.18 show a powertrain efficiency survey of some of the recent HEV models on city and highway standard drive cycles as defined by EPA.

It can be noticed that hybrid vehicles show a remarkable efficiency improvement in the city cycle with respect to conventional mid-size gasoline vehicles. As it can be expected, the efficiency gets higher as the level of hybridization increases (from mild HEVs, such as vehicles equipped with BSG, to parallel HEVs to power split HEVs): for instance power split HEVs have the highest city cycle powertrain efficiency of almost 0.2, doubling the gasoline vehicle efficiency.

In the highway cycle, although the average efficiency is higher than in the city cycle, the use of hybrid vehicles is more sacrificed and the improvements are limited. Power split HEVs have again the highest highway cycle powertrain efficiency, which is between 0.27 and 0.29, about 15% higher than the gasoline vehicle efficiency.

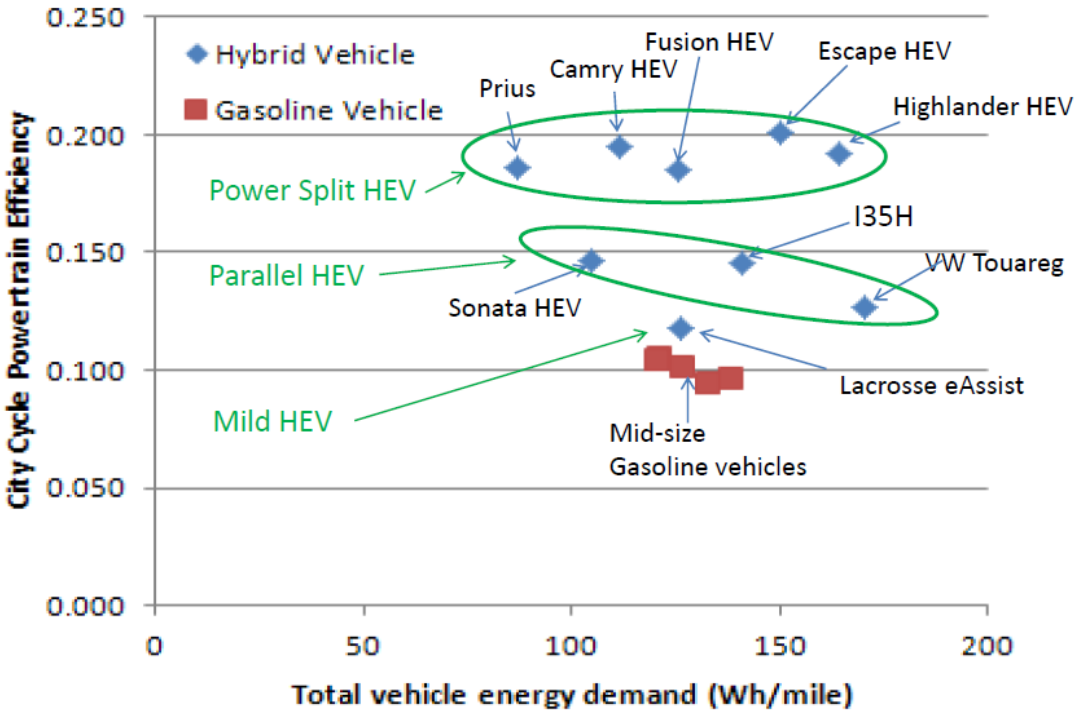

Figure 3.17 - Powertrain efficiency of recent HEV models on city cycle [58].

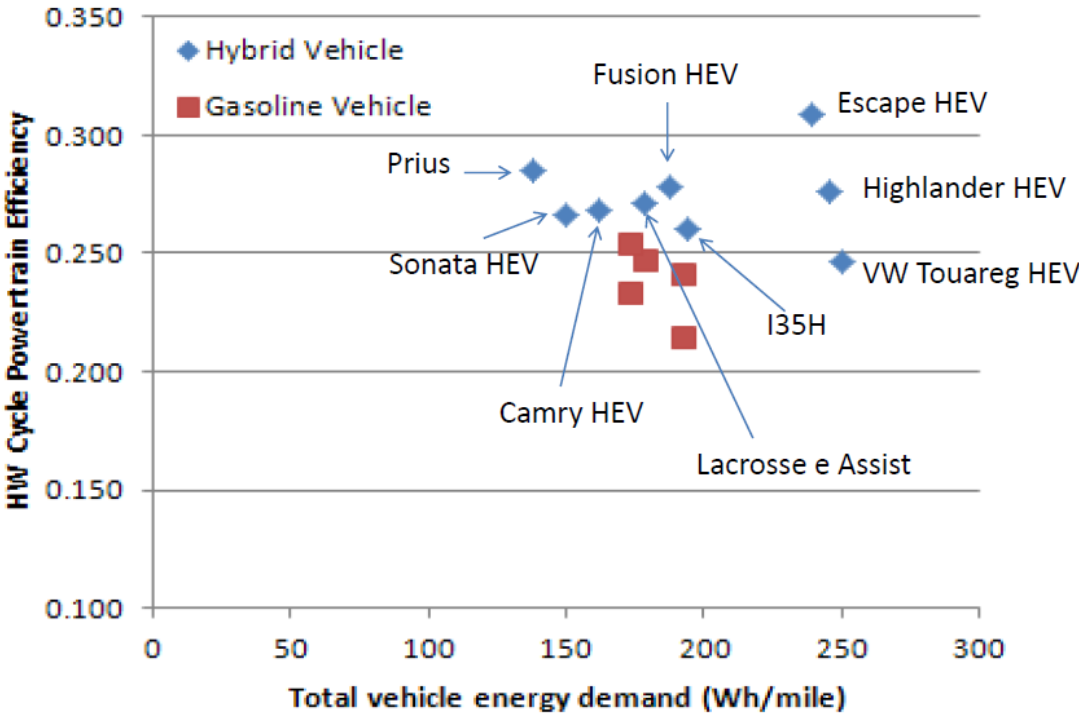

Figure 3.18 - Powertrain efficiency of recent HEV models on highway cycle [58].

3.2.1.4 Study cases

The main purpose of the simulations and tests is to assess the improvements in fuel consumption related to the BSG system and its features. Four cases were studied to evaluate the effects of the main BSG functions, i.e., engine stop-start, electric e-assist and regenerative braking. Table 3.5 shows which features were selected for each case: knowing the fuel consumption of the conventional vehicle, to be used as reference, the idea was to first estimate the fuel consumption benefits with stop-start only, then to add electric assist in order to observe the improvements related to the load shifts, and finally to include regenerative braking.

Table 3.5 - Fuel consumption study cases

	Case 0 (conventional)	Case 1	Case 2	Case 3
Engine stop-start	✗	✓	✓	✓
Electric assist	✗	✗	✓	✓
Regenerative braking	✗	✗	✗	✓

3.2.1.5 Drive cycles

A drive cycle is a series of data points representing the speed of a vehicle versus time. Drive cycles are established by various countries and organizations to assess the vehicle performance [59]. Implementing them in simulations or real tests, in order to replay real world driving conditions, fuel consumption and emissions can be estimated.

Drive cycles were created in different ways. Some were derived theoretically, and others were obtained based on measurement data from real world driving tests [60]. The European Union prefers the former while the United States and Japan like the latter.

Drive cycles are further classified into two different types:

1. Transient drive cycles: the speed changes a lot in these drive cycles based on typical on-road driving conditions; the American Urban Dynamometer Driving

Schedule (UDDS), the Federal Test Procedure (FTP) and the Highway Fuel Economy Driving Schedule (HWFET) drive cycles belong to this type.

2. Modal drive cycles: they involve protracted periods at constant speeds; the European New European Driving Cycle (NEDC) and the Japanese 10-15 Mode cycles are included in this type.

For all the kinds of approaches considered in this thesis (analytical, simulations and tests), it has been decided to utilize three different drive cycles: two of them are US standard drive cycles, the UDDS to simulate city driving and the HWFET to simulate highway driving; the third one is the European standard drive cycle, the NEDC.

The UDDS is commonly called the "LA4" or the "city test", representing complex city driving conditions. It is only suitable for light duty vehicle testing. The speed profile is shown in Figure 3.19. The characteristics are listed in Table 3.6.

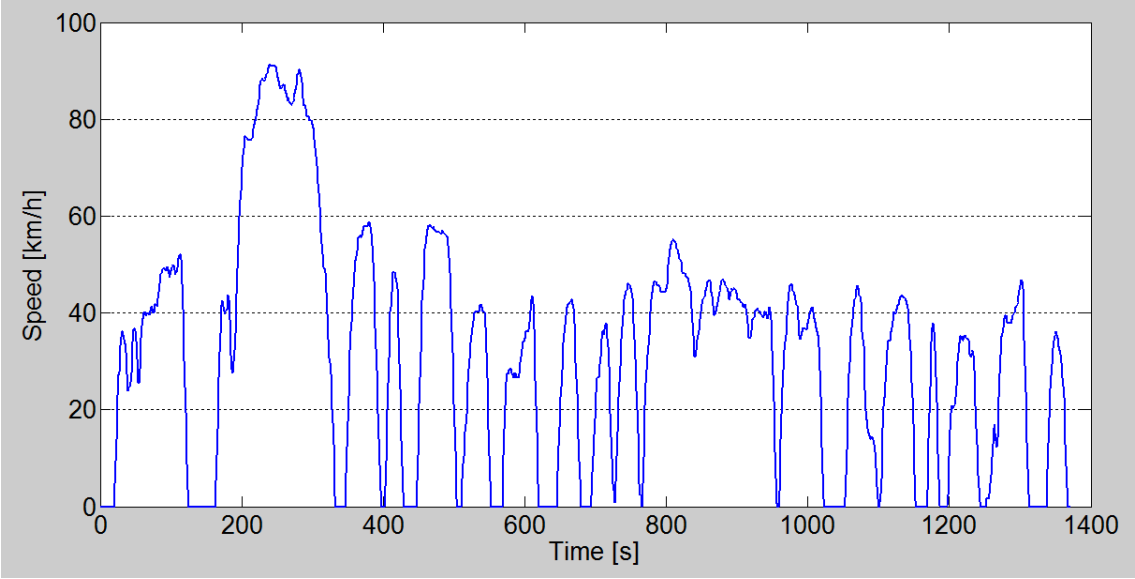

Figure 3.19 - UDDS speed profile.

Table 3.6 - UDDS main characteristics.

Time	1369 s
Distance	11.99 km
Maximum speed	91.25 km/h
Average speed	31.51 km/h
Maximum acceleration	1.48 m/s^2
Maximum deceleration	-1.48 m/s^2
Average acceleration	0.5 m/s^2
Average deceleration	-0.58 m/s^2
Idle time	244 s
No. of stops	17

The HWFET represents highway driving conditions under 60 mph (100 km/h) and it is characterized by no stops. Figure 3.20 shows its speed profile and Table 3.7 its characteristics.

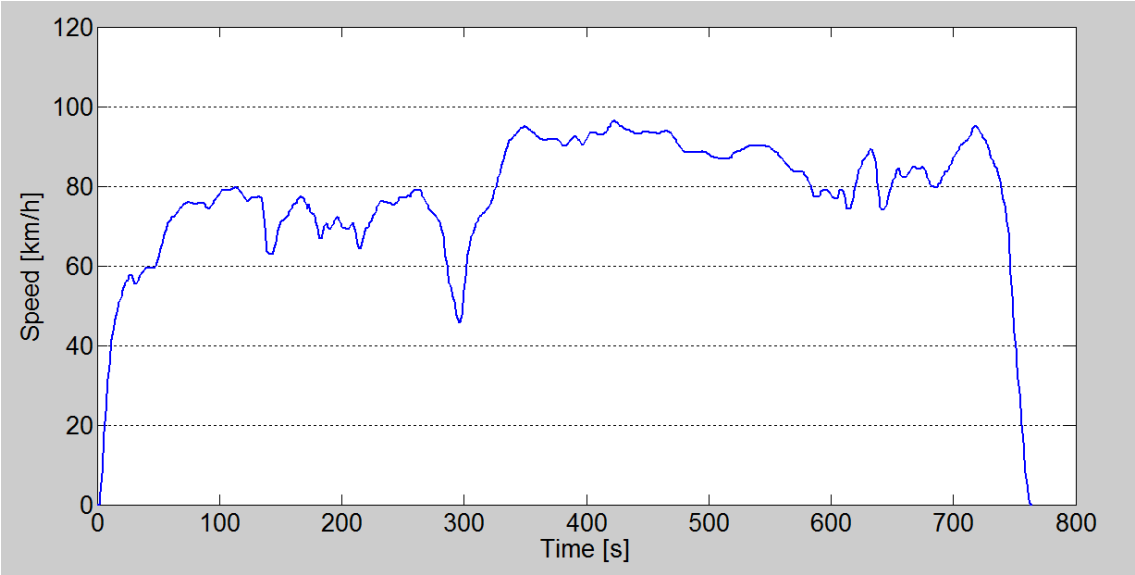

Figure 3.20 - HWFET speed profile.

Table 3.7 - HWFET main characteristics.

Time	765 s
Distance	16.51 km
Maximum speed	96.40 km/h
Average speed	77.58 km/h
Maximum acceleration	1.43 m/s^2
Maximum deceleration	-1.48 m/s^2
Average acceleration	0.19 m/s^2
Average deceleration	-0.22 m/s^2
Idle time	3 s
No. of stops	1

The NEDC, also referred as Motor Vehicle Emission Group (MVEG) cycle, is a drive cycle consisting of four repeated ECE-15 drive cycles and an Extra-Urban drive cycle (EUDC). The ECE-15 is a urban drive cycle which is employed to represent city driving conditions and is characterized by low vehicle speeds, low engine load and low exhaust gas temperature. The EUDC, which has more aggressive and high speed drive modes simulating highway driving, is added after the fourth ECE-15 to produce a NEDC cycle. The NEDC is used for emission certification of light duty vehicles in Europe. The speed profile and characteristics are shown in Figure 3.21 and Table 3.8.

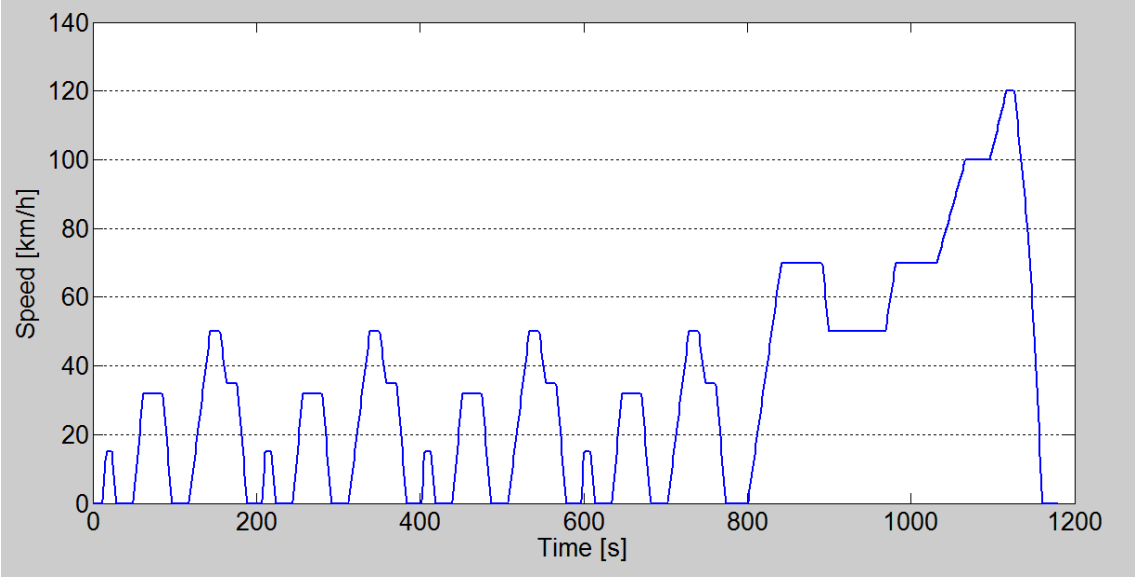

Figure 3.21 - NEDC speed profile.

Table 3.8 - NEDC main characteristics.

Time	1184 s
Distance	10.93 km
Maximum speed	120 km/h
Average speed	33.21 km/h
Maximum acceleration	1.06 m/s^2
Maximum deceleration	-1.39 m/s^2
Average acceleration	0.54 m/s^2
Average deceleration	-0.79 m/s^2
Idle time	257 s
No. of stops	13

3.2.1.6 Data and assumptions

For the calculation of the fuel consumption, some data were available, while others had to be assumed.

In order to evaluate the effect of the Belt Starter Generator on vehicles of different size, two D-segment, one E-segment and one mid-size SUV vehicles have been considered. For all of them, calculations were made both for the conventional version and for the version equipped with BSG. Since the study was focused on the BSG effect only, the road load coefficients were held constant (same rolling and aerodynamic resistance as conventional), while weight was increased to take into account the heavier components which make up the BSG. Most of the weight increase is due to the motor-generator, the power electronics with cooling system and the battery pack. These components were considered equal to those used in the simulations and tests, which will be explained in the following sections. With an 18 kW motor generator and a high voltage 72 cells lithium-ion battery, the weight increase was assumed of 70 kg. Table 3.9 shows weights and road load coefficients for all the discussed versions.

Table 3.9 - Characteristics of the vehicles for simulations with analytical approach

Vehicle	Estimated test weight $[kg]$	$F_0\ [N]$	$F_1\left[\frac{N}{km/h}\right]$	$F_2\left[\frac{N}{(km/h)^2}\right]$
D-segment 1 (conventional)	1746	142.966	0.854	0.026
D-segment 1 (BSG)	1816	=	=	=
D-segment 2 (conventional)	1814	201.104	-0.086	0.035
D-segment 2 (BSG)	1884	=	=	=
E-segment (conventional)	1934	205.864	-0.074	0.036
E-segment (BSG)	2004	=	=	=
SUV (conventional)	2495	201.816	2.778	0.038
SUV (BSG)	2565	=	=	=

The average engine efficiency over the drive cycle is defined as:

$$\eta_{engine} = \frac{E_{fw}}{E_{fuel}} = \frac{\int_{cycle} P_{fw}\, dt}{m_{fuel} \cdot LHV_{fuel}} = \frac{\int_{cycle} T_{fw} \cdot n_{fw}\, dt}{m_{fuel} \cdot LHV_{fuel}} \tag{3.35}$$

E_{fw} represents the total produced mechanical energy available at the flywheel, calculated integrating over the cycle the flywheel power P_{fw}, which in turn is computed knowing torque T_{fw} and speed n_{fw} at the flywheel at each time instant. E_{fuel} instead is obtained multiplying the mass of burned fuel during the cycle by the fuel lower heating value. These data were obtained from tests on a vehicle running with a V6 3.6 liter engine (maximum torque: 353 Nm @ 4800 rpm; maximum power: 211 kW @ 6400 rpm), taking into account the differences in calibrations occurring among the four study cases previously introduced. Table 3.10 summarizes the engine efficiency values used for the study cases and drive cycles.

Table 3.10 - Adopted engine efficiency values for the various study cases

	Case 0 (conventional)	Case 1	Case 2	Case 3
UDDS	23,12%	23,12%	25,71%	23,85%
HWFET	27,94%	27,94%	30,07%	29,30%
NEDC	24,04%	24,04%	25,78%	24,89%

The efficiency values don't change between Case 0 and Case 1 because in the calculation, since the car was running with stop-start enabled, only the operating points for which the vehicle speed was greater than zero were taken into account. For Case 0, an engine power at idle of 3 kW was assumed, originating from an engine speed of 720 rpm and torque of 40 Nm. From the fuel consumption map of the engine, a specific fuel consumption of 450 g/kWh was extrapolated.

These efficiency values could actually be improved if more time is spent on calibrating the vehicle for a specific study case. For instance, gear shift maps, battery power limits and other calibrations can be further modified (still with some limitations) to find an optimum for the efficiency.

The values of mechanical efficiency and energy conversion efficiency were instead assumed. For the latter, two equivalent values were hypothesized for the path going from the crankshaft to the battery and for the opposite one. The value of the engine friction power was obtained from friction data of the considered engine, assuming that during regenerative braking speed was constant and equal to 1000 rpm. Table 3.8 shows all these values.

Table 3.11 - Mechanical and electrical losses data.

Mechanical efficiency	$\eta_m = 95\ \%$
Engine friction power	$P_{friction} = 1350\ W$
Energy conversion efficiency (crankshaft – battery)	$\eta_{cs-b} = 90\ \%$
Energy conversion efficiency (battery – crankshaft)	$\eta_{b-cs} = 90\ \%$
Energy conversion efficiency (crankshaft – battery – crankshaft)	$\eta_{cs-b-cs} = 90\ \% \cdot 90\ \% = 81\ \%$

Then, regarding the accessory power consumption, a distinction must be made between mechanical and electric accessories. It was assumed that the mechanical accessory power consumption was already included in the engine efficiency, while the electric power consumption was considered constant throughout the cycle and entirely provided by the battery (the energy conversion efficiency then must be taken into account). Its value was set to 200 W.

Last but not least, talking about the cases in which electric assist and regenerative braking are present, some constraints had to be stated on the battery power. It was assumed to limit the battery charge power to 15 kW, which is reasonable for a mid-size mild hybrid vehicle with a high voltage battery. Also in this case, the energy conversion efficiency must be considered to calculate the energy that is effectively recovered in the battery and then supplied to the crankshaft with the electric assist. The battery discharge power could instead be higher, and in this case the maximum electric assist power was supposed constrained by the motor-generator to 18 kW.

3.2.1.7 Analytical model for fuel consumption evaluation

Once all the data were available, they were implemented in a Matlab code to estimate the fuel consumption values. All the energy terms previously mentioned were summed together in an energy balance equation, to obtain as a first result the mechanical energy produced by the engine and available at the flywheel E_{fw}:

$$E_{fw} = E_{traction} + E_{acc} + E_{\substack{energy \\ conversion \\ losses}} + E_{\substack{mech \\ losses}} + E_{braking} - E_{regen} + E_{\substack{regen \\ losses}} \quad (3.36)$$

- $E_{traction}$ is the tractive energy and in Equation 3.32 it was found that it is equal to the energy required to overcome the road loads. It can be further divided in "positive" road load energy for vehicle acceleration equal or higher than zero and "negative" road load energy for vehicle acceleration lower than zero:

$$E_{road\ loads\ (+)} = E_{traction}(\dot{v} \geq 0) \quad (3.37)$$

$$E_{road\ loads\ (-)} = E_{traction}(\dot{v} < 0) \quad (3.38)$$

$$E_{traction} = E_{road\ loads} = E_{road\ loads\ (+)} + E_{road\ loads\ (-)} \quad (3.39)$$

- E_{acc} is the energy absorbed by the electric accessories evaluated at the battery output, and is calculated as:

$$E_{acc} = \int_{t=t_i}^{t=t_f} P_{acc}\, dt = P_{acc} \cdot t_{cycle} \quad (3.40)$$

- $E_{\substack{energy \\ conversion \\ losses}}$ represents the loss due to energy conversion from mechanical at the crankshaft to chemical in the battery, required to run the electric accessory loads. It is obtained as:

$$E_{\substack{energy \\ conversion \\ losses}} = (1 - \eta_{cs-b}) \cdot E_{acc} \quad (3.41)$$

- $E_{\substack{mech \\ losses}}$ is the energy lost in the gearbox. It is calculated using the mechanical efficiency defined in Table 3.11, and it applies to all the power going from the

flywheel to the differential through the gearbox:

$$E_{\substack{mech \\ losses}} = (1 - \eta_m) \int_{t=t_i}^{t=t_f} (P_{road\ loads\ (+)} + P_{accel} + P_{extra})\, dt \qquad (3.42)$$

where P_{accel} is the mechanical power needed to accelerate the vehicle and make it follow the drive cycle speed profile:

$$P_{accel} = m_v a \cdot v \qquad for\ \ a > 0 \qquad (3.43)$$

while P_{extra} needs a more detailed explanation. The drive cycle requires that the vehicle follows a specific speed (and acceleration) profile. During decelerations, the force equilibrium equation can be rewritten as:

$$F - F_{road\ loads\ (-)} = m_v a = F_{decel} \qquad for\ \ a < 0 \qquad (3.44)$$

where F is the force applied by the driver (which can be positive or negative), $F_{road\ loads\ (-)}$ is the force opposed to the motion by the road loads and F_{decel} represent the inertia force related to the deceleration a imposed by the cycle (it a negative value since a is negative). Three situations can happen in this case:

- If $|F_{decel}| < F_{road\ loads\ (-)}$, it means that the road loads would brake the car more than what is requested by the cycle, so the driver has to add an extra positive tractive force (called F_{extra}) to follow the correct profile;
- If $|F_{decel}| > F_{road\ loads\ (-)}$, the speed profile requires a deceleration that the road loads only cannot provide, so the driver has to apply a braking force ($F_{braking}$);
- If $|F_{decel}| = F_{road\ loads\ (-)}$, the road load exactly provide the deceleration required by the cycle, so no action is requested from the driver.

Powers are simply calculated multiplying the corresponding forces by the speed.

- $E_{braking}$ is the energy that has to be absorbed by either friction braking or regenerative braking to decelerate the vehicle accordingly to the cycle. Since during decelerations part of the kinetic energy is dissipated by road loads, the

effective value of $E_{braking}$ is calculated as:

$$E_{braking} = \int_{cycle} P_{braking}\, dt = \int_{cycle|_{\dot{v}<0}} (|P_{decel}| - P_{road\ loads\ (-)})\, dt \quad (3.45)$$

provided the condition

$$|P_{decel}| > P_{road\ loads\ (-)} \quad (3.46)$$

- E_{regen} represents the energy recovered through regenerative braking. It depends on the instantaneous $P_{braking}$ value and on the maximum regenerative power capability $P_{\substack{regen \\ max}}$ (both of them are calculated at the wheels):

$$if\ P_{braking} \geq P_{\substack{regen \\ max}} \rightarrow P_{regen} = P_{\substack{regen \\ max}} \quad (3.47)$$

$$if\ P_{braking} < P_{\substack{regen \\ max}} \rightarrow P_{regen} = P_{braking} \quad (3.48)$$

This means that when the braking power exceeds the regenerative power capability the braking power is split between friction braking and regenerative braking, while in the other case it is entirely covered by regenerative braking. After this step, it must be checked if the power which arrives at the engine is able to overcome the engine friction and go up to the battery; if not, regenerative braking cannot apply:

$$if\ P_{regen} \cdot \eta_m > P_{friction} \rightarrow P'_{regen} = P_{regen} \quad (3.49)$$

$$if\ P_{regen} \cdot \eta_m \leq P_{friction} \rightarrow P'_{regen} = 0 \quad (3.50)$$

where P'_{regen} is the final effective value of regenerative power. E_{regen} is simply calculated as:

$$E_{regen} = \int_{cycle} P'_{regen}\ dt \quad (3.51)$$

- $E_{\substack{regen \\ losses}}$ takes into account the losses due to the flow of E_{regen} from the wheels to the battery and then back again to the wheels with electric assist. Its value is:

$$E_{\substack{regen \\ losses}} = \int_{cycle} \left[P'_{regen} - \left(P'_{regen} \cdot \eta_m - P_{friction}\right) \cdot \eta_{cs-b-cs} \cdot \eta_m\right]\, dt \quad (3.52)$$

Lastly, E_{idle} is the energy necessary to run the engine at minimum when the vehicle is stopped. Obviously this quantity applies only for Case 0, i.e., for the conventional vehicle.

It is calculated as:

$$E_{idle} = \int_{cycle|_{v=0}} P_{idle}\, dt = \int_{cycle|_{v=0}} T_{idle} \cdot n_{idle}\, dt = T_{idle} \cdot n_{idle} \cdot \Delta t|_{v=0} \tag{3.53}$$

Once the energy at the flywheel E_{fw} and E_{idle} have been determined, the fuel energy E_{fuel} can be calculated knowing engine efficiency and specific fuel consumption at idle:

$$E_{fuel} = \frac{E_{fw}}{\eta_{engine}} + E_{idle} \cdot sfc_{idle} \cdot LHV_{fuel} \tag{3.54}$$

where sfc_{idle} is the specific fuel consumption at idle and LHV_{fuel} is the lower heating value of the fuel.

From E_{fuel}, fuel consumption can be easily determined, either in $\mathrm{l}/100\mathrm{km}$ or in mpg:

$$\frac{l}{100km} = \frac{E_{fuel}[J]}{LHV_{fuel}\left[\frac{J}{kg}\right] \cdot \rho_{fuel}\left[\frac{kg}{l}\right] \cdot \frac{distance\_covered\ [km]}{100}} \tag{3.55}$$

$$mpg = \left(\frac{l}{100km} \cdot \frac{1}{100} \cdot \frac{0.2642\ Gallon}{0.6219\ miles}\right)^{-1} \tag{3.56}$$

3.2.1.8 Preliminary analysis

As a preliminary analysis, it is interesting to take a look at the differences in road load resistance for the four vehicles. Figure 3.22 shows the road load resistance curves as a function of the vehicle speed. Since all the components of the powertrain are considered equal among the vehicle cases, it is certainly expected that the D-segment 1 will produce the lowest fuel consumption while the SUV the highest, for all the considered study cases. More uncertain are the results of the D-segment 2 and the E-segment: since the road load resistance curves are so close, it may be possible that the different masses play an important role in certain study cases, such as the one including regenerative braking

(from one side higher mass increase the energy required to accelerate the vehicle, but from the other it allows more energy to be recovered during braking).

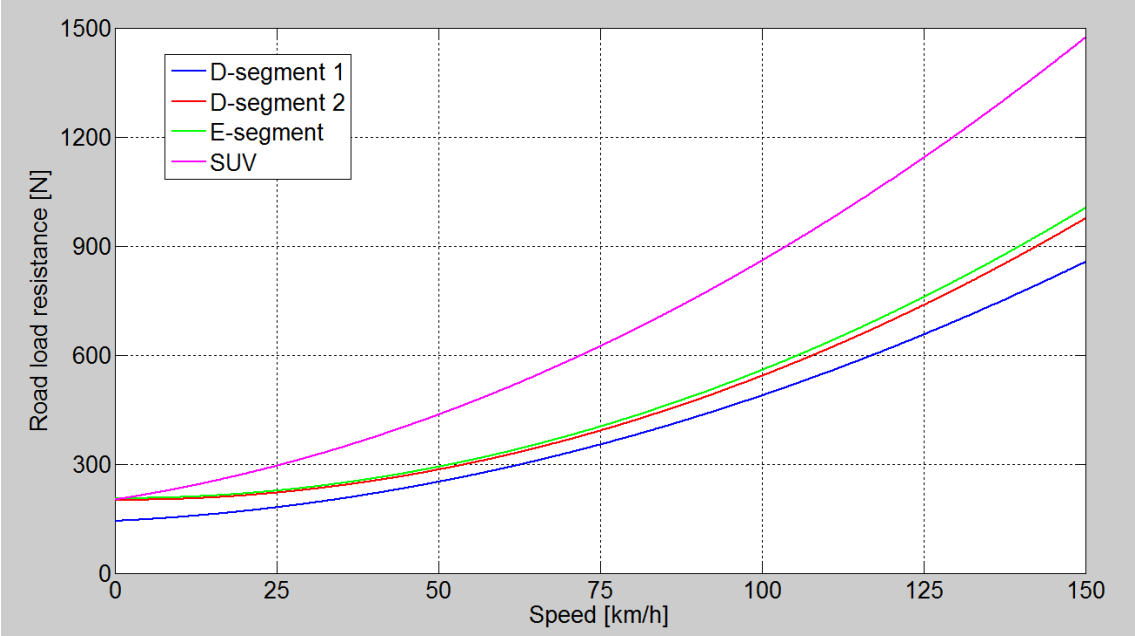

Figure 3.22 - Road load resistance curves of the vehicles analyzed with the analytical approach

Table 3.12 shows some energy quantities of particular interest, expressed in Wh/km. The total vehicle energy demand is the sum of road load and accessory energy. It depends on the cycle profile and on the road load coefficients, as defined in Equation 3.27. The total braking energy is calculated in Equation 3.45 and is based on the deceleration profile of the cycles and on the vehicle mass. For Case 3, the regenerative braking energy is obtained from the braking power as defined in Equation 3.51. Higher vehicle mass and lower load road resistance allows recovery of more regenerative braking energy, since more kinetic energy must be absorbed either by the friction brakes or by the generator. Lastly the flywheel energy for Case 1 and Case 3 are reported to show how regenerative braking affects the mechanical energy produced at the flywheel (for Case 1, the idle energy does not influence the flywheel energy value since idle consumption is accounted separately for the calculation of the fuel energy - see Equation 3.54). A neat decrease from Case 1 to Case 3 can be observed for UDDS and NEDC, while the few braking opportunities of the HWFET induce a limited effect on the flywheel energy reduction.

Table 3.12 - Preliminary outcomes of the analytical approach.

$\left[\frac{Wh}{km}\right]$		Total vehicle energy demand	Total braking energy	Regenerative braking energy	Flywheel energy Case 1	Flywheel energy Case 3
D-segment 1	**UDDS**	78.6	70.0	47.7	156.4	128.5
	HWFET	110.8	14.7	8.8	131.9	126.7
	NEDC	95.2	45.4	33.0	147.9	128.6
D-segment 2	**UDDS**	88.3	70.6	47.4	167.2	139.4
	HWFET	120.8	14.8	8.6	142.4	137.3
	NEDC	105.7	45.8	33.0	159.3	140.0
E-segment	**UDDS**	89.8	76.0	48.9	174.4	145.5
	HWFET	122.4	16.2	9.2	145.6	140.2
	NEDC	107.2	49.4	34.4	164.8	144.5
SUV	**UDDS**	130.1	93.9	51.5	235.5	204.8
	HWFET	191.2	18.2	8.8	220.0	214.7
	NEDC	159.4	60.1	37.7	230.8	208.1

Finally, another interesting preliminary result is represented by the powertrain efficiency, defined in Equation 3.34, of the different vehicles for the considered cycles and study cases. Figures 3.23 to 3.25 show the powertrain efficiency values for UDDS, HWFET and NEDC cycles respectively. The numbers indicate the corresponding case study. For UDDS and NEDC, the efficiencies increase moving from Case 0 to Case 3 for all the vehicles. For HWFET instead Case 0 efficiency is higher than Case 1, indicating that the fuel economy introduced by stop-start is offset by the weight increase relative to the introduction of the BSG on the vehicle.

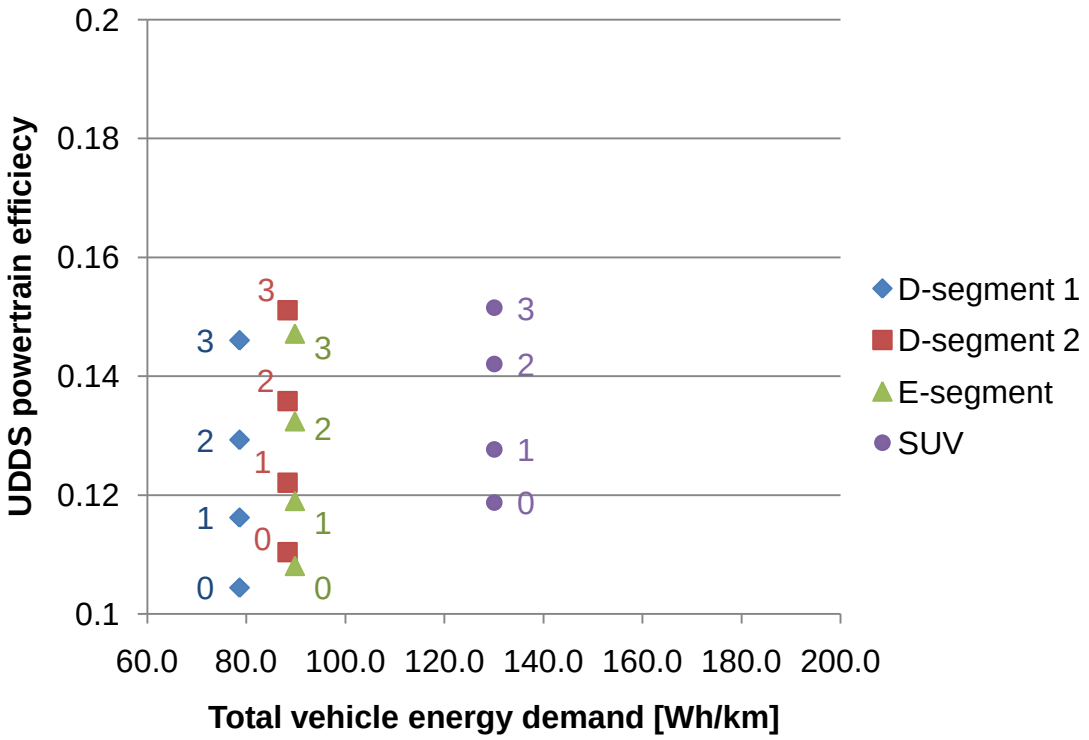

Figure 3.23 - Powertrain efficiency of the analyzed vehicle on UDDS cycle.

The numbers refer to the study cases.

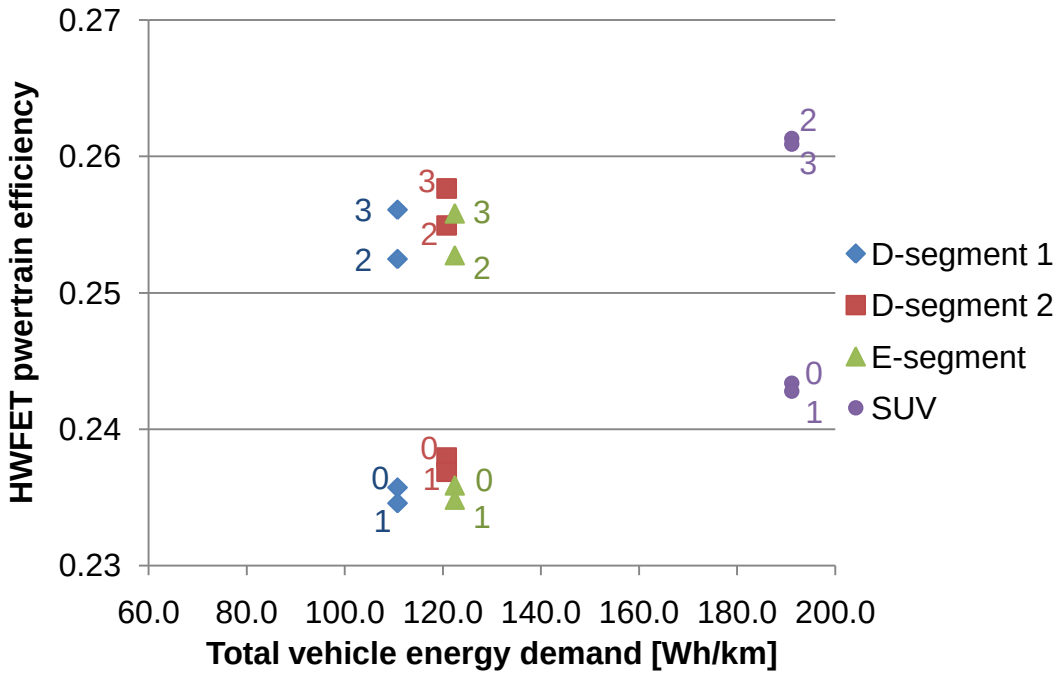

Figure 3.24 - Powertrain efficiency of the analyzed vehicle on HWFET cycle.

The numbers refer to the study cases.

Comparing the efficiencies in Figures 3.23 and 3.24 with those previously shown in Figures 3.17 and 3.18 for conventional (Case 0) and "full" BSG (Case 3), it can be noticed that in the HWFET values are quite close, while in the UDDS the values appear higher with the analytical approach, indicating that the model may underestimate the fuel consumption.

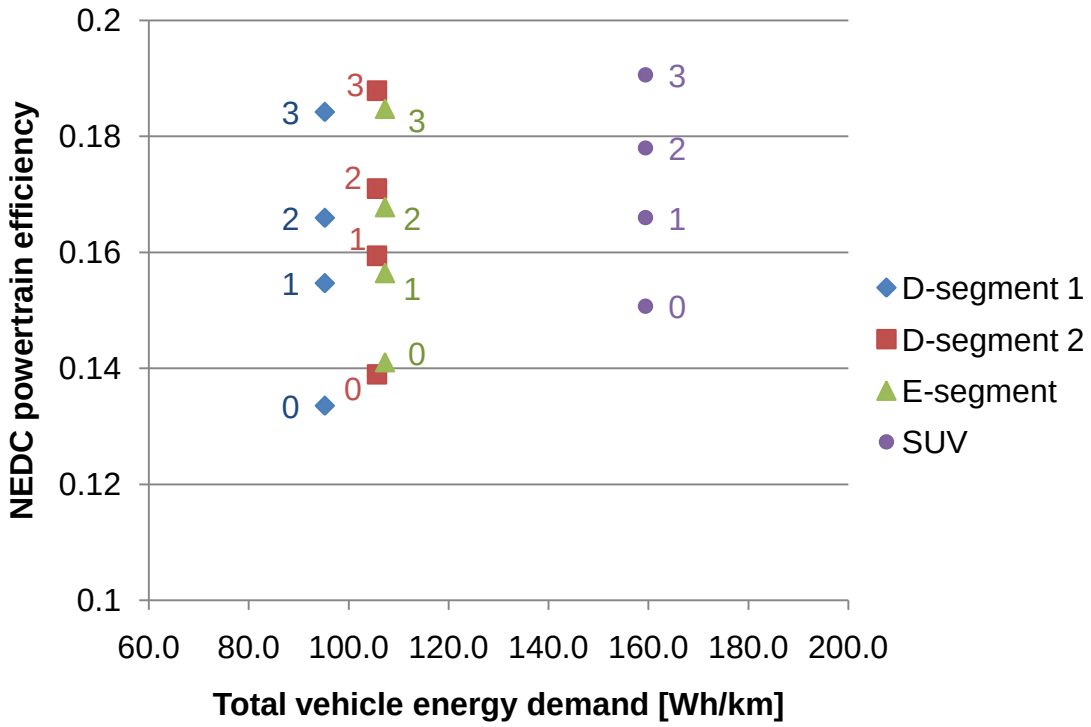

Figure 3.25 - Powertrain efficiency of the analyzed vehicle on NEDC cycle.
The numbers refer to the study cases.

The efficiency values for the NEDC are reasonably intermediate between those of the other two cycles, considering that such cycle is composed of both city and highway sections.

3.2.2 Fuel consumption simulations

In this section, the fuel consumption simulations of vehicles equipped with Belt Starter Generator are presented. As in the section about the analytical approach, the study cases will be introduced first, followed by a list of the required data, the description of the model and some preliminary results.

3.2.2.1 Simulation study cases and data

The simulations which were performed can be divided in two main sets, with different scopes:

1. Simulations aimed to assess the sensitivity of a vehicle with BSG to different component characteristics and sizes. The interest was focused on the effect of different vehicles, engines, electric motors and batteries on the fuel consumption. While changing a specific component, the others were usually kept the same.
2. Simulations intended to obtain fuel consumption values corresponding to the study cases introduced in the previous section (Table 3.5), which will also be applied for the fuel consumption tests on a real vehicle. The results of the simulations will be compared with those of the analytical approach to validate the analytical model.

3.2.2.1.1 Set 1

For the first set of simulations, three different vehicles, six engines, two motor generators and two batteries were considered. In the following, they will be listed and labeled, and after that the combinations that make up the study cases will be shown.

The vehicles are the two D-segment and the E-segment vehicles, which parameters have been already listed in Table 3.9. In this case only the BSG versions were simulated. For the sake of completeness, their characteristics are reported in Table 3.13. Engine, motor-generator and battery characteristic are listed in Tables 3.14 to 3.16.

Table 3.13 - Characteristics of the vehicles for the simulations - set 1.

Vehicles					
Vehicle label	**Estimated test weight** $[kg]$	$F_0\ [N]$	$F_1\ \left[\frac{N}{km/h}\right]$	$F_2\ \left[\frac{N}{(km/h)^2}\right]$	**Transmission**
D-segment 1	1816	142.966	0.854	0.026	6-speeds automatic
D-segment 2	1884	201.104	-0.086	0.035	6-speeds automatic
E-segment	2004	205.864	-0.074	0.036	8-speeds automatic

Table 3.14 - Characteristics of the engines for the simulations - set 1.

Engines					
Engine label	**Displacement**	**Layout**	**Type**	**Maximum torque**	**Maximum power**
A	1.8 L	I4	Aspirated	170 Nm @ 5200 rpm	110 kW @ 6500 rpm
B	2.4 L	I4	Aspirated	210 Nm @ 4800 rpm	119 kW @ 5800 rpm
C	2.4 L	I4	Aspirated	232 Nm @ 4800 rpm	137 kW @ 6250 rpm
D	2.4 L	I4	Turbo	363 Nm @ 2000–5600 rpm	213 kW @ 5700–6400 rpm
E	3.6 L	V6	Aspirated	353 Nm @ 4800 rpm	211 kW @ 6400 rpm
F	5.7 L	V8	Aspirated	529 Nm @ 4000 rpm	272 kW @ 5400 rpm

Table 3.15 - Characteristics of the motor-generators for the simulations - set 1.

Motor-generators					
Motor-generator label	**Type**	**Rated power**	**Max. motoring torque**	**Max. generating torque**	**Maximum speed**
A	Induction	11.9 kW	107 Nm	107 Nm	18000 rpm
B	Induction	18 kW	57 Nm	57 Nm	17000 rpm

Table 3.16 - Characteristics of the batteries for the simulations - set 1.

Batteries						
Battery label	**Type**	**No. of cells**	**Nominal voltage**	**Nominal capacity**	**Peak charging power**	**Peak discharging power**
A	Lithium-ion	31 series	115 V	4.5 Ah	15 kW	-15 kW
B	Lithium-ion	32 series	270 V	4.4 Ah	30 kW	-30 kW

Now that all the component data have been listed, the simulation study cases are presented in Table 3.17 as combinations of the components.

Table 3.17 - Simulation study cases - set 1.

Study cases					
Simulation scope	**Case label**	**Vehicle**	**Engine**	**Motor generator**	**Battery**
Sensitivity to the vehicle	Veh1	D-segment 1	B	A	A
	Veh2	D-segment 2	B	A	A
Sensitivity to the engine	Eng1	E-segment	A	B	B
	Eng2	E-segment	C	B	B
	Eng3	E-segment	D	B	B
	Eng4	E-segment	E	B	B
	Eng5	E-segment	F	B	B
Sensitivity to the motor generator	MoGen	E-segment	E	A	B
Sensitivity to the battery	Batt	E-segment	E	B	A
Sensitivity to the mogen & the battery	MoGen&Batt	D-segment 1	B	B	B

The Cases “MoGen” and “Batt” will be referenced to the Case “Eng4”, since vehicle and engine remain unchanged, while the Case “MoGen&Batt” will be referenced to the Case “Veh1” for the same reason. These simulation cases were run on the UDDS cycle.

3.2.2.1.2 Set 2

The second set of simulations followed the same logic explained in section 3.2.1.4. The conventional vehicle was simulated first in order to have a reference value of fuel consumption. Then, in sequence, stop-start, electric assist and regenerative braking were

added. The vehicle and the components for this set of simulations were selected in order to match the real proof-of-concept vehicle which was used for fuel consumption tests (discussed in Section 3.2.4). They are listed in Tables 3.18 to 3.21.

Table 3.18 - Characteristics of the vehicle for the simulations - set 2.

Vehicle					
Segment	**Estimated test weight** $[kg]$	$F_0\ [N]$	$F_1\ \left[\frac{N}{km/h}\right]$	$F_2\ \left[\frac{N}{(km/h)^2}\right]$	**Transmission**
E	2004	205.864	-0.074	0.036	8-speeds automatic

Table 3.19 - Characteristics of the engine for the simulations - set 2.

Engine				
Displacement	**Layout**	**Type**	**Maximum torque**	**Maximum power**
3.6 L	V6	Aspirated	353 Nm @ 4800 rpm	211 kW @ 6400 rpm

Table 3.20 - Characteristics of the motor-generator for the simulations - set 2.

Motor-generator				
Type	**Rated power**	**Max. motoring torque**	**Max. generating torque**	**Maximum speed**
Induction	18 kW	54 Nm	54 Nm	18000 rpm

Table 3.21 - Characteristics of the battery for the simulations - set 2.

Battery					
Type	**No. of cells**	**Nominal voltage**	**Nominal capacity**	**Peak charging power**	**Peak discharging power**
Lithium-ion	72 series	270 V	5.2 Ah	30 kW	-30 kW

The simulations were performed on UDDS, HWFET and NEDC cycles.

3.2.2.2 Model description

The model used for the simulations was a proprietary model realized in Matlab-Simulink, able to evaluate performance and fuel consumption of a vehicle, provided the selection of the powertrain components from a library. All the powertrain has been modeled in detail, from the engine to the wheels, on the basis of the losses occurring in each component for every operating point. The energy conservation is granted thanks to energy balance equations present in each powertrain subsystem.

Figure 3.26 shows the main Simulink interface, with blocks and connections. Starting from the drive cycle, the controller block evaluates the torque and power request in order to run the vehicle at the speed specified in the cycle. The controller then calculates a cost function based on the losses in the system, which are included in the vehicle and transmission kinematics block. For a hybrid vehicle, it splits the output power request between the two available power sources, engine and electric machine, with the purpose of finding the optimum operating point, minimizing the losses in the system and obtaining the best fuel consumption. More in particular, the controller is characterized by two levels of optimization, called static and dynamic: during the static optimization, the controller calculates the best operating point for the engine at a specific time, on the basis of the requested power, its division between engine and electric machine and the constraints in the system; after that, the dynamic optimization defines the most efficient path for the engine transient in order to reach the static optimum, starting from the current operating point.

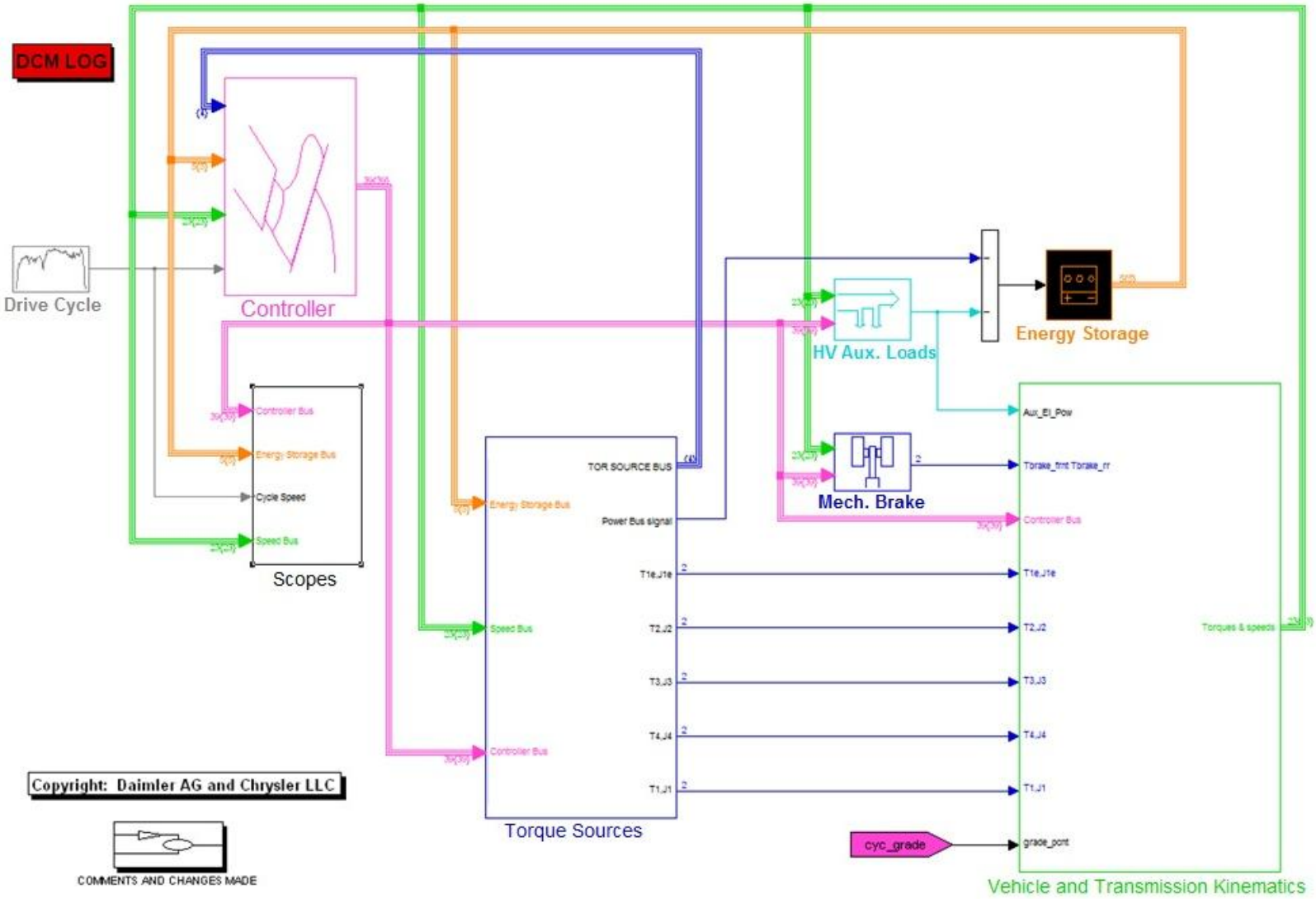

Figure 3.26 - Simulink interface of the model utilized for the fuel economy simulations.

3.2.2.3 Preliminary analysis

As preliminary analysis, some graphs and diagrams related to vehicle functioning and performance will be shown. The outputs of the simulation model were engine and motor maps with operating points, plots of speeds, torques, powers, fuel consumption, SOC and other parameters. The parameters of interest will be defined for each simulation set.

3.2.2.3.1 Set 1

For this set, it is interesting to see the differences among the operating points on the engine maps for the various engines considered for the sensitivity analysis. As it can be noted in Figures 3.27 to 3.31, increasing the engine dimension, the areas of high efficiency draw away from the cloud of the operating points (the pink line represents the wide open throttle limit). Bigger engines work in less efficient areas than smaller engines, for the power levels requested by the drive cycle, so a higher fuel consumption is then expected. Moreover, between the 2.4 L aspirated engine and the 2.4 L turbo engine there is not much difference, since the turbo engine is forced to work mainly at low rpm, where the performance and the fuel consumption is similar to the aspirated engine.

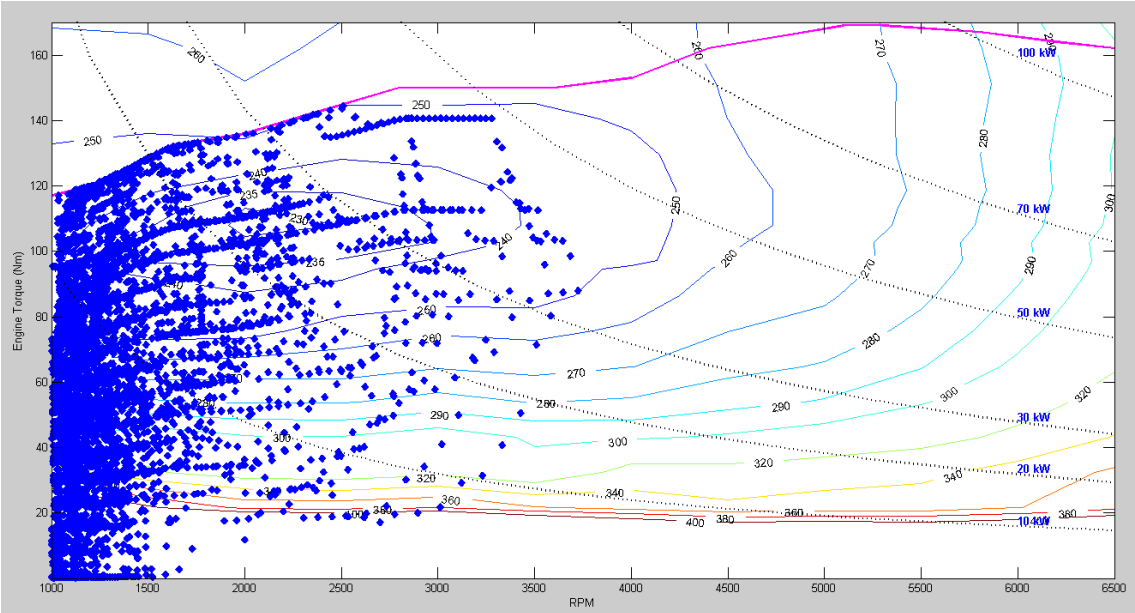

Figure 3.27 - 1.8 L engine map with operating points obtained with simulations - set 1.

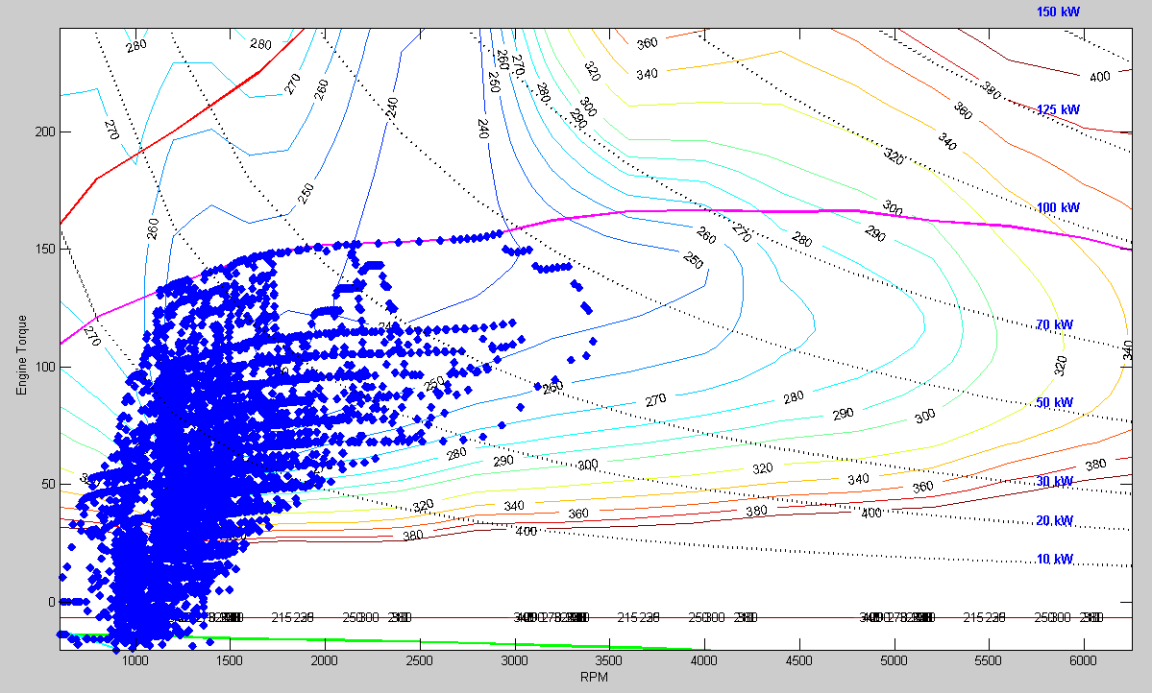

Figure 3.28 - 2.4 L aspirated engine map with operating points obtained with simulations - set 1 (torque is expressed in lb·ft).

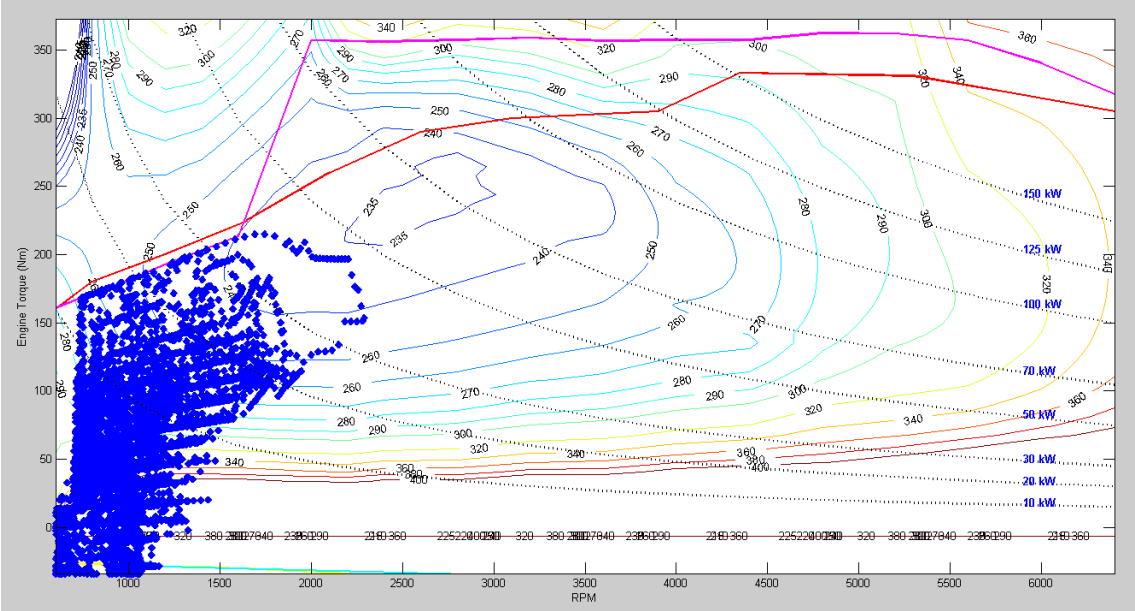

Figure 3.29 - 2.4 L turbo engine map with operating points obtained with simulations - set 1.

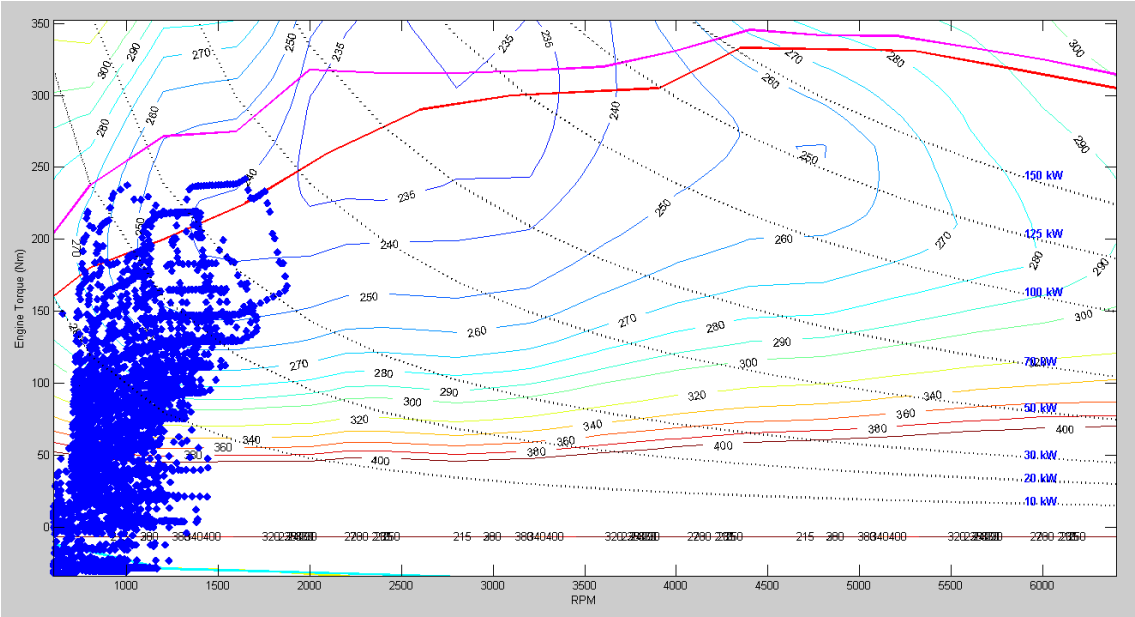

Figure 3.30 - 3.6 L engine map with operating points obtained with simulations - set 1.

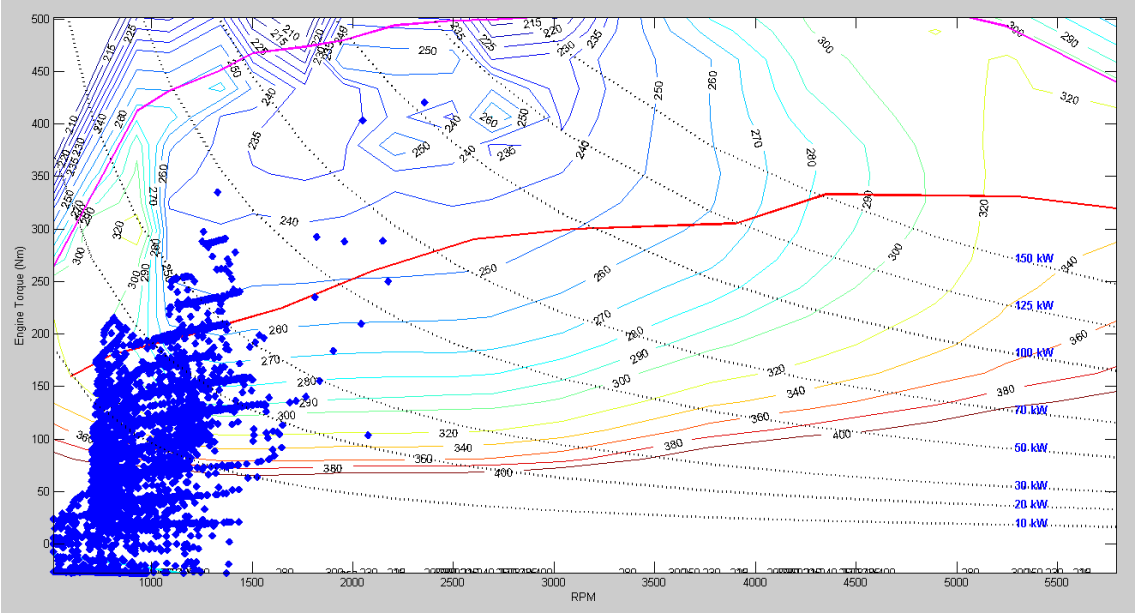

Figure 3.31 - 5.7 L engine map with operating points obtained with simulations - set 1.

Figures 3.32 and 3.33 show the motor generator maps with the operating point of the Cases “MoGen” (11.9 kW machine) and “Eng4” (18 kW machine). It can be seen that for the city cycle the powers in play are quite contained inside the limits imposed by the motor generator maps, except during energy recuperation characterized by very low (negative) torque. For the rest, the clouds are very similar between the two cases. Since

the operating engine speeds are rather low (around 1000 rpm) also the machine speeds are small (the pulley ratio is 2.5). This prevents the machines to work in a high efficiency area. Therefore, the fuel consumption values are expected to be very close.

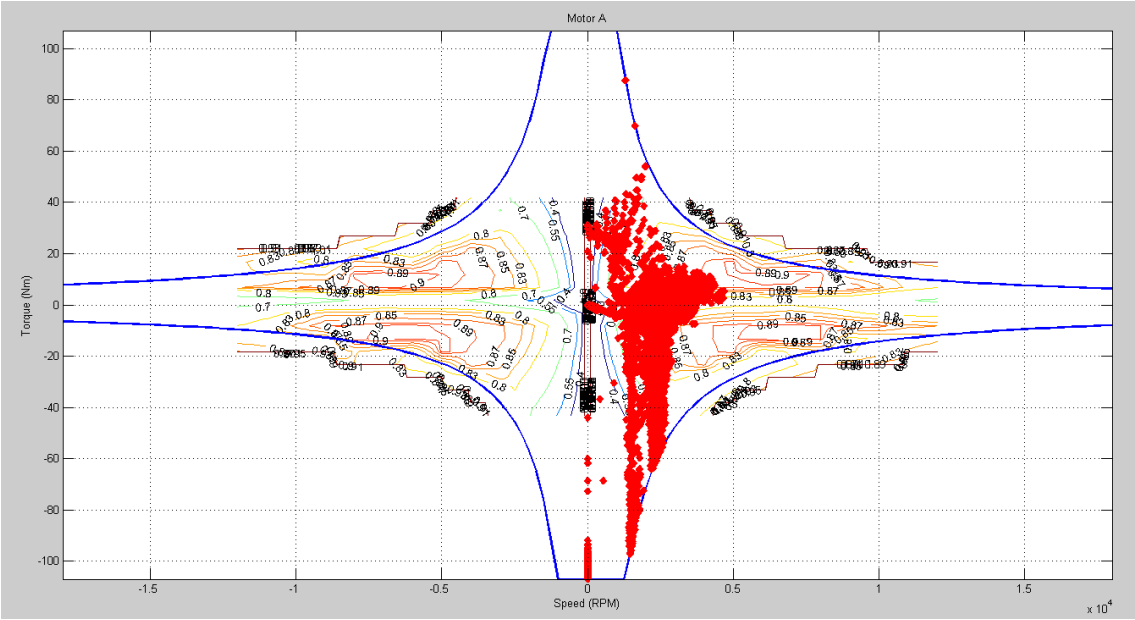

Figure 3.32 - 11.9 kW machine map with operating points obtained with simulations - set 1.

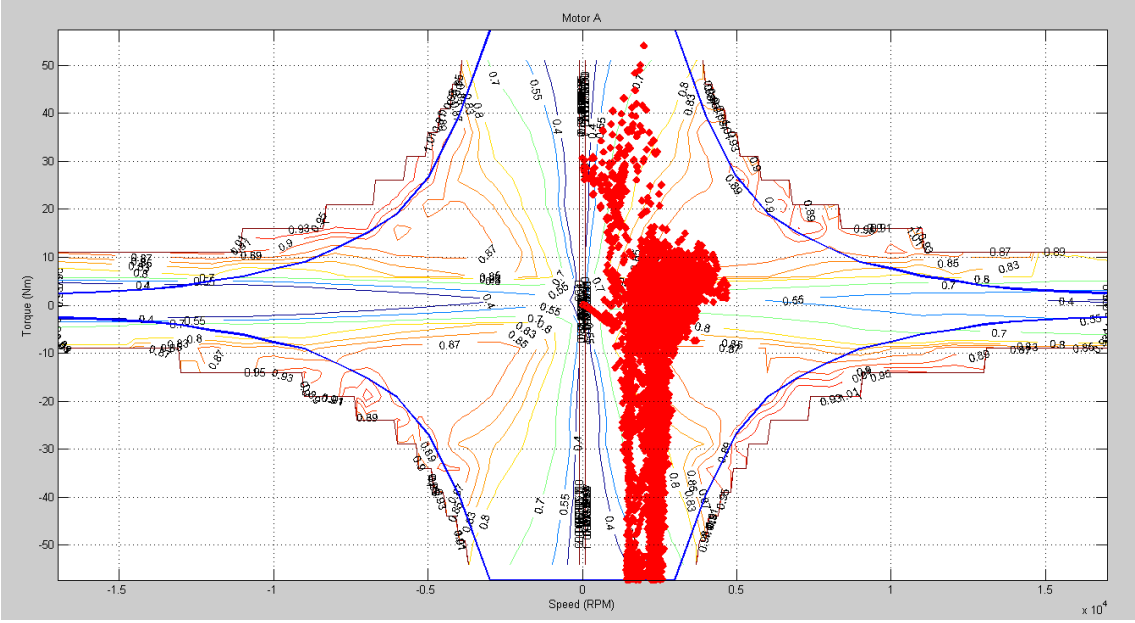

Figure 3.33 - 18 kW machine map with operating points obtained with simulations - set 1.

3.2.2.3.2 Set 2

For this simulation set, it is interesting to see how the operating points of engine and motor generator change from case to case, since the electric contribution increases from the stop-start only to the full BSG case. It is also remarkable to observe the trend of the power profiles during the cycle (or part of that), to see the effect of the electric machine on the output power production.

Figures 3.34 to 3.36 show the engine map for the three simulation cases for the UDDS cycle. The main difference that can be noticed between the first and the other two pictures is that the operating points characterized by high torque and high speed disappear, because of the effect of the electric assist. When high power is requested by the drive cycle and electric assist is present, some of it is provided by the motor generator.

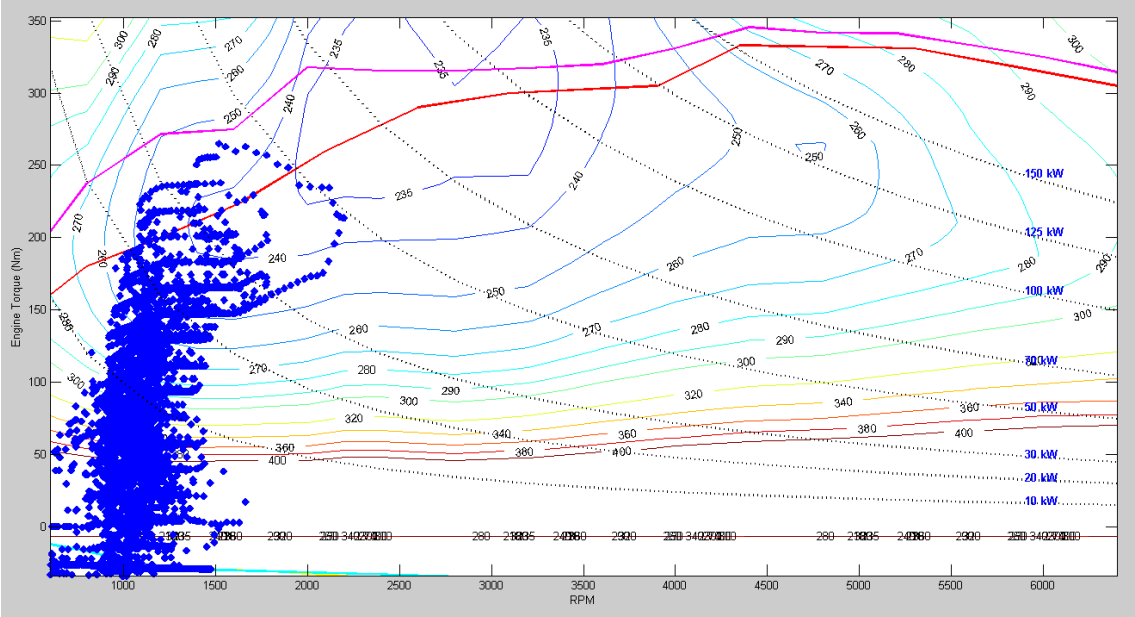

Figure 3.34 - Engine map with operating points obtained with simulations - set 2, Case 1, UDDS.

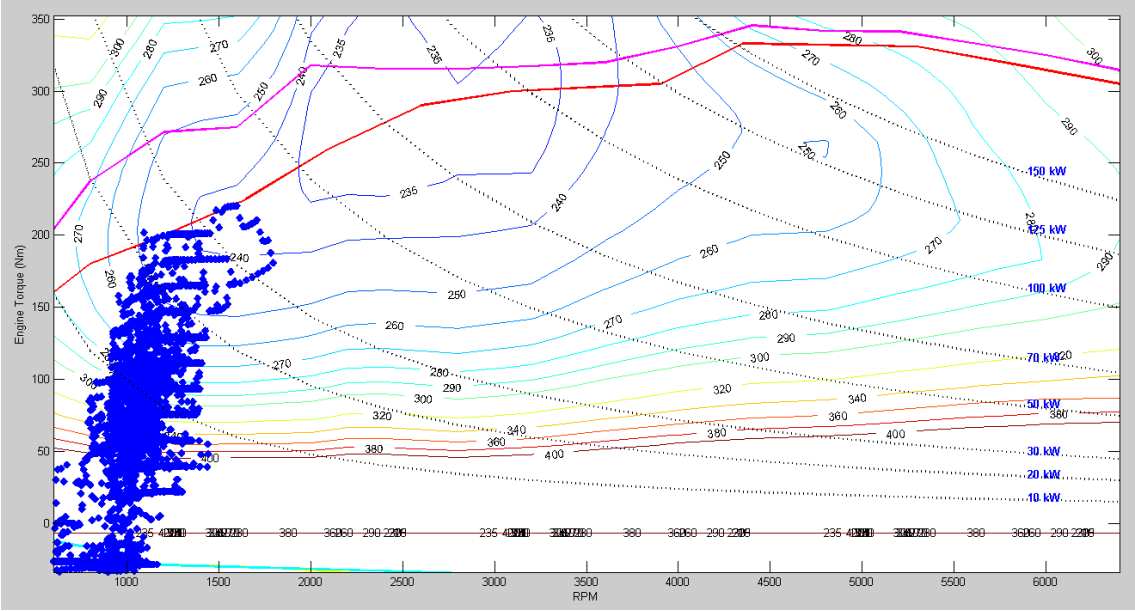

Figure 3.35 - Engine map with operating points obtained with simulations - set 2, Case 2, UDDS.

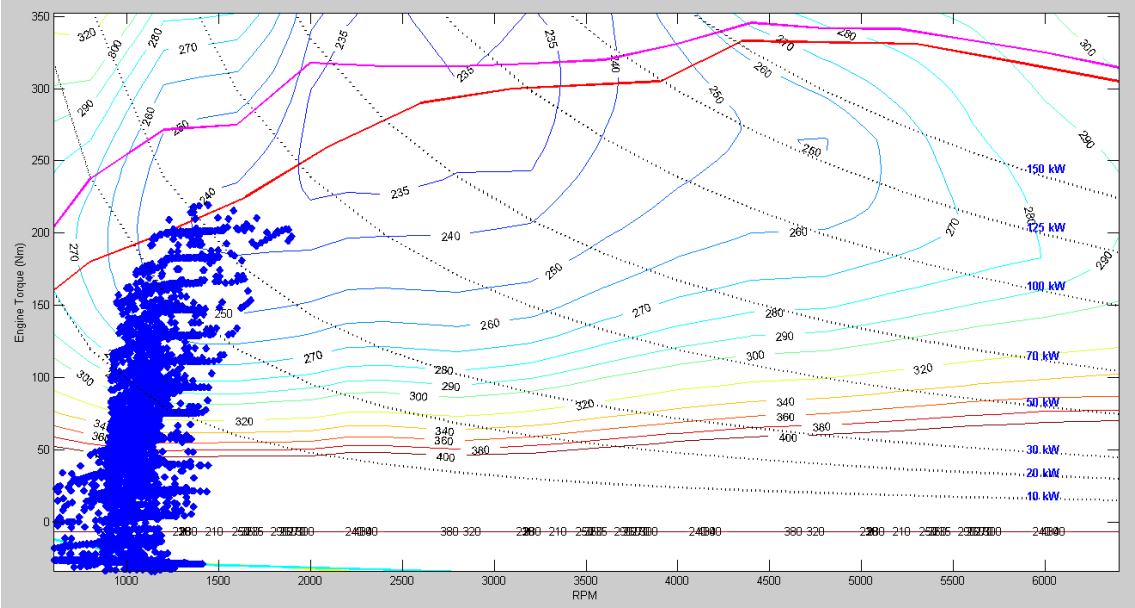

Figure 3.36 - Engine map with operating points obtained with simulations - set 2, Case 3, UDDS.

It is also interesting to see the motor generator map with its operating points for the UDDS (Figures 3.37 to 3.39). It can be clearly seen how the cloud of the operating point grows from Case 1 to Case 2 towards positive torque values due to electric assist, and from Case 2 to Case 3 towards negative values due to regenerative braking. Moving from Case 1 to Case 2 it can be noticed a slight enlargement of the cloud towards negative

torque values as well. This is related to the necessity of the battery to be charged in order to be able to support the electric assist during a subsequent discharge phase. In Case 2 it can only obtained using the engine to run the motor generator as a conventional alternator, thus producing electric energy.

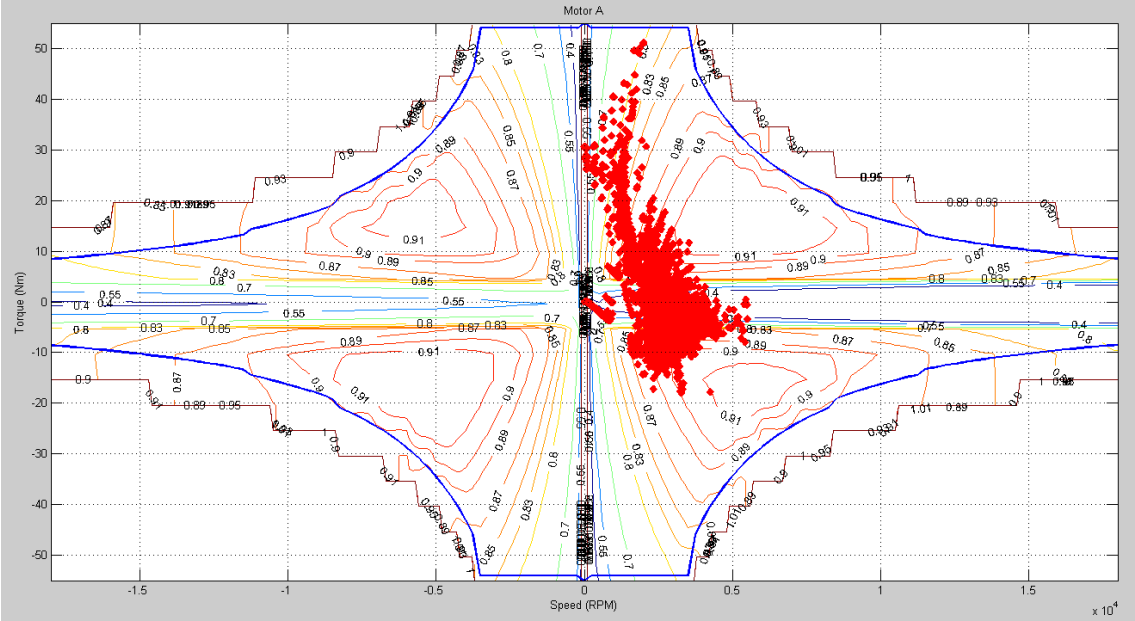

Figure 3.37 - Electric motor map with operating points obtained with simulations - set 2, Case 1, UDDS.

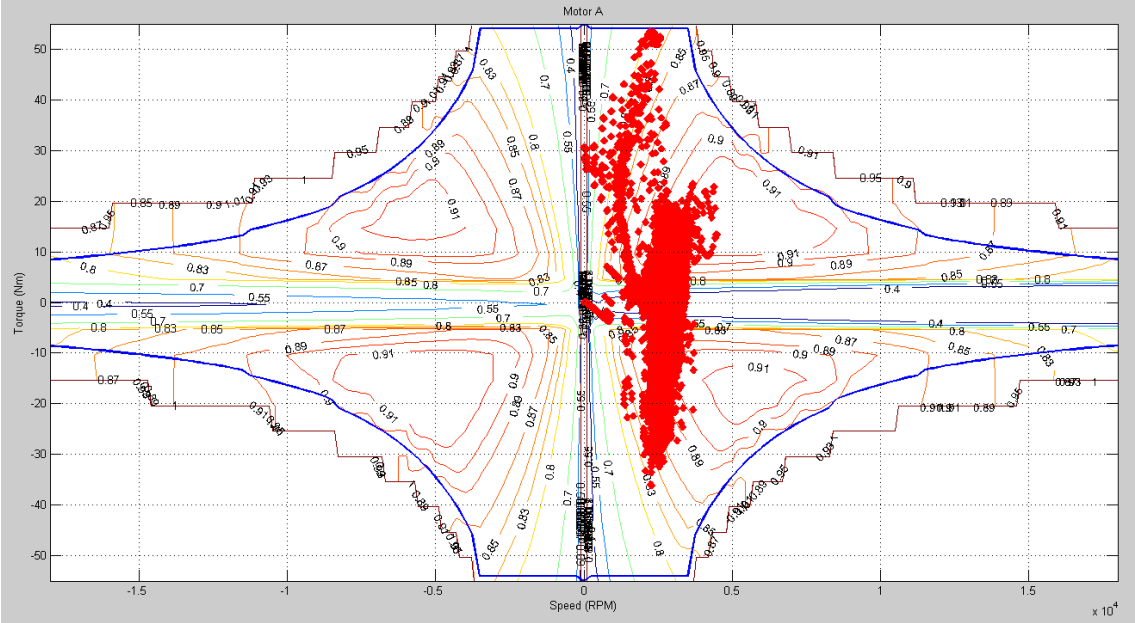

Figure 3.38 - Electric motor map with operating points obtained with simulations - set 2, Case 2, UDDS.

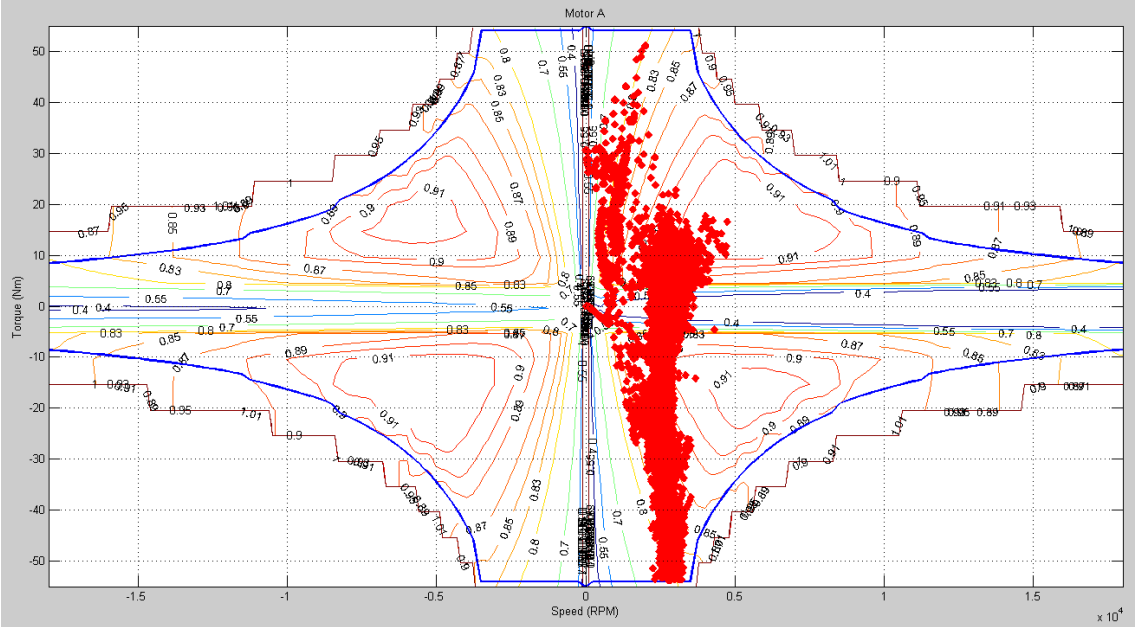

Figure 3.39 - Electric motor map with operating points obtained with simulations - set 2, Case 3, UDDS.

Figures 3.40 to 3.42 show instead the trend of the powers during part of each of the three cycles. For Case 1, the battery power (magenta line) is very close to zero as expected. The electric power in this case is only necessary to drive the electric accessory loads. In Case 2 instead, the battery power starts to have higher fluctuations, but no energy is recovered during braking (the magenta line is close to zero for negative output power (yellow line). Instead, in Case 3 all the potentialities of the BSG are exploited, and the negative power during decelerations indicates the presence of regenerative braking (the battery power during charging is limited to -15 kW, as previously said). Looking at the differences between the cycles, it can be seen that the UDDS and the NEDC present some peaks characterized by high power request (30 kW and more), while in the HWFET the power request is usually lower. As a consequence, the former cycles give more opportunities of using the electric assist, dividing high power requests between engine and electric motor.

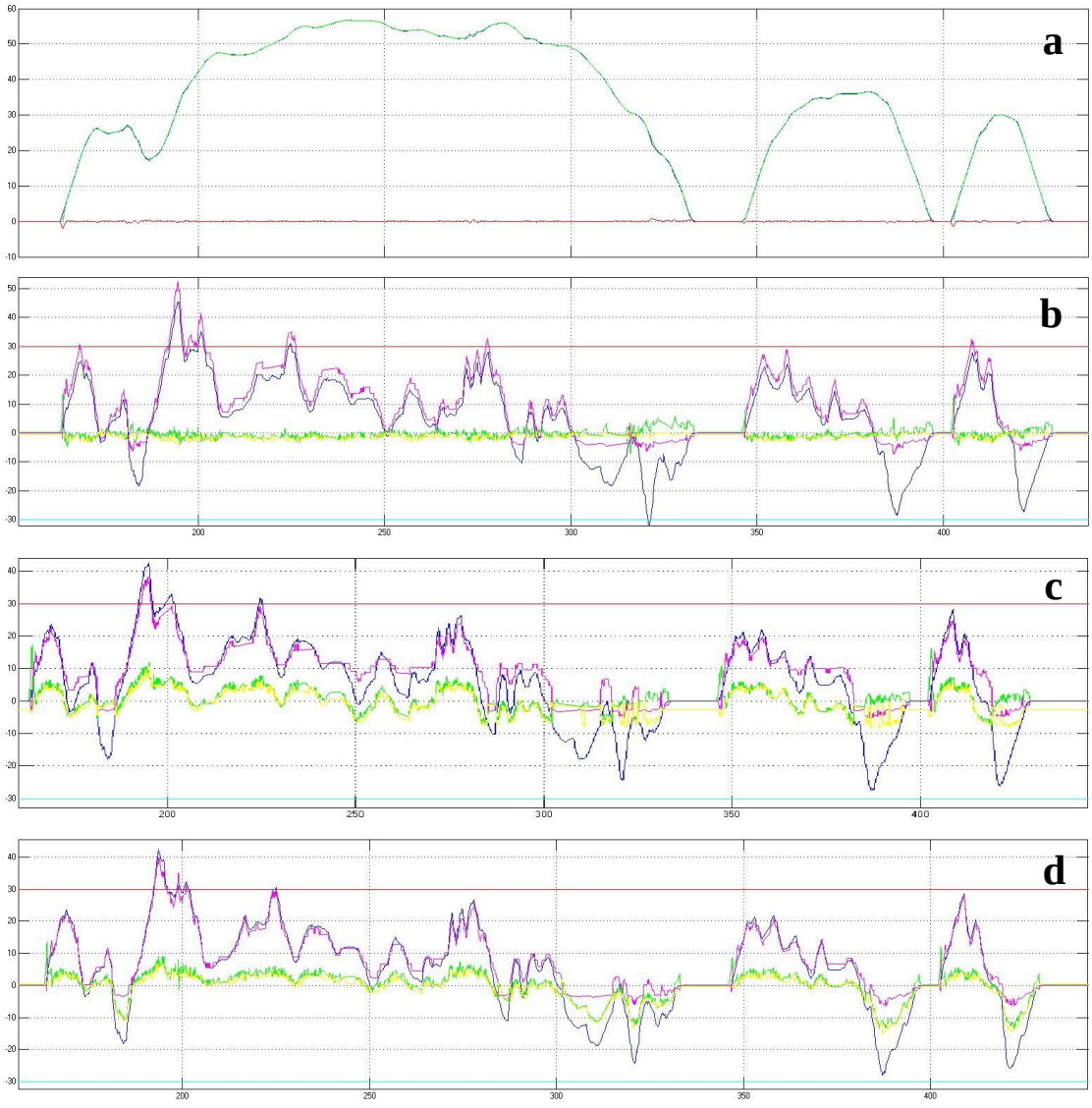

Figure 3.40 - Trend of the powers on UDDS cycle. (a) speed profile [mph]; (b) Case 1 powers [kW]; (c) Case 2 powers [kW]; (d) Case 3 powers [kW]. Blue: output power; magenta: engine power; green: battery power; yellow: desired battery power.

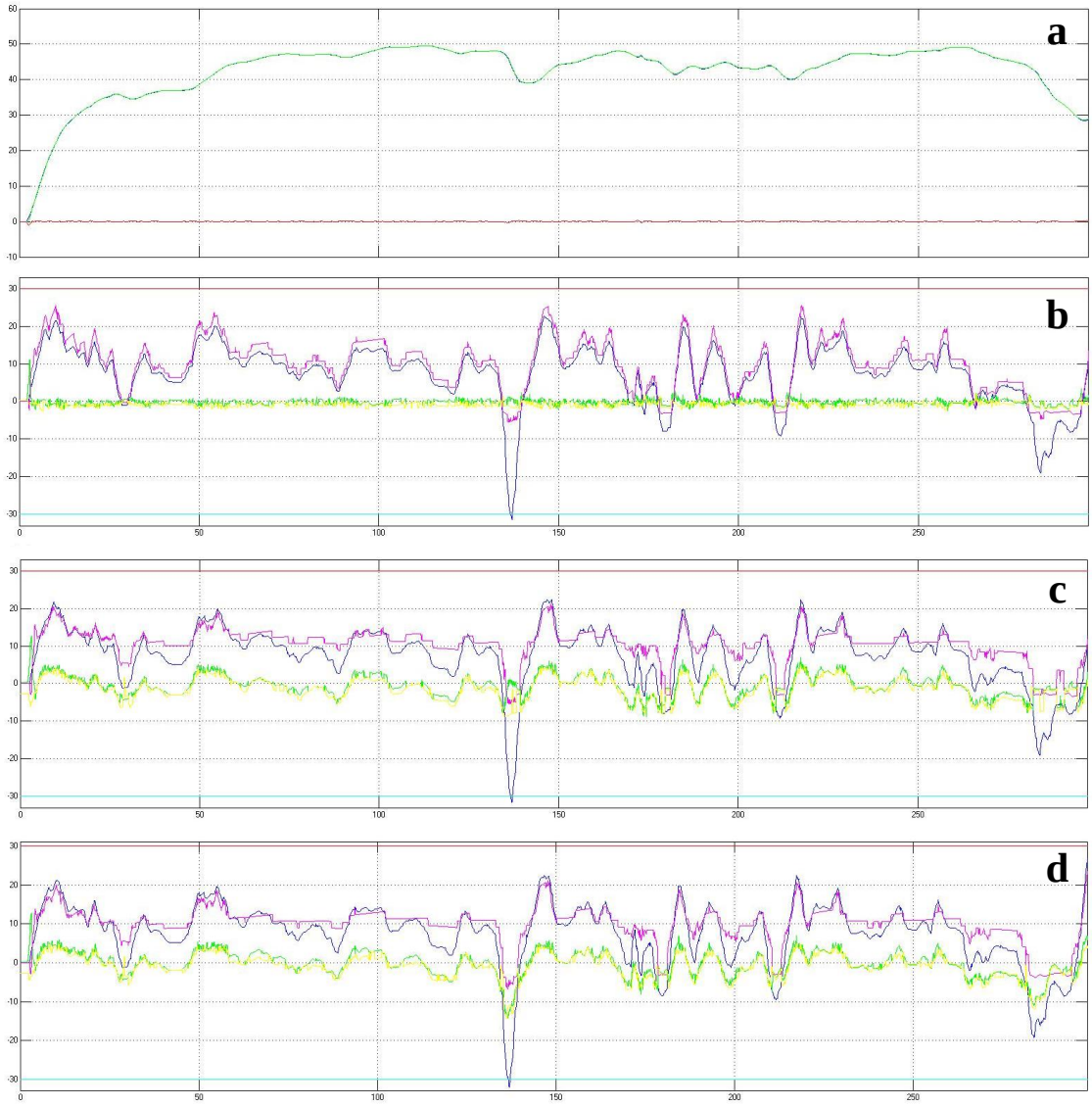

Figure 3.41 - Trend of the powers on HWFET cycle. (a) speed profile [mph]; (b) Case 1 powers [kW]; (c) Case 2 powers [kW]; (d) Case 3 powers [kW]. Blue: output power; magenta: engine power; green: battery power; yellow: desired battery power.

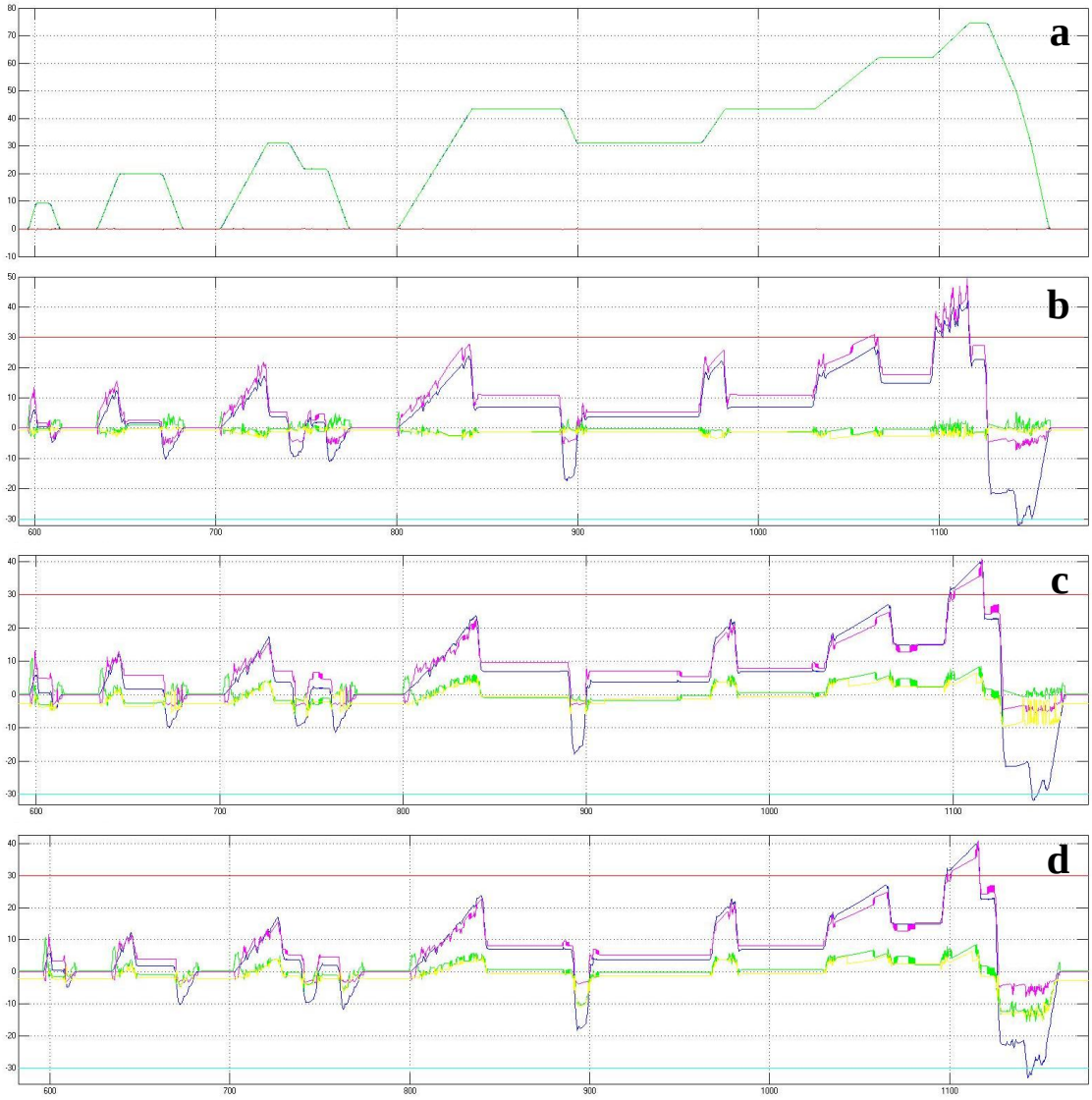

Figure 3.42 - Trend of the powers on NEDC cycle. (a) speed profile [mph]; (b) Case 1 powers [kW]; (c) Case 2 powers [kW]; (d) Case 3 powers [kW]. Blue: output power; magenta: engine power; green: battery power; yellow: desired battery power.

Finally, Figure 3.43 illustrates the trend of the battery SOC for the three cases during the UDDS cycle. The energy exchanged during Case 2 and Case 3 is remarkably higher than in Case 1. It can also noticed that for Cases 2 and 3, after the discharge during hill 2, it takes more time in Case 2 than in Case 3 for the SOC to return to the original value. Regenerative braking allows faster recharges, especially in drive cycles characterized by multiple brake phases, such as the UDDS.

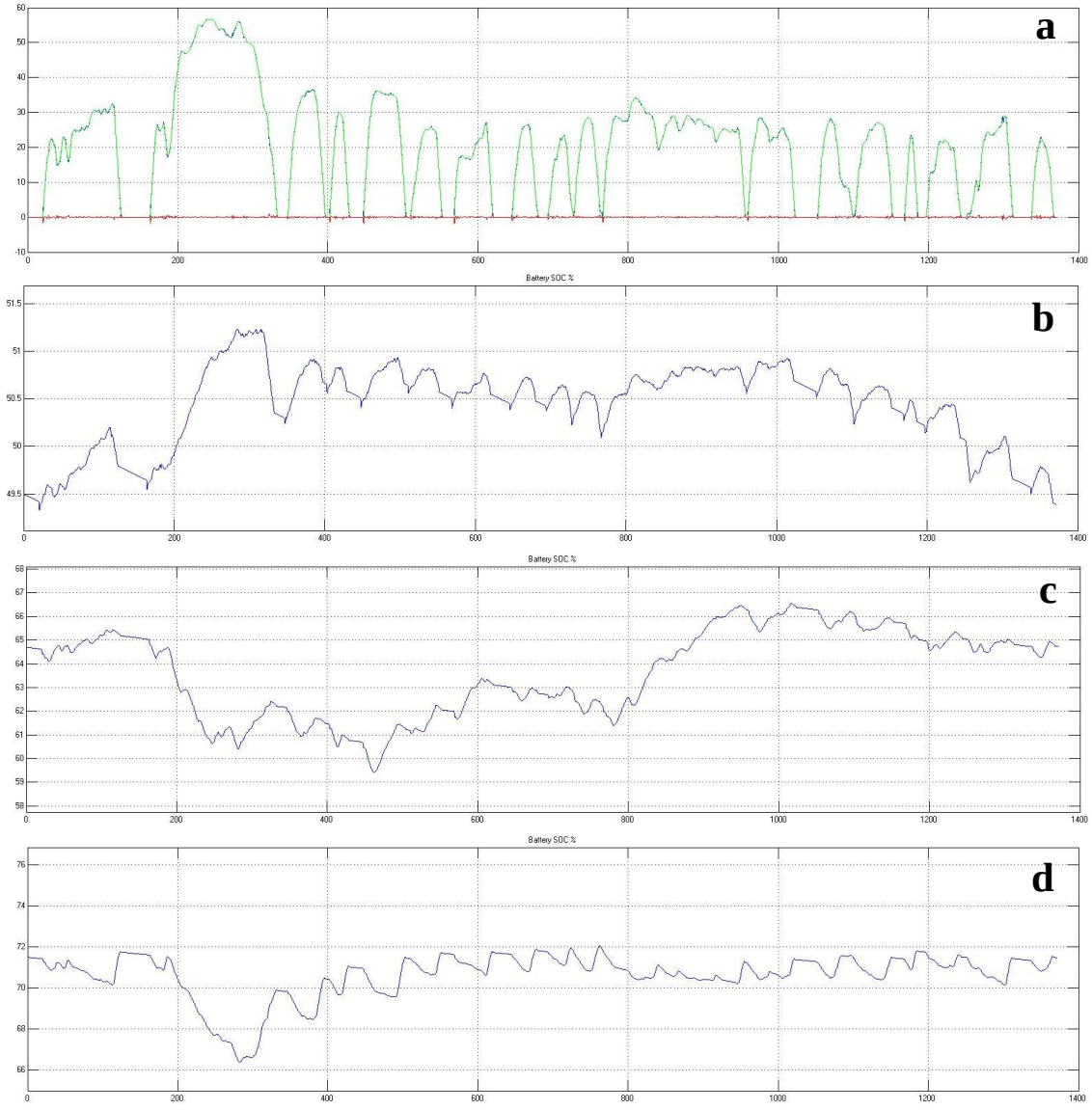

Figure 3.43 - Trend of battery SOC on UDDS cycle. (a) speed profile [mph]; (b) Case 1 SOC [%]; (c) Case 2 SOC [%]; (d) Case 3 SOC [%].

3.2.3 Fuel consumption testing

The last approach for fuel consumption evaluation is through testing on a proof-of-concept hybrid vehicle. The results of the tests will be compared with those obtained from the analytical approach and the simulations for validation purposes. The test car (a full hybrid prototype calibrated to run as BSG vehicle) was placed on a dynamometer, simulating the road loads, and run through a few drive cycles. To estimate the fuel consumption, the exhaust gas was collected from the tailpipe and its chemical composition was analyzed. The following sections describe the vehicle structure and the test setup and process more in detail.

3.2.3.1 Proof-of-concept vehicle description

The vehicle used for the tests is an E-segment, rear-wheel drive (RWD) car, with a powertrain that has been modified to become a parallel full hybrid electric vehicle. It is the same E-segment vehicle for which the parameters have been defined in Table 3.18.

The architecture is composed of the engine and two electric subsystems: an 18 kW Belt Starter Generator (called P1f) on the front end accessory drive and a 30 kW traction motor (called P2) integrated in the transmission. Figure 3.44 shows a simplified sketch of the powertrain, with the two electric machines highlighted, while Figure 3.45 provides a more detailed diagram.

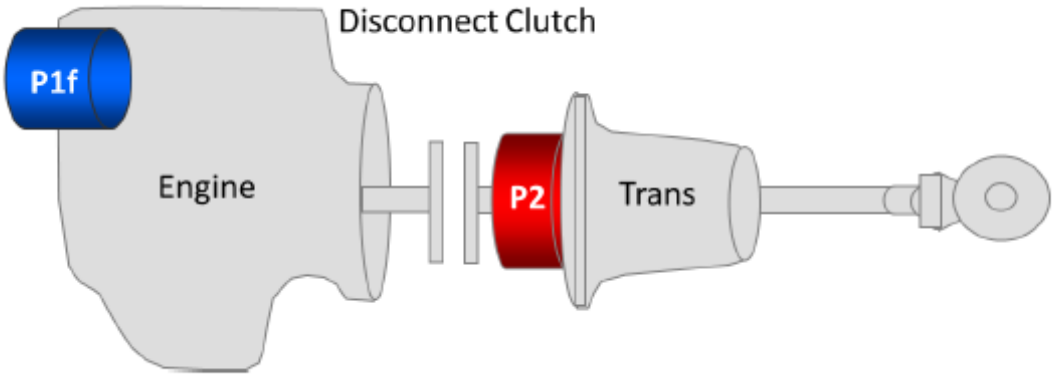

Figure 3.44 - Sketch of the proof-of-concept test vehicle powertrain.
The main electric machines are highlighted.

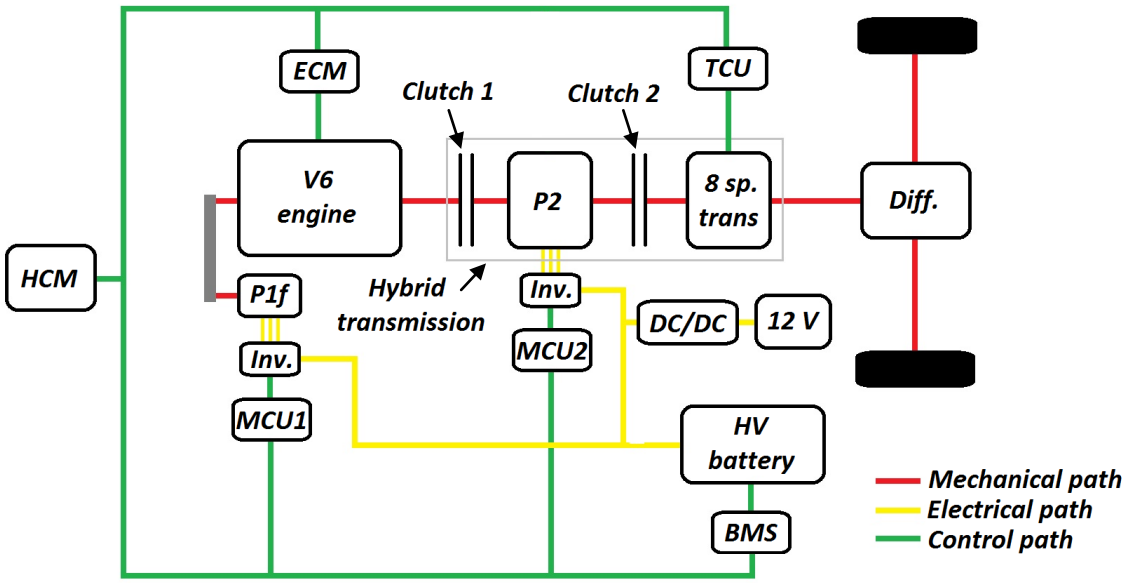

Figure 3.45 - Diagram of the proof-of concept test vehicle architecture.

The BSG is in charge of the stop-start of the engine. This task is made easier by the disconnect clutch, which allows separation of the engine from the rest of the drivetrain. In this way the smoothness of the restart events is improved, since there is no direct connection between engine and wheels. The second electric machine is positioned after the clutch in place of the torque converter, before an eight-speed automatic transmission. This motor is characterized by high torque and high power, and when the clutch is disengaged it allows the vehicle to run in pure electric mode. It can also help P1f to start the engine during cold starts, since in some situations P1f torque may not be enough to overcome the cranking torque of the engine. Finally, the two electric motors can also be coordinated to boost the engine or produce electric energy through regenerative braking.

The parameters of vehicle, engine, motor generator and battery are the same as those shown in Section 3.2.3.1.2, which were used for the simulations.

Figure 3.46 presents a CAD model of the vehicle architecture, where the main components are labeled.

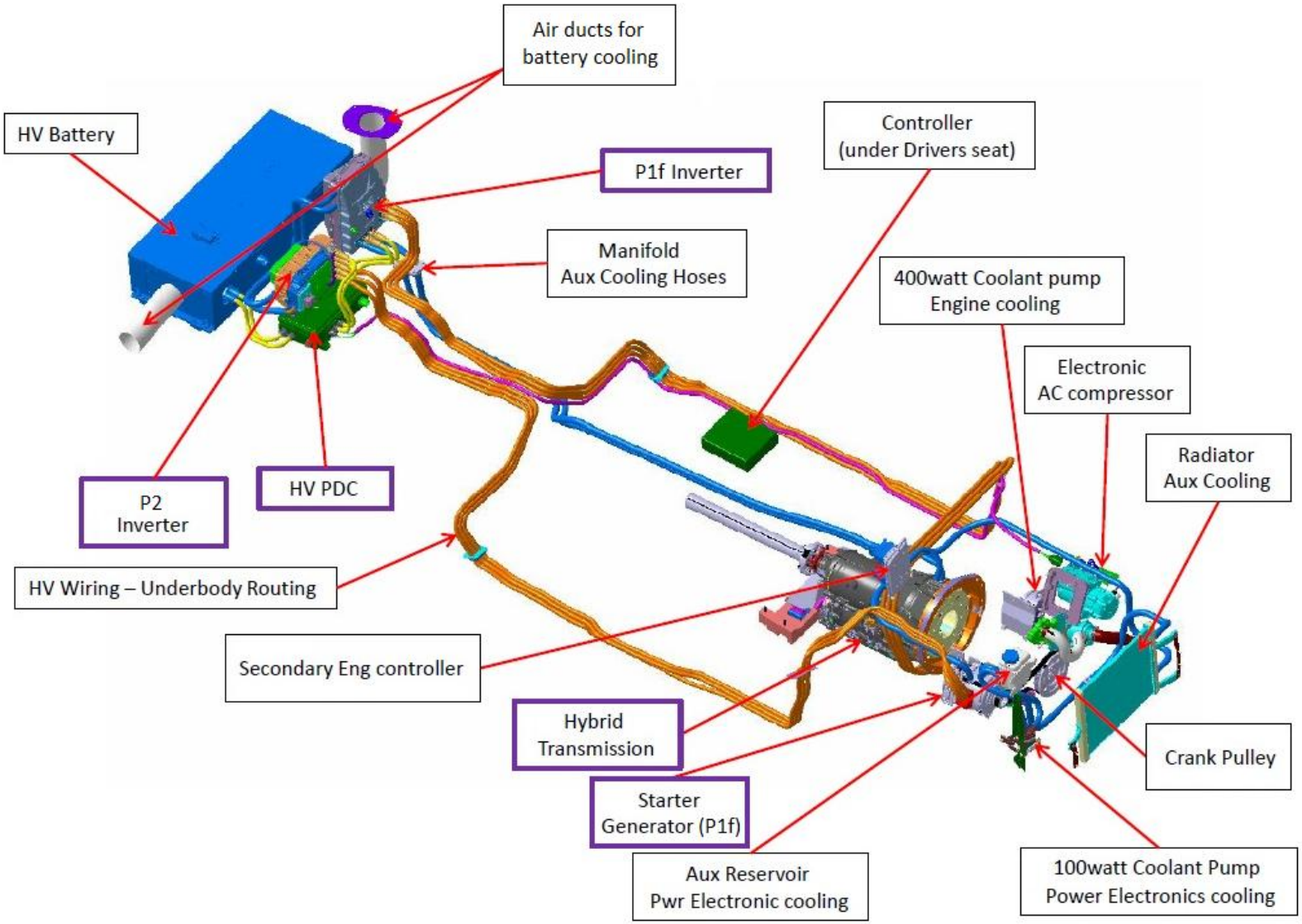

Figure 3.46 - Proof-of-concept test car powertrain layout, with labels of the main components

3.2.3.2 Test setup

Three test cases were scheduled in order to evaluate the effects of the three main BSG functions, i.e., engine stop-start, electric assist and regenerative braking. The procedure was once again to first estimate the fuel consumption benefits with stop-start only, then to add electric assist in order to observe the improvements related to the load shifts, and finally to include regenerative braking. Unfortunately, it was not feasible to test the vehicle as conventional, because the prototype was designed to work as a full hybrid vehicle, and it was impossible to completely get rid of the effects of the clutch and the P2 motor.

Nevertheless, to proceed in the way the tests were scheduled, the test car required modifications in the controls and in the calibrations in order to run it as close as possible to a vehicle equipped with a BSG only. This was not an easy task, since the clutch and the P2 motor introduced complexity in the system.

The original control system launches the car in pure electric mode through P2 motor with the clutch open, and closes the clutch adding the engine contribution when a threshold of either requested power or wheel speed is reached. Instead, in a vehicle equipped with BSG, the engine is firstly cranked and after that the car starts to move. Since the hybrid transmission controls didn't allow closing of the clutch before the vehicle motion, a compromise was found setting the threshold wheel speed for clutch engagement to a very small value (such as 0.1 km/h). The effect was that the car started to creep electrically, and after a very short time interval the engine cranked and the clutch closed.

For the first test, it was almost impossible to completely eliminate electric assist and regenerative braking, so they were limited to very small amounts. This was obtained by modifying the calibrations related to the power going in and out of the battery as a function of the output power levels at the wheels. Anyway, the battery could still be recharged as in a conventional car, using the engine to run the generator and produce electric energy.

For the second test, the calibrations for the outgoing battery power were loosened. The gear shift map was also modified to force the engine to run in the low rpm range,

where engine torque is limited but e-assist can be better exploited, due to the torque-speed characteristic of electric motors (higher torque at lower speed).

Lastly, for the third test, also the calibrations for the ingoing battery power were loosened to increase the level of regenerative braking, and the shift map was kept the same to have good amount of e-assist. In these last two test cases, the calibrations needed to be adjusted in order to obtain battery power limits which resembled those of a vehicle equipped with a 18 kW starter generator.

Adjusting the battery power limits didn't make a distinction on the choice of the electric motor providing e-assist or regenerative braking. As a consequence, both motors are involved in these processes, and this is the reason why it was necessary to introduce these limits on the battery side: the power capability of the two machines summed together was potentially much higher than that of a simple BSG system.

In order to obtain a correct value of fuel consumption at the end of each cycle, it was important to pursue the so-called "charge balance". It means that the SOC level of the battery at the beginning and at the end of a cycle must be the same; if not, the fuel consumption value is offset of a certain amount proportional to the energy added or subtracted to the original energy level of the battery. Usually, the procedure that provides charge balance consists in running each drive cycle twice; at the end of the first cycle, the battery SOC should stabilize at the correct value to achieve charge balance in the subsequent cycle. If a small discrepancy is still present for the second cycle (few percentage points of SOC), the fuel consumption value can be adjusted knowing the characteristics of the battery and the average efficiency of the engine.

The tests were run on a dynamometer in a test cell, and the selected drive cycles were UDDS, HWFET and NEDC. The vehicle drive wheels were placed on the dynamometer roller, which simulated the driving environment. The energy required to move the rollers could be adjusted to account for the road load parameters of the vehicle. A screen placed over the windshield in front of the driver’s seat showed in real time the speed profile of the driving schedule, along with the vehicle “simulated” speed, while a professional driver, acting on the pedals, accelerated and decelerated the vehicle to follow the cycle. Fuel economy tests were performed with the vehicle's air conditioning and other accessories turned off.

Figures 3.47 and 3.48 show the proof-of-concept vehicle on the dynamometer, ready to run the tests.

Figure 3.47 - Proof-of-concept test car on the dynamometer. The screen over the windshield shows the speed profile of the cycle.

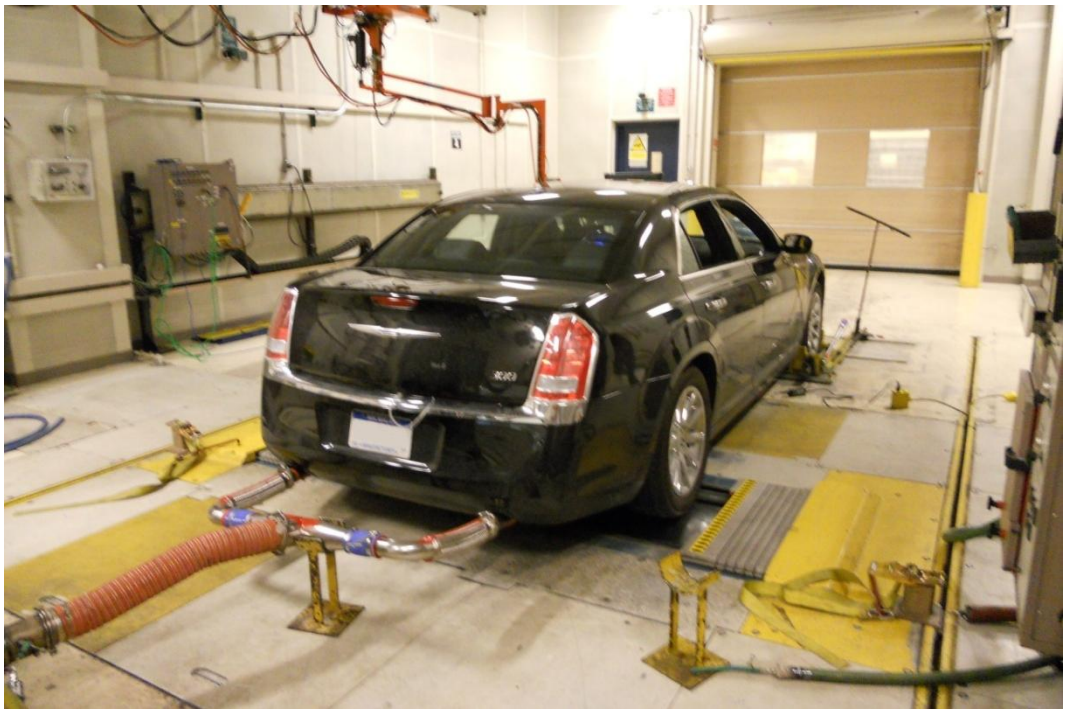

Figure 3.48 - Proof-of-concept test car on the dynamometer. The exhaust collecting hoses can be noticed.

To calculate the fuel consumption for vehicles using carbon-based fuels, such as the one under investigation, a hose was connected to the tailpipe to collect the engine exhaust during the tests. The exhaust gas was chemically analyzed to find the amount of carbon-containing components (i.e., unburned hydrocarbons, carbon monoxide and carbon dioxide). Knowing the chemical composition of the fuel, the quantity of carbon in the exhaust was used to calculate the amount of fuel burned during the test. The EPA claims this method is more accurate than using a fuel-gauge to physically measure the amount of gasoline being burned [61].

3.2.3.3 Preliminary analysis

For these tests it is interesting to show the power trend of engine and battery. Figure 3.49 shows the profiles along the hill 5 of the UDDS cycle for Case 3 ("full" BSG). Here it is possible to see how much battery power is requested to crank the engine and how much power is possible to recover thanks to regenerative braking. Observing the engine power trace, it can be noticed that it becomes negative during deceleration, indicating that the car is in fuel shut-off mode while recovering energy through the electric motors.

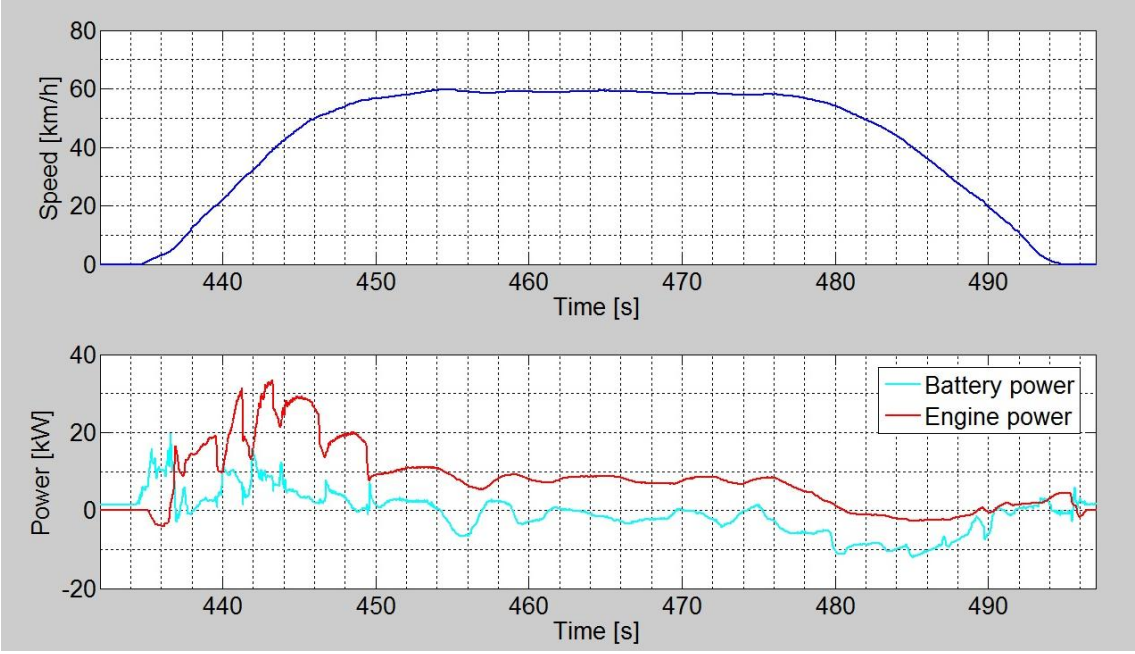

Figure 3.49 - UDDS hill 5 speed profile and battery + engine power trends - Case 3.

Figure 3.50 zooms even more on the starting phase of the hill. Here it can be clearly seen how the engine cranks up. At first, engine power is null, while battery power is stable at a small value to run the accessory loads. Then, the latter starts to increase, and by means of P2 motor the car begins to move, while the engine is still off. When the speed threshold is overcome, the clutch is closed and the engine power increases towards negative values. In this phase the electric machines are motoring the engine (as it can be seen from the increase in battery power). It takes another while for the control algorithm to order the engine to start firing: from this moment on the engine power begins to increase, overshoots and then stabilizes.

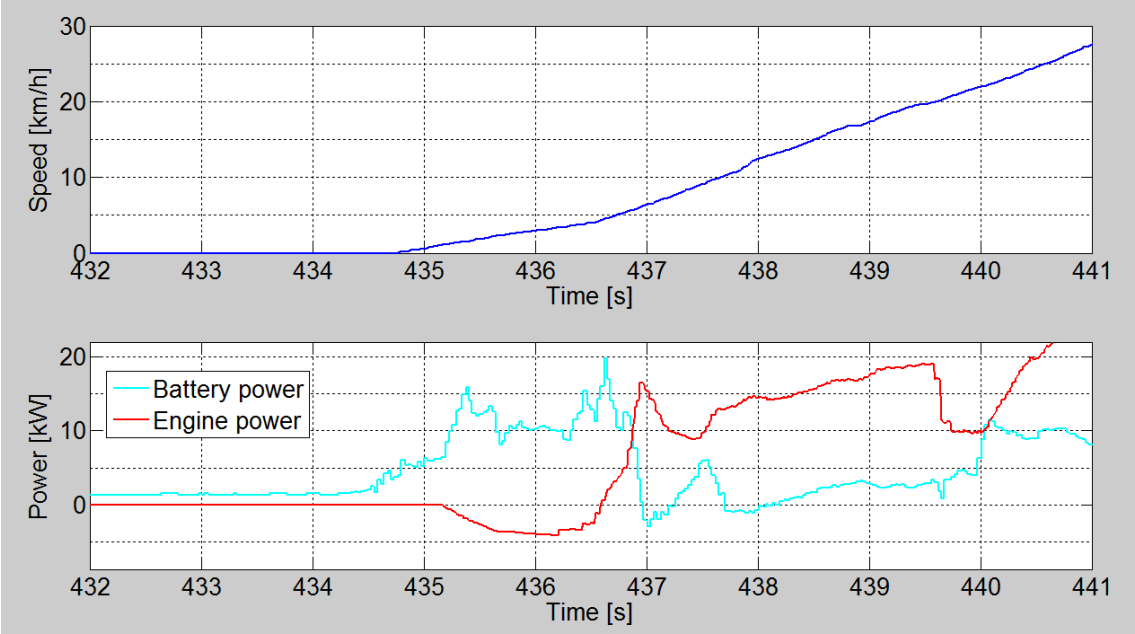

Figure 3.50 - UDDS hill 5 zoom speed profile and battery + engine power trends - Case 3.

From the power data, it is possible to approximately estimate the amount of energy spent to start the engine. During the start-up phase, the battery power is required both to move the car and to crank the engine. Integrating the engine power during motoring, and taking the absolute value, it is possible to calculate the amount of energy that goes from the battery to the engine. To be more precise, the engine spends some more fuel energy to spin up to idle speed, so the integral of engine power between zero and idle power must be also considered, and added to the previous quantity.

This calculation can be extended to the whole cycle to calculate the total cranking energy. Then, assuming a value of idle power and knowing the total amount of time during which the engine is off, the idle energy can be computed. In this way the energy involved in the stop-start strategy can be estimated:

$$E_{stop-start} = E_{idle} - \left|E_{cranking}\right| \tag{3.57}$$

Since it was not possible to test the proof-of-concept vehicle as a conventional, this calculation was used to make a backward projection of the fuel consumption, starting from the fuel consumption obtained in Case 1.

CHAPTER 4

ANALYSIS OF RESULTS

This chapter provides the results of the research and their analysis. As the previous chapter, it is divided into two main sections, related to the two research topics.

In the first section, the results of the engine cranking simulations are shown and analyzed, and the model is validated against experimental test data obtained from the start cart.

In the second part, the fuel consumption results of the three approaches are shown at first singularly and then compared among each other. The contribution of the BSG functions to fuel savings are analyzed and justified, considering also the effect of different vehicle types and calibrations.

4.1 Stop-start performance evaluation and modeling of the belt starter generator system

Some simulations were run to verify the correct functioning of the BSG model. The main purpose of the research was to investigate behavior of the BSG during an engine start in motoring condition, providing as input the electric machine torque versus time and obtaining as output the speed profile of the engine. The influence of different temperature and the occurrence of slip will be analyzed as well. The results will be also compared with engine cranking tests on the start cart for validation purpose.

4.1.1 Simulation results

Figure 4.1 shows an engine start at ambient temperature (20°C). The torque provided as input was in the form of a step, and the values were chosen so that the engine revs up to idle speed (assumed equal to 800 rpm) in 0.4 seconds and then stays at that speed. The oscillations due to the compression pulses can be clearly seen, overlapped with smaller and higher frequency fluctuations due to belt elasticity.

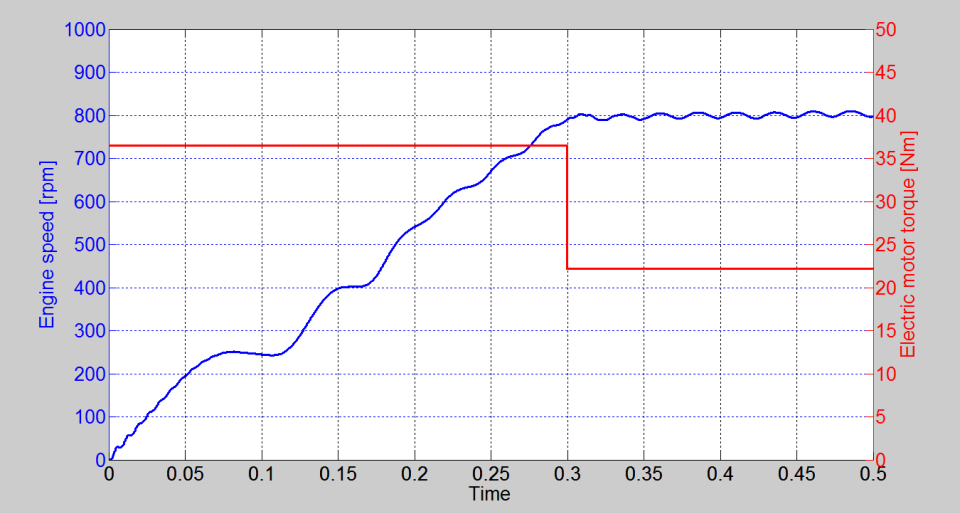

Figure 4.1 - Engine motored start at 20°C. Idle speed is 800 rpm.

Figure 4.2 illustrates how different engine temperatures affect the start. The selected engine temperatures were -40, 20 and 100°C, and the torque was kept the same for the three simulations. Its value was chosen so that during cold start (-40°C) the engine spins up to 800 rpm in 0.4 seconds. It can be noticed that temperature, which affects engine friction, has a major impact on the cranking time. At 20°C it takes 0.21 seconds for the engine to reach idle speed, while at 100°C only 0.15 seconds. It must be however mentioned that in these simulations other effects such as belt slip (which may occur at high acceleration rates) were not considered. Moreover, a very quick cranking usually produce more vibrations than a slower one, so a tradeoff must be found to obtain a rapid but also smooth start.

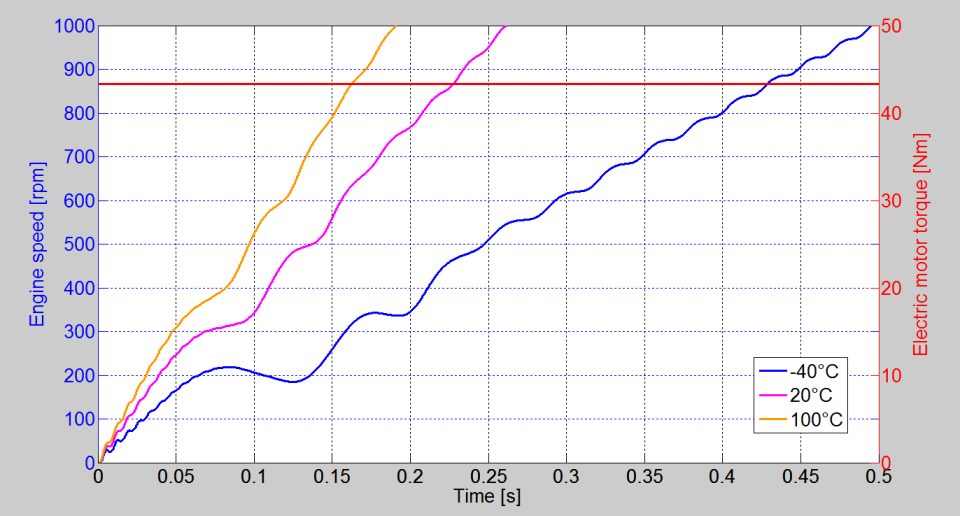

Figure 4.2 - Engine motored start at different temperatures.

In Figure 4.3 the belt slip phenomenon was investigated. The belt static friction capacity of the belt was lowered (to simulate low grip conditions, such as when the belt is wet) and a torque profile equal to that reported in Figure 4.1 was provided to the electric machine. Figure 4.3 shows the speed profiles of engine and motor; the latter was scaled up to overlap with the profile of the engine, in order to observe how much the speeds diverge during slip. In this simulation, slip occurs three times: at very low speed, the motor starts to spin faster than the engine, due to its lower inertia and belt elasticity, until the friction torque at the belt-pulley interface T_f saturates and belt starts to slip; at intermediate speeds it occurs two other times, when the engine generates a higher resistant torque due to air compression in the cylinders (as can be seen by the dips in engine speed), inducing T_f to saturate again.

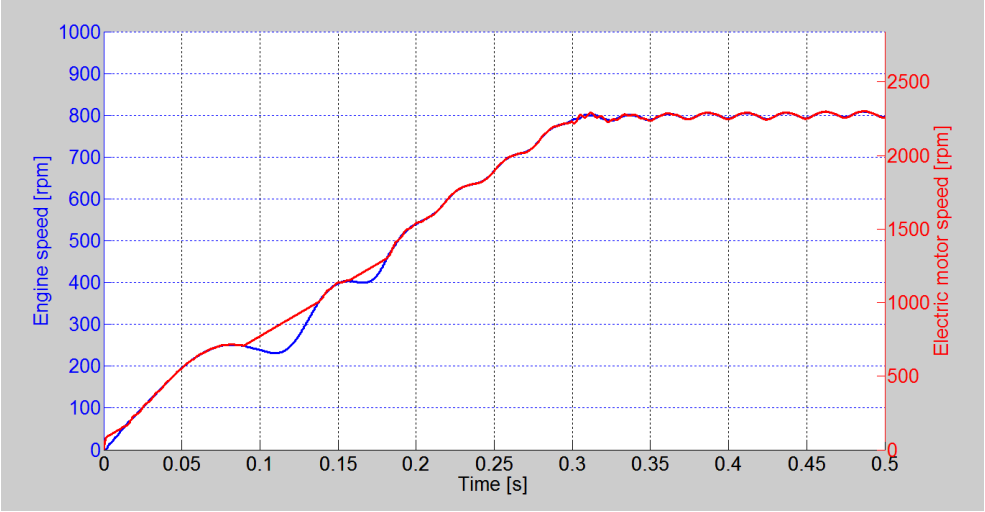

Figure 4.3 - Engine motored start with slip occurrence.

4.1.2 Model validation

Finally, the Simulink model was validated against experimental data from the start cart. The motor torque of the experimental test was imported in the model and used as input. Engine speed profiles from simulation and test were then compared. The results are shown in Figure 4.4.

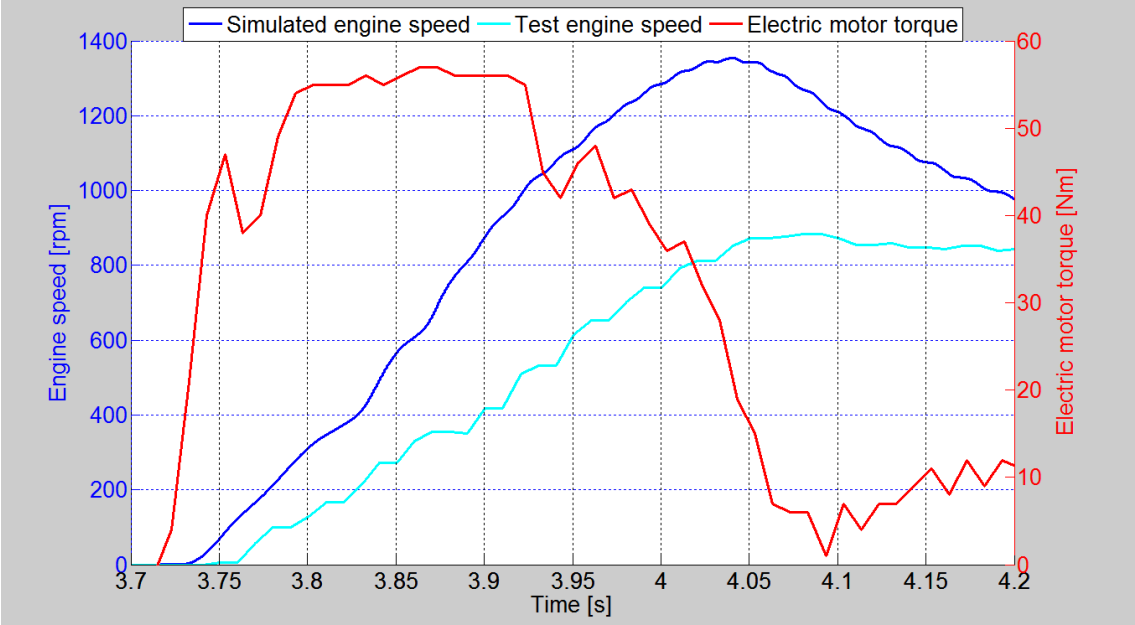

Figure 4.4 - Validation of the model.

Unfortunately, it can be noticed that the matching of the data is very poor. The experimental speed has a longer delay before it starts to increase, and the acceleration rate is lower than for the simulation profile; therefore, simulated speed reaches a much higher peak speed (1450 rpm vs. 900 rpm). Another major difference is that while experimental speed keeps constant at idle once motor torque is reduced, simulated speed instead decreases, indicating that the experimental motor torque during idle is not sufficient to balance the resistant torques in the model. The discrepancy in the speed profiles can be related to a combination of the following factors:

- assumptions in constructing the model: the model was built with some simplifications; for example, the tensioners were not considered, and this may have induced a different behavior of the system at very low speed, where the displacement of the tensioners is not negligible; moreover, the higher acceleration obtained in the simulation may be related to the fact that the inertia torque of the reciprocating masses was neglected, leading to an underestimation of the overall engine inertia;
- engine data: some of the data related to the engine used in the model were obtained with test setups different from the start cart, which produced the

experimental data for the validation; as a consequence, data such as engine inertia, friction torque and compression pulses may be incorrect;

- input resolution: as it can be noticed in Figure 4.4, electric motor resolution is quite low, which may have caused the loss of some high frequency components; in this case, such aspect would be reflected in the simulated speed profile with a loss in accuracy.

In conclusion, the mismatch of the data can be reduced if the factors just described are tackled and solved. Some of them may have a greater impact than others on the simulation results. For instance, it's very likely that a remarkable improvement would be attained if a new experimental test is run using the start cart setup and the collected data are used to calibrate the engine model in Simulink. Once the model is capable to correctly simulate engine start condition, it can also be extended to simulate complete engine stop-start events. If the speed oscillations are accurately predicted, a control strategy for the electric motor can be developed, capable of starting and stopping the engine rapidly with no or little unwanted vibrations.

4.2 Fuel consumption analysis: results and discussion

This section presents the main results of the fuel consumption simulations and the tests which were described in Chapter 3. For all the considered cases, and for all the types of approaches (analytical, simulations and tests) the obtained fuel consumption values will be provided and compared. For the cases in which the purpose was to assess the improvements in fuel consumption due to stop-start, electric assist and regenerative braking, it will be interesting to observe the different contributions and compare absolute and relative values.

The fuel consumption results will be presented in the same order the three approaches were described: firstly, the outcomes of the analytical approach will be shown, followed by the simulation results, both for the first and second set; then, the results obtained in the tests will be introduced. All of them will be discussed and compared, and the test results will be used to validate the models used for the simulations.

The proof-of-concept test car was actually a full HEV which was modified to run as if it was equipped with a BSG only. To show the potential of the vehicle when run as a full hybrid, the fuel consumption results in this configuration (i.e., taking advantage of the whole capability of the two electric motors and of a specific control strategy) will be reported as well.

4.2.1 Analytical approach results

This approach was developed to analytically predict the fuel consumption improvements related to the BSG and its features. The study cases introduced the BSG features one at a time: knowing the fuel consumption of the conventional vehicle to be used as reference (Case 0), the fuel economy related to stop-start only was estimated first (Case 1), then electric assist was added in order to observe the improvements related to the load shifts (Case 2), and finally regenerative braking was included (Case 3). Table 4.1 reports the study cases in a schematic form.

Table 4.1 - Fuel consumption study cases

	Case 0 (conventional)	Case 1	Case 2	Case 3
Engine stop-start	✗	✓	✓	✓
Electric assist	✗	✗	✓	✓
Regenerative braking	✗	✗	✗	✓

In the following, the main parameter variations that were operated to switch from one case to another are recalled:

- Weight: the BSG contribution in Case 1, 2 and 3 was assumed to come with a weight increase due to the heavier components that make up this system (battery, motor-generator, water cooled power electronics). The weight increase was assumed to be of 70 kg.

- Idle engine power: moving from Case 0 to the following cases, the vehicle turned the engine off during idle, so idle engine power and the related fuel consumption were set to 0.
- Engine efficiency: the engine efficiency was assumed to vary from case to case, according to Table 3.10. The values were obtained from tests on a vehicle running with a V6 3.6 liter engine, taking into account the differences in calibrations occurring among the four study cases.
- Maximum regenerative braking power: when regenerative braking has been introduced in Case 3, a limit on the regenerative power at the wheels must be set, taking into account battery and motor-generator capabilities. At first sight, the bottleneck was represented by the maximum charging power of the battery, assumed equal to 15 kW. Actually, this power could not be reached, because during decelerations the engine speed is usually kept low (for comfort issues), so the motor-generator, mechanically linked to the crankshaft, runs in low speed regions as well, where the maximum achievable power is lower than in the constant power region. The bottleneck was then represented by the motor-generator. Moreover, regenerative braking is usually disabled at very low vehicle speeds (lower than 5 km/h) because of difficulties in the control of the motor-generator. These and other factors constrain the maximum available regenerative power, which also could be time dependent (because of thermal protection issues of motor and battery). For these reasons, such parameter is very hard to predict. Anyways, in the effort of taking into account all the constraints, the maximum regenerative braking power was set to be constant and equal 10 kW at the wheels.

Tables 4.2 to 4.5 show the fuel consumption values for each vehicle, study case and drive cycle, along with the absolute variation of each case from the previous one and the corresponding percentage variation relative to Case 0, defined as:

$$\%\ \text{variation} = \frac{fc_i - fc_{i-1}}{fc_0} \tag{4.1}$$

Table 4.2 - Fuel consumption results obtained with analytical approach - D-segment 1.

D-segment 1				
$\left[\frac{l}{100km}\right]$	**Case 0 (conventional)**	**Case 1 (Case 0 + stop-start)**	**Case 2 (Case 1 + e-assist)**	**Case 3 (Case 2 + regen)**
UDDS	8.49	7.54	6.78	6.00
	Abs. variation →	- 0.85	- 0.76	- 0.78
	% variation →	- 10.14 %	- 9.05 %	- 9.27 %
HWFET	5.24	5.26	4.89	4.82
	Abs. variation →	+ 0.04	- 0.47	- 0.07
	% variation →	+ 0.49 %	- 7.12 %	- 1.42 %
NEDC	7.94	6.85	6.49	5.76
	Abs. variation →	- 1.08	- 0.46	- 0.64
	% variation →	- 14.67 %	- 5.84 %	- 8.00 %

Table 4.3 - Fuel consumption results obtained with analytical approach - D-segment 2.

D-segment 2				
$\left[\frac{l}{100km}\right]$	**Case 0 (conventional)**	**Case 1 (Case 0 + stop-start)**	**Case 2 (Case 1 + e-assist)**	**Case 3 (Case 2 + regen)**
UDDS	8.91	8.05	7.24	6.51
	Abs. variation →	- 0.85	- 0.81	- 0.74
	% variation →	- 9.58 %	- 9.11 %	- 8.24 %
HWFET	5.65	5.68	5.28	5.22
	Abs. variation →	+ 0.04	- 0.40	- 0.06
	% variation →	+ 0.45%	- 7.11 %	- 0.99 %
NEDC	8.47	7.48	6.88	6.26
	Abs. variation →	- 1.09	- 0.50	- 0.62
	% variation →	- 12.82 %	- 5.88 %	- 7.42 %

Table 4.4 - Fuel consumption results obtained with analytical approach - E-segment.

E-segment				
$\left[\frac{l}{100km}\right]$	**Case 0 (conventional)**	**Case 1 (Case 0 + stop-start)**	**Case 2 (Case 1 + e-assist)**	**Case 3 (Case 2 + regen)**
UDDS	9.25	8.40	7.55	6.80
	Abs. variation →	- 0.85	- 0.85	- 0.76
	% variation →	- 9.21 %	- 9.15 %	- 8.20 %
HWFET	5.78	5.81	5.49	5.44
	Abs. variation →	+ 0.04	- 0.41	- 0.07
	% variation →	+ 0.44 %	- 7.12 %	- 1.14 %
NEDC	8.72	7.64	7.12	6.46
	Abs. variation →	- 1.08	- 0.52	- 0.65
	% variation →	- 12.44 %	- 5.91 %	- 7.51 %

Table 4.5 - Fuel consumption results obtained with analytical approach - SUV.

SUV				
$\left[\frac{l}{100km}\right]$	**Case 0 (conventional)**	**Case 1 (Case 0 + stop-start)**	**Case 2 (Case 1 + e-assist)**	**Case 3 (Case 2 + regen)**
UDDS	12.20	11.44	10.20	9.56
	Abs. variation →	- 0.85	- 1.14	- 0.64
	% variation →	- 7.01 %	- 9.47 %	- 5.24 %
HWFET	8.75	8.77	8.15	8.14
	Abs. variation →	+ 0.02	- 0.62	- 0.01
	% variation →	+ 0.28 %	- 7.12 %	- 0.14 %
NEDC	11.78	10.69	9.97	9.41
	Abs. variation →	- 1.09	- 0.72	- 0.66
	% variation →	- 9.22 %	- 6.14 %	- 5.59 %

For illustrative purposes, Figure 4.5 and 4.6 show how much each function of the BSG (stop-start, electric assist and regenerative braking) contributes to the reduction of fuel consumption, according to the results of the analytical approach. The illustrated case refers to the E-segment car (which is the same used for the simulations and tests), and the data are represented both as absolute and percentage values.

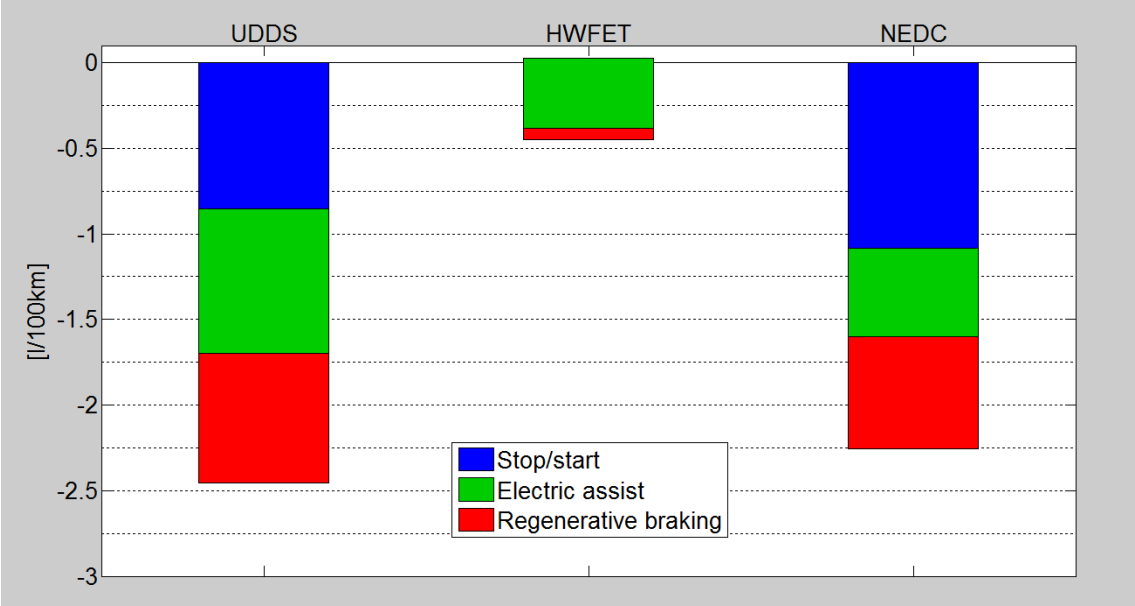

Figure 4.5 - Contribution of BSG functions on fuel savings - analytical approach, absolute values.

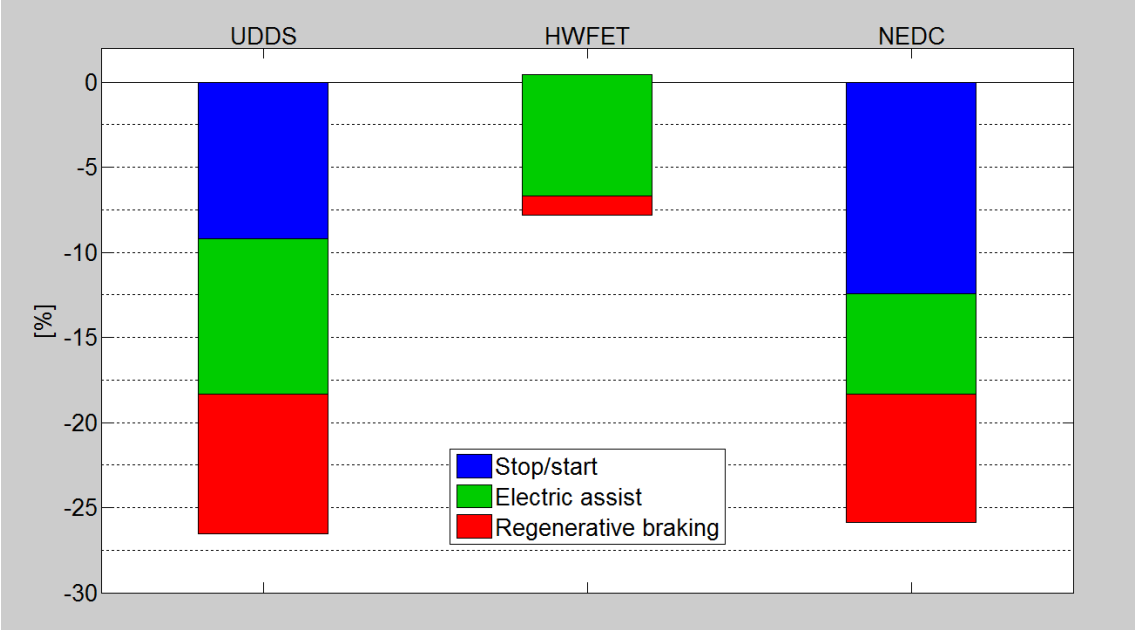

Figure 4.6 - Contribution of BSG functions on fuel savings - analytical approach, relative values.

It can be noticed that in the HWFET cycle, Case 1 fuel consumption is higher than Case 0 (the blue bar is not visible because covered by the green one). This happens because the weight increase which was assumed for the BSG outbalanced the savings related to stop-start (which however were quite small for this type of drive cycle). For UDDS and NEDC, the fuel consumption reduction associated with stop-start is proportional to the idle time of the cycles (UDDS has 244 second of idle against 257 of NEDC).

The savings related to electric assist represent a large portion in the overall fuel economy. They will be compared with those obtained with simulations and tests to check if they were overestimated in the analytical approach. The fuel consumption reductions associated with regenerative braking depends heavily on the assumed maximum regenerative braking power, but when compared among each cycle they seem sensible, because the red areas are proportional to the number of brakings of the respective cycles (UDDS presents the most numerous and aggressive decelerations, followed by NEDC; HWFET instead is characterized by very few decelerations, so the space for improvement is quite limited).

Table 4.6 shows the overall absolute and percentage variations of the "full" BSG version (Case 3) with respect to the conventional one (Case 0), for all the considered vehicles and drive cycles. Figure 4.7 illustrates in the form of bar plots the fuel consumption of each vehicle under investigation in the conventional and BSG versions over the three cycles.

Table 4.6 - Absolute and percentage fuel consumption variations between Case 0 and Case 3, for the analytical approach.

Variation Case 0 → Case 3				
$\left[\frac{l}{100km}\right]$	**D-segment 1**	**D-segment 2**	**E-segment**	**SUV**
UDDS	-2.49	-2.40	-2.46	-2.64
	-28.47%	-26.92%	-26.55%	-21.61%
HWFET	-0.42	-0.44	-0.45	-0.60
	-7.95%	-7.66%	-7.80%	-6.71%
NEDC	-2.18	-2.20	-2.25	-2.47
	-27.49%	-26.02%	-25.86%	-20.94%

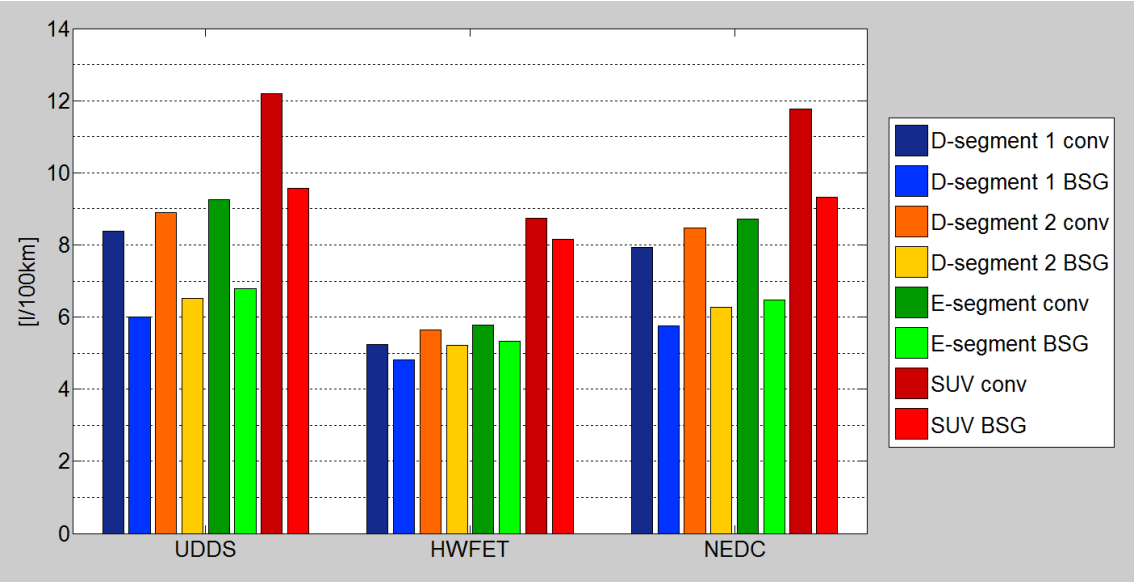

Figure 4.7 - Bar plots showing the fuel consumption results of the analytical approach.

As it was expected from the road load resistance of each vehicle (Figure 3.20), it can be noted that moving up of segment size, from the D-segment to the SUV, the fuel consumption increases. Furthermore, the absolute value of the fuel savings from conventional to BSG increases with the size of the car (it is maximum for the SUV), but the percentage value reduces instead. From these results, it looks like the benefits

introduced by BSG are more effective on smaller size vehicles, since the percentage improvement is higher for them. Nevertheless, the use of BSG on bigger size vehicles like SUVs, which usually have worse fuel consumption, could be a smart way to save on fuel. In fact, they have a greater potential to better exploit regenerative braking due to their heavy weight, so if the size of the components are intelligently studied and the limits on regenerative braking power can be increased, fuel consumption will further benefit.

4.2.2 Simulation results

4.2.2.1 Set 1

This simulation set was focused on the sensitivity analysis of different vehicles and powertrain components on fuel consumption. All the cases considered a vehicle equipped with a Belt Starter Generator, so the components changed in this analysis were engine, motor-generator and battery (see Table 3.16 for details about the study cases).

The first two study cases compared two different D-segment vehicles, corresponding to the simulation study cases "Veh1" and "Veh2". The first vehicle (D-segment 1) is characterized by a lower road load resistance at each speed, as it can be noted in Figure 4.8.

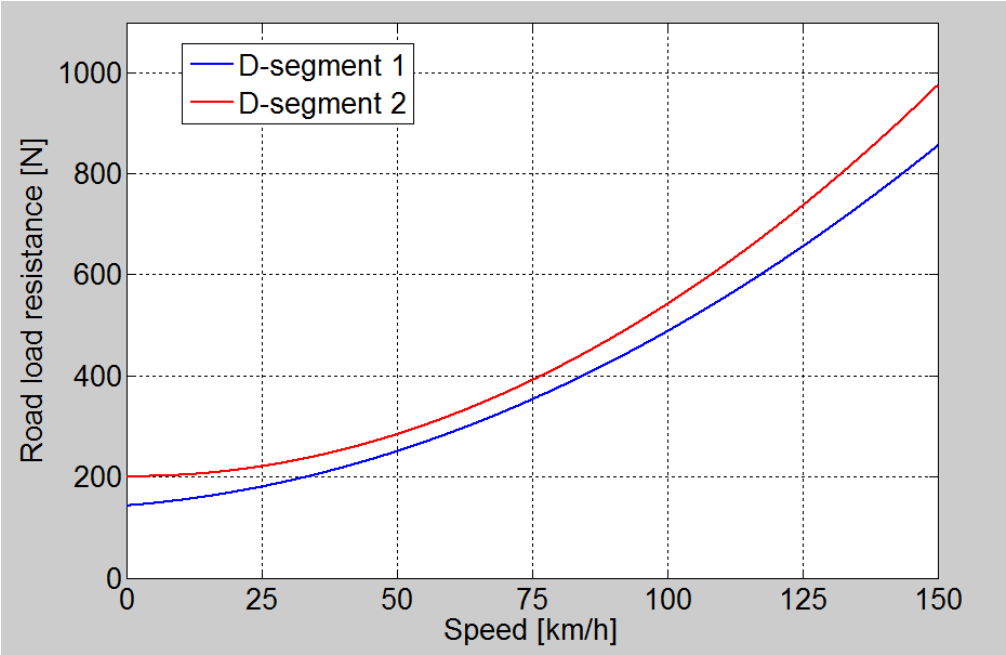

Figure 4.8 - Road load resistance curves of the vehicles analyzed with simulations - set 1.

This aspect, with all the other components being equal, causes a lower fuel consumption for vehicle D-segment 1 than for D-segment 2 (see Table 4.7 and Figure 4.9).

Table 4.7 - Fuel consumption results of the vehicle comparison obtained with simulations - set 1.

Vehicle comparison		
Vehicle	D-segment 1	D-segment 2
Fuel consumption [l/100km]	6.67	7.48

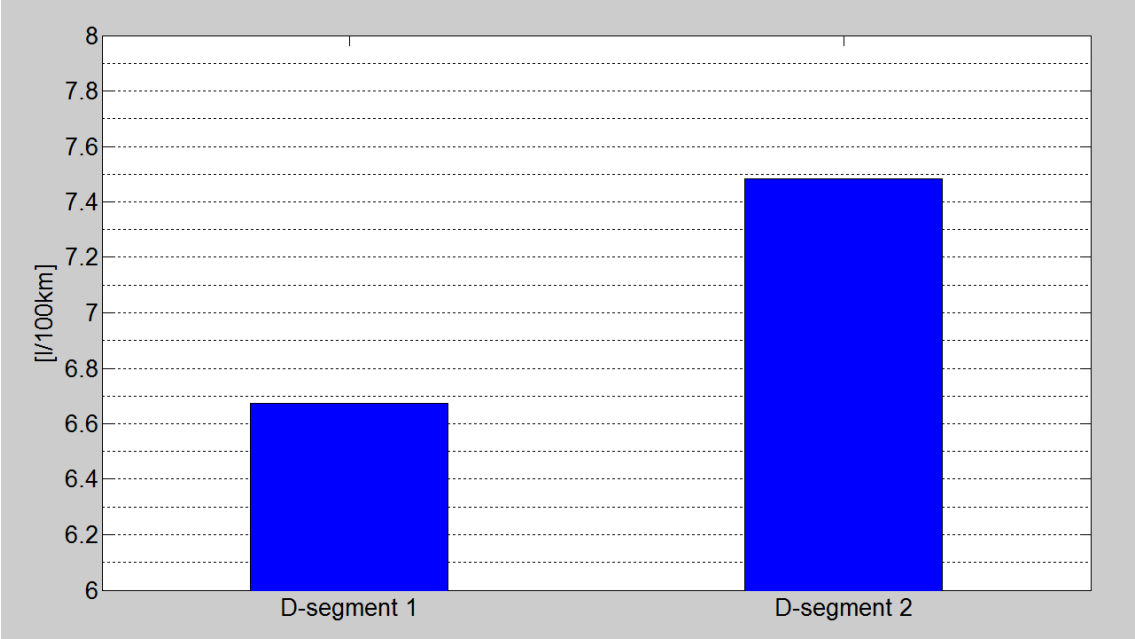

Figure 4.9 - Bar plots showing the results of the vehicle comparison with simulations - set 1.

Next, five different engine types were simulated using an E-segment as vehicle base (study cases from "Eng1" to "Eng5"). The engine characteristics have been shown in Table 3.10. As it was expected, the fuel consumption increased with the engine displacement. Obviously, the engine displacement has also a major impact on the vehicle performance, so acceleration simulations were run as well. Table 4.8 and Figure 4.10 show the results of fuel consumption and 0-100 km/h time for each engine.

Table 4.8 - Fuel consumption results of the engine comparison obtained with simulations - set 1.

Engine comparison					
Engine displacement	1.8 L	2.4 L	2.4 L turbo	3.6 L	5.7 L
Fuel consumption [l/100km]	6.17	6.22	6.28	6.81	8.12
0-100 km/h time [s]	14.40	9.95	6.75	7.05	5.65

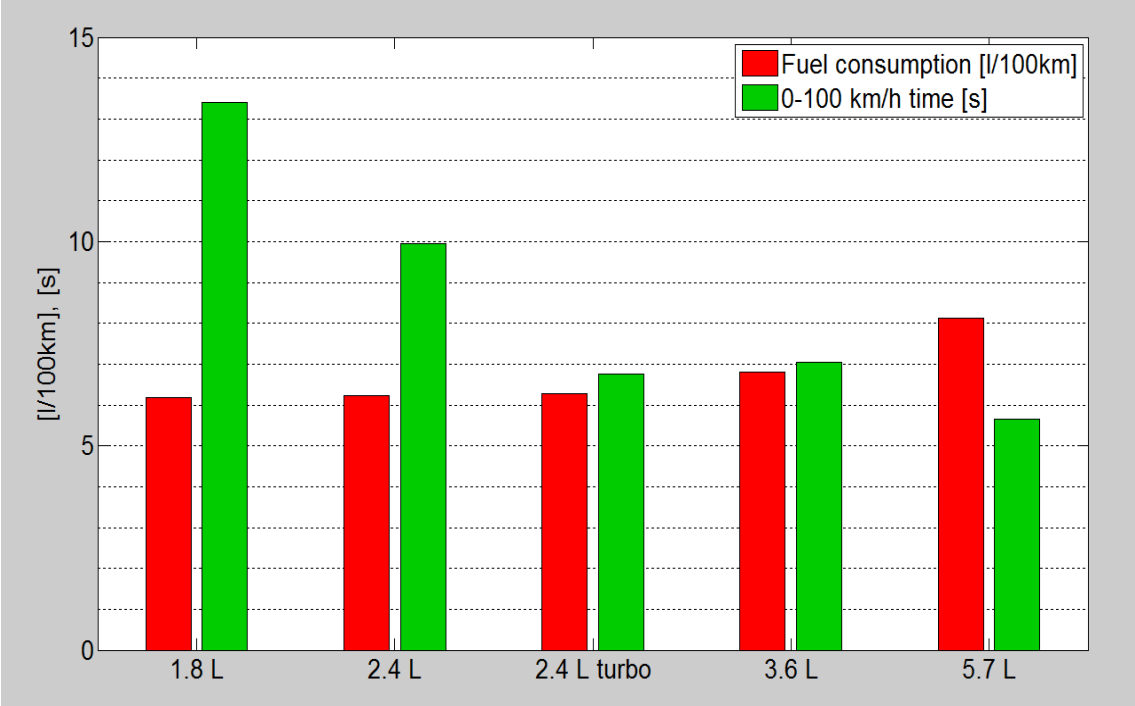

Figure 4.10 - Bar plots showing the results of the engine comparison with simulations - set 1.

Normally, a smaller displacement entails a lower fuel consumption but a higher acceleration time. In the simulations, the only exception is represented by the 2.4 liter turbocharged engine, which thanks to its characteristics shows both lower fuel consumption and lower acceleration time than the 3.6 liter aspirated engine.

The following study cases compared two different motor-generators (cases "Mogen" and "Eng4"). The motor-generators were respectively an 11.9 kW with 107 Nm of maximum torque and a 18 kW with 57 Nm maximum torque induction machines. In Section 3.3.2.3.1 their torque-speed maps with operating points have already been illustrated, showing a similar behavior (the clouds of the operating points were almost

identical, except for the area characterized by low speed and very negative torque, which only the 11.9 kW machine was capable to provide). As expected, the fuel consumption values were very close. The small difference can be related to the fact that with the 11.9 kW motor it was possible to recover a little more energy with regenerative braking. Table 4.9 and Figure 4.11 report the results.

Table 4.9 - Fuel consumption results of the motor-generator comparison obtained with simulations - set 1.

Motor-generator comparison		
Motor-generator power	11.9 kW	18 kW
Fuel consumption [l/100km]	6.85	6.81

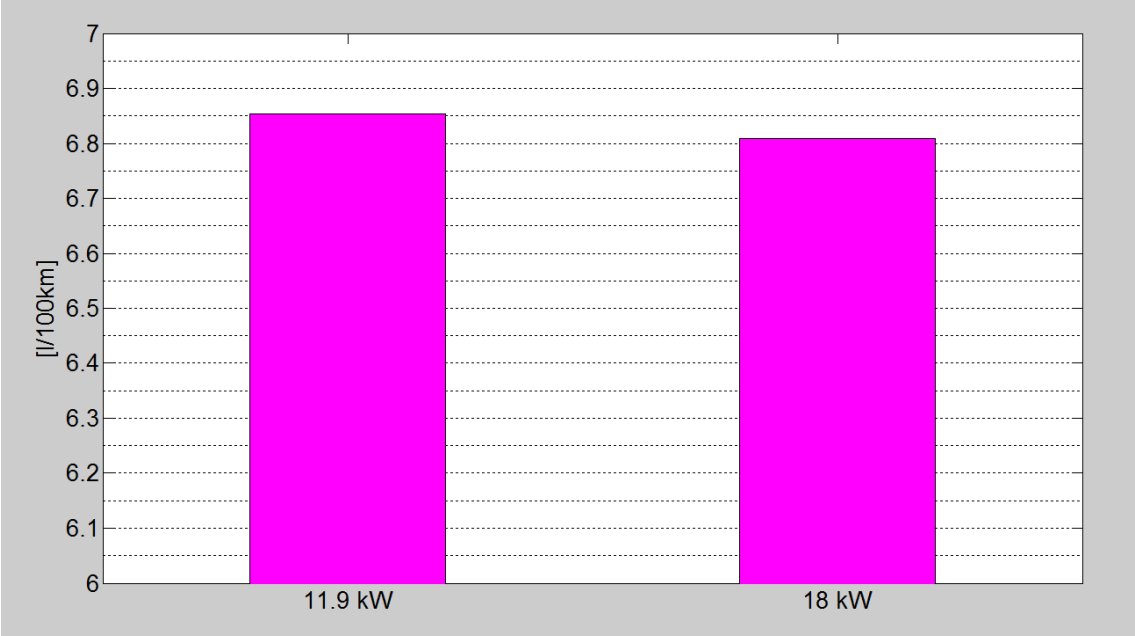

Figure 4.11 - Bar plots showing the results of the motor-generator comparison with simulations - set 1.

Afterward, two different batteries were compared (study cases "Batt" and "Eng4"). The batteries present two specific voltage levels (115 V vs. 270 V), similar nominal capacity but different maximum charging and discharging power (±15 kW vs. ±40 kW). If it was possible to completely exploit the power limits, the second battery would have provided a higher level of regenerative braking and electric assist. However, two other circumstances shrank this limits to lower values: using an 18 kW motor-generator, the

limits for the second battery were reduced to the machine power limits; then, since the engine ran generally at low speed (no more than 1500 rpm), also the motor-generator ran at low speed, mostly in the constant torque region, where power is proportional to speed and lower than the maximum. Consequently, because of external operating conditions, the two batteries worked almost in the same way, and the fuel consumption values for the two cases were close. Table 4.10 and Figure 4.12 show these results. The difference can be caused by the efficiencies of the batteries: for the same power, the second battery current is lower than the first one, because of its higher voltage level. This means lower losses and higher efficiency, and in turn lower fuel consumption.

Table 4.10 - Fuel consumption results of the battery comparison obtained with simulations - set 1.

Battery comparison		
Battery power	115 V, 4.5 Ah	270 V, 4.4 Ah
Fuel consumption [l/100km]	7.05	6.81

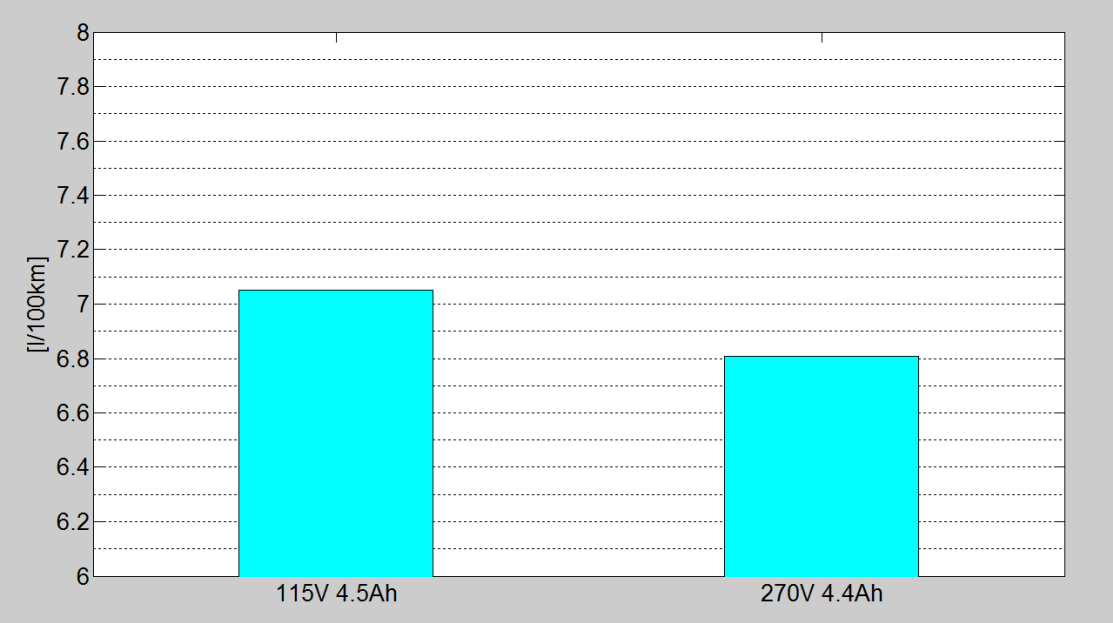

Figure 4.12 - Bar plots showing the results of the battery comparison with simulations - set 1.

The last test cases compared the combined effect of motor-generator and battery (cases "Veh1" and "MoGen&Batt"). The first one used the lower power motor-generator and the lower voltage battery, while the second case simulated the higher power machine

and the higher voltage battery. As in the previous comparisons, the powers in play were limited by the fact that the engine ran at low speeds. The fuel consumption values were again very close, with a slight difference due to motor-generator and battery efficiencies. The results are illustrated in Table 4.11 and Figure 4.13.

Table 4.11 - Fuel consumption results of the mo-gen & battery comparison obtained with simulations-set 1.

Motor-generator & battery comparison		
Motor-generator	11.9 kW	18 kW
Battery	115V 4.5Ah	270V 4.4Ah
Fuel consumption [l/100km]	6.67	6.54

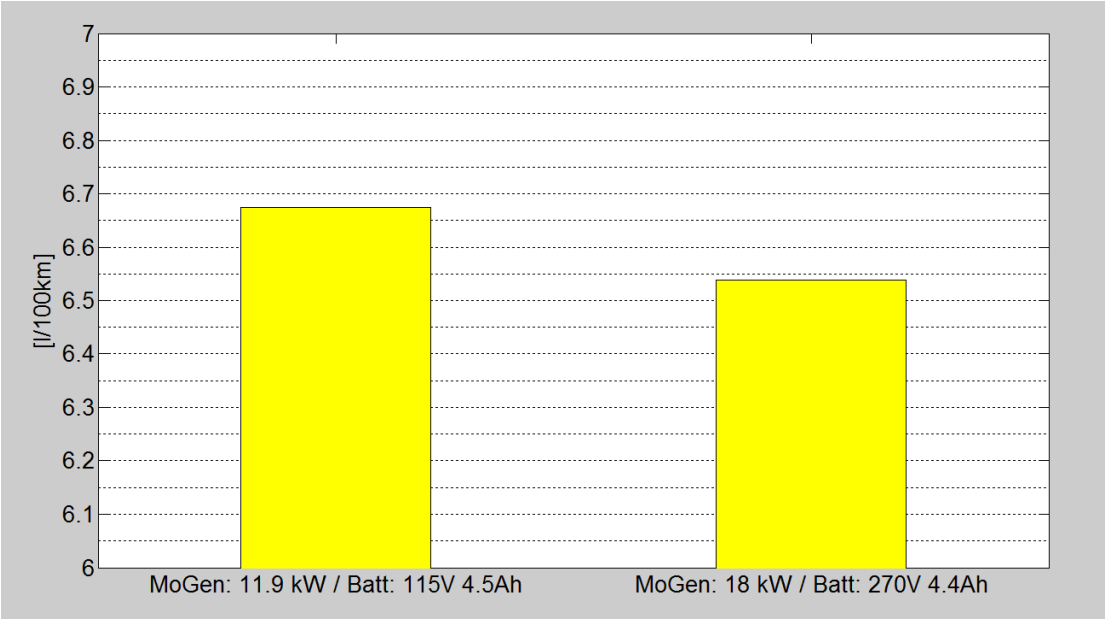

Figure 4.13 - Bar plots showing the results of the mo-gen & battery comparison with simulations - set 1.

In conclusion, the two last comparisons didn't provide a "better" motor-generator or battery, because in none of the cases the potential of the components could be completely exploited. Further simulations would be necessary, changing the operating parameters and the power limits in play in order to make a fairer comparison.

4.2.2.2 Set 2

The second set of simulations had the same purpose of the analytical approach, i.e., to investigate the fuel consumption benefits of the three features that the BSG introduces: stop-start, electric assist and regenerative braking. The vehicle under study is the same E-segment that was analyzed with the analytical approach.

Table 4.12 shows the fuel consumption values for each study case and drive cycle, along with the absolute variation of each case from the previous one and the corresponding percentage variation relative to Case 0. Table 4.13 illustrates instead the overall absolute and percentage variation of the "full" BSG version (Case 3) with respect to the conventional vehicle (Case 0).

Table 4.12 - Fuel consumption results obtained with simulation set 2.

Simulations set 2				
$\left[\frac{l}{100km}\right]$	**Case 0 (conventional)**	**Case 1 (Case 0 + stop-start)**	**Case 2 (Case 1 + e-assist)**	**Case 3 (Case 2 + regen)**
UDDS	8.71	7.81	7.67	6.94
	Abs. variation →	- 0.9	- 0.14	- 0.74
	% variation →	- 10.44 %	- 1.61 %	- 8.50 %
HWFET	5.97	5.74	5.71	5.58
	Abs. variation →	- 0.24	- 0.02	- 0.14
	% variation →	- 4.02 %	- 0.44 %	- 2.18 %
NEDC	8.14	7.56	7.45	6.74
	Abs. variation →	- 0.58	- 0.21	- 0.62
	% variation →	- 7.12 %	- 2.58 %	- 7.62 %

Table 4.13 - Absolute and percentage fuel consumption variations between Case 0 and Case 3, simulation set 2.

Variation Case 0 → Case 3	
$\left[\frac{l}{100km}\right]$	**Simulation set 2**
UDDS	- 1.78
	- 20.44 %
HWFET	- 0.49
	- 6.54 %
NEDC	- 1.41
	- 17.42 %

Figures 4.14 and 4.15 show graphically the individual contribution of each BSG function on the total fuel consumption reduction, in absolute and relative values, for the considered cycles.

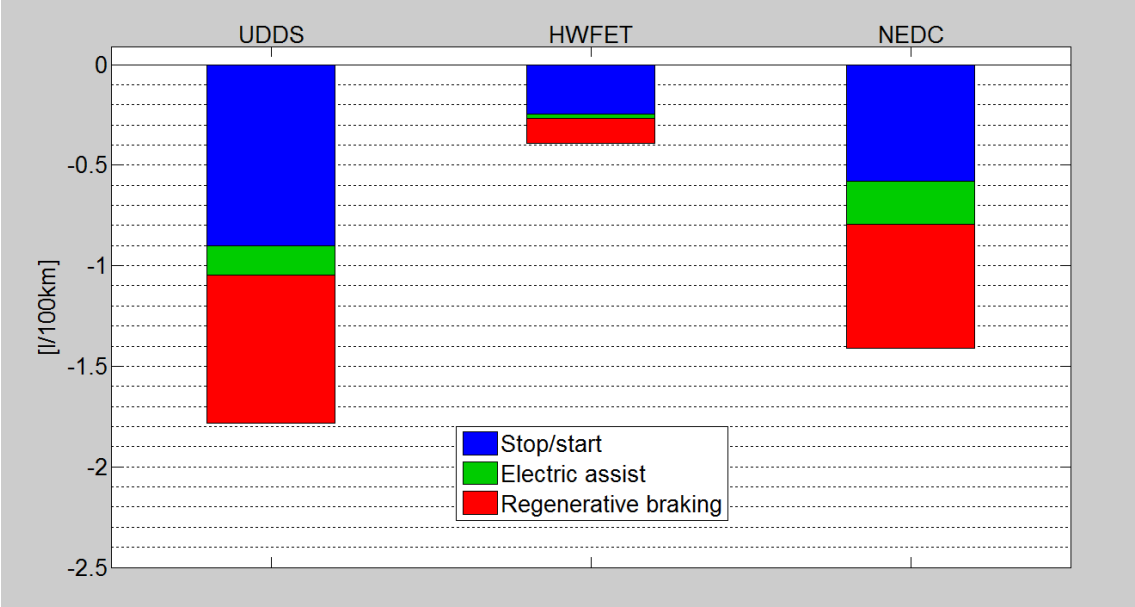

Figure 4.14 - Contribution of BSG functions on fuel savings - simulation set 2, absolute values.

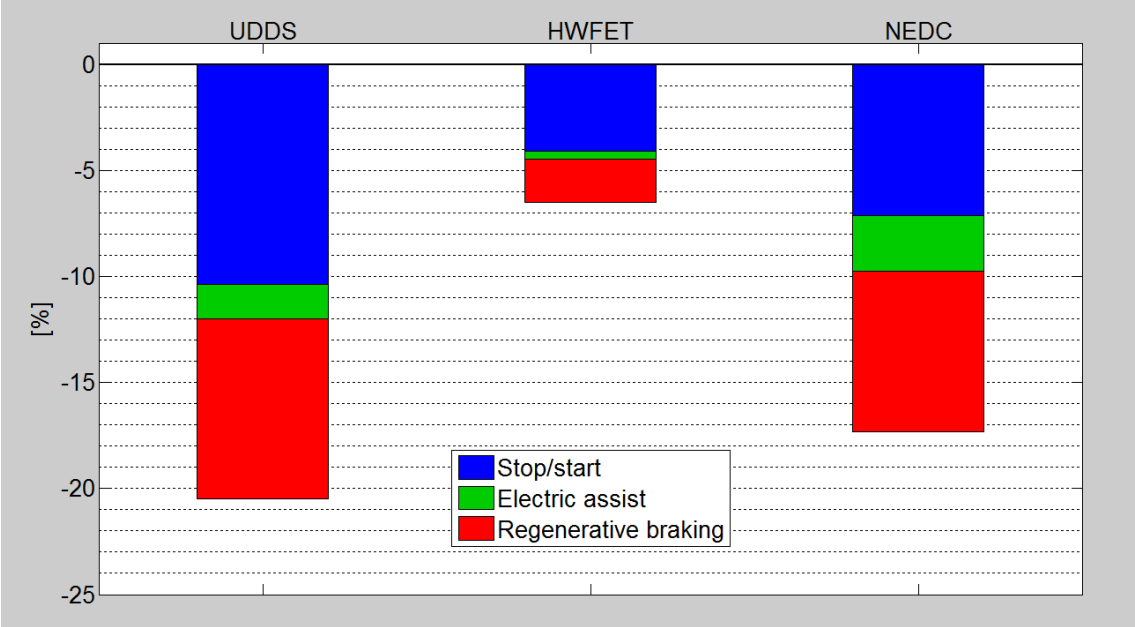

Figure 4.15 - Contribution of BSG functions on fuel savings - simulation set 2, relative values.

A large part of the fuel savings came from the stop-start strategy. While this is reasonable for the UDDS and the NEDC cycles, where the idle time on the whole cycle is relevant, it is not for the HWFET cycle, which has a negligible amount of idle time. Moreover, the fuel savings due to stop-start should be proportional to the idle time in the cycle, so the larger blue portion for the UDDS than for the NEDC is in contrast with the previsions.

Apparently, for this simulation set some other factors came into play, influencing the results. Further investigations would be required to identify them and reduce their effect. Probably for the same reasons, the fuel economy associated with electric assist (green portion) is very small compared to the others (blue and red portions). The savings brought by regenerative braking seem instead reasonable, since they appear proportional to the number and aggressiveness of the braking phases of each cycle.

4.2.3 Experimental test results

The fuel consumption tests on the proof-of-concept hybrid vehicle had the purpose of obtaining an experimental validation of the analytical approach and the simulations. Nevertheless, it must be considered that running the vehicle as it was equipped with a BSG only was not easy to obtain. The results may be offset of a certain amount due to

higher losses occurring in the powertrain, related to the greater number of components, and to the fact that it was not possible to completely disable electric assist and regenerative braking for Case 1 and regenerative braking for Case 2. To reduce this error, some more time should be spent tuning the calibrations, so that the car behaves more and more as a normal vehicle with BSG.

Although the results may be not completely accurate, it is still interesting to look at the differences in fuel consumption among the different cases. In this way, it is possible to get rid of those errors which keep constant from one case to the other.

Unfortunately, it was not feasible to test the vehicle as a conventional type, because the prototype was designed to work as a full hybrid vehicle, and it was impossible to completely get rid of the effects of the clutch and the P2 motor. Therefore, the fuel consumption for the conventional vehicle was analytically calculated starting from the fuel consumption obtained in Case 1. Firstly, analyzing the engine power in Case 1 it was possible to estimate the energy required to crank the engine on each drive cycle; then, assuming an idle power of 4 kW, and knowing the total amount of time during which the engine was off, the idle energy could be computed. Summing these two quantities with the respective signs, the energy involved in the stop-start could be estimated.

Tables 4.14 and 4.15 show the fuel consumption results, with the same layout used for the analytical approach and the second set of simulations.

Table 4.14 - Fuel consumption results obtained with experimental tests.

Experimental tests				
$\left[\frac{l}{100km}\right]$	**Case 0 (conventional)**	**Case 1 (Case 0 + stop-start)**	**Case 2 (Case 1 + e-assist)**	**Case 3 (Case 2 + regen)**
UDDS	10.82	9.87	9.44	8.64
	Abs. variation →	- 0.95	- 0.44	- 0.8
	% variation →	- 8.78 %	- 4.07 %	- 7.49 %
HWFET	6.12	6.14	5.81	5.59
	Abs. variation →	+ 0.01	- 0.42	- 0.22
	% variation →	0.16 %	- 5.24 %	- 4.59 %
NEDC	10.48	9.17	8.90	8.26
	Abs. variation →	- 1.21	- 0.27	- 0.64
	% variation →	- 11.66 %	- 2.60 %	- 6.16 %

Table 4.15 - Absolute and percentage fuel consumption variations between Case 0 and Case 3, experimental tests.

Variation Case 0 → Case 3	
$\left[\frac{l}{100km}\right]$	**Experimental tests**
UDDS	- 2.19
	- 20.24 %
HWFET	- 0.54
	- 8.66 %
NEDC	- 2.12
	- 20.42 %

Figures 4.16 and 4.17 present the results in a graphical way. Both absolute and relative values are reported.

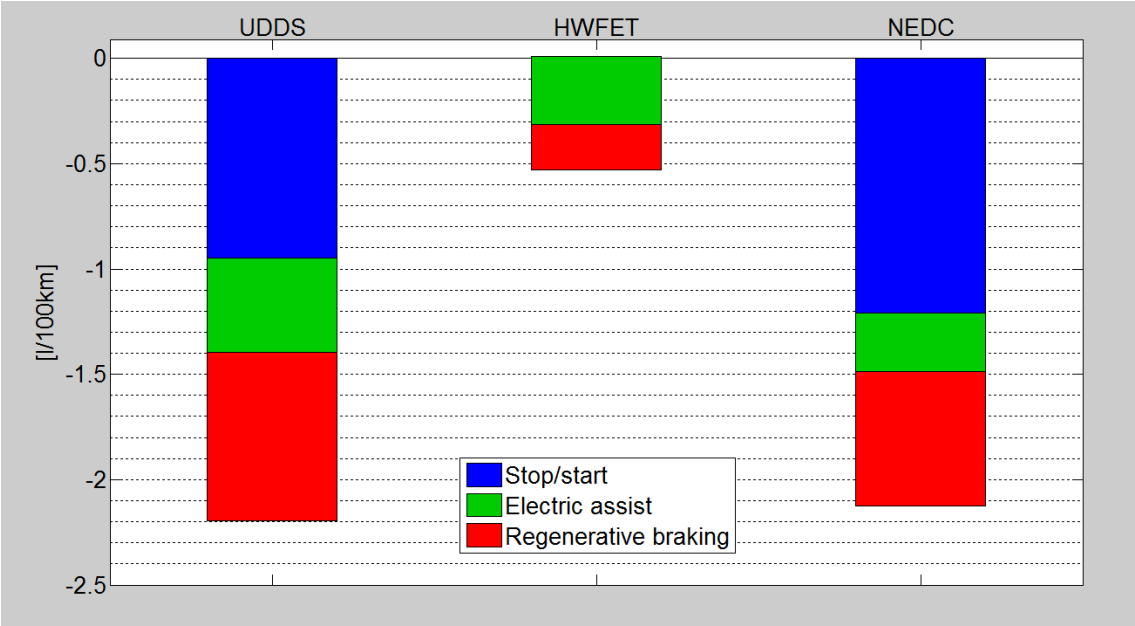

Figure 4.16 - Contribution of BSG functions on fuel savings - experimental tests, absolute values.

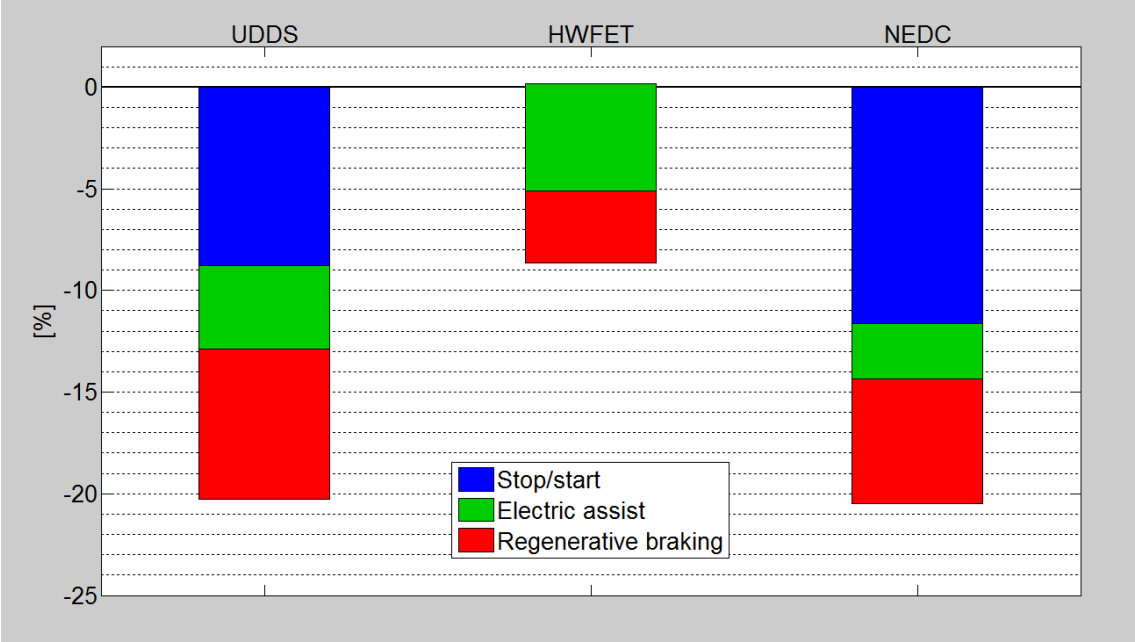

Figure 4.17 - Contribution of BSG functions on fuel savings - experimental tests, relative values.

The analytical calculations of the conventional fuel consumption bring reasonable results on the fuel savings related to stop-start. The savings in the NEDC are greater than in the UDDS, and in the HWFET the energy required to crank the engine is even higher than the energy saved during idle, so the fuel consumption slightly increases instead of decreasing. Fuel economy associated with electric assist is greater in the UDDS if the absolute value is considered, and in the HWFET if percentages are taken into account. The savings due to regenerative braking seem proportional to the number and aggressiveness of the braking phases of each cycle.

4.2.4 Comparison of the results obtained with the different approaches

In this section, the results which have been previously shown will be compared and analyzed. Analytical approach, simulation and test results will be put side by side for each drive cycle in order to observe differences and similarities. The study cases which are compared consist in the E-segment vehicle with and without the BSG.

Figure 4.18 shows the fuel consumption results obtained with each approach and drive cycle.

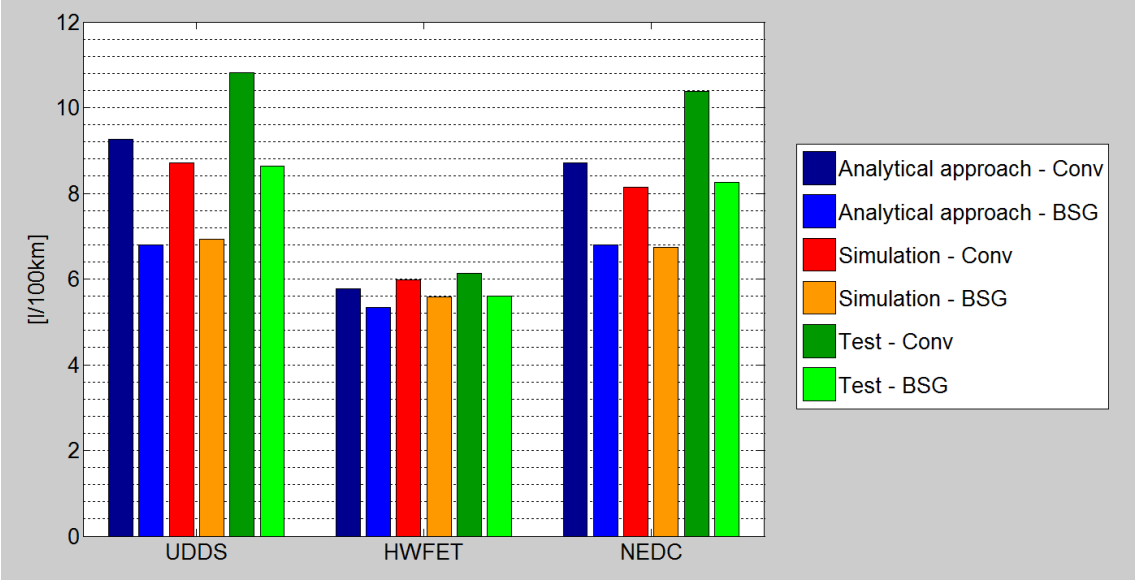

Figure 4.18 - Comparison of the fuel consumption results obtained with each approach.

It can be seen that the tests generated the highest fuel consumption values (especially for the UDDS and the NEDC, while for the HWFET they are closer to the other approaches). This is likely to be related to the fact that the test proof-of-concept

vehicle was not just a car equipped with BSG, but also included a series of other components that consumed energy, increasing fuel consumption. Moreover, the calibrations played an important role in the determination of the consumption: since the vehicle was not designed to run as it was forced to do in the test, the controls and the calibrations most probably were not optimal. Spending more time tuning the calibrations or developing an ad hoc control strategy would surely bring a better fuel consumption.

Looking at analytical approach and simulation results only for the UDDS and the NEDC cycles, they are different in the conventional version (higher for the analytical approach than the simulations) but very close in the BSG version. In the HWFET instead, the values remain different, and the trend is reversed (lower for analytical approach than simulations).

In order to better evaluate the effect of the introduction of the BSG, the contribution of each function (stop-start, electric assist and regenerative braking) will be compared for the different approaches considering a drive cycle at a time.

Figure 4.19 and 4.20 illustrate the difference in fuel consumption introduced by each function with the three approaches on the UDDS cycle. The data are presented both as absolute and percentage values.

Observing the absolute values, it can be noted that the benefits associated with stop-start and regenerative braking are very similar for the three approaches. A big difference is instead reported for the electric assist contribution. The green portion in the simulation bar seems excessively small, probably because of other factors that came into play and influenced the results. At the same time, the e-assist benefit in the analytical approach is almost the double than in the test. For the analytical approach, it is probable that the losses related to this function have been underestimated, while for the test surely the additional components introduced more losses, so very likely the correct value lays in between these two.

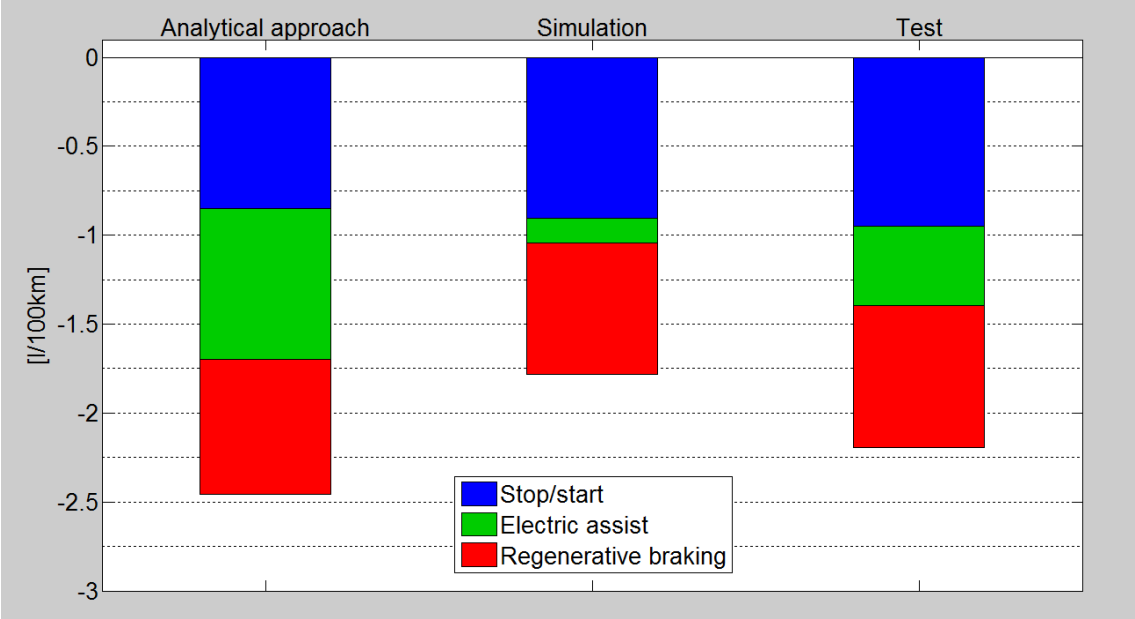

Figure 4.19 - Comparison of effect of BSG functions on fuel savings for the three approaches, on UDDS cycle, absolute values.

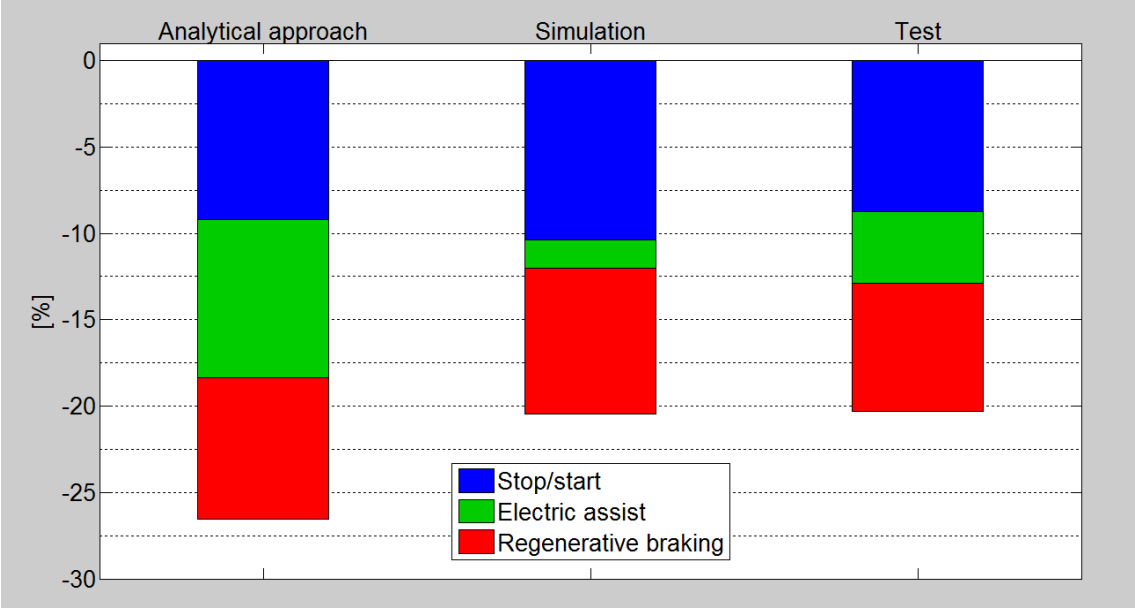

Figure 4.20 - Comparison of effect of BSG functions on fuel savings for the three approaches, on UDDS cycle, relative values.

The percentage values are instead influenced by the fuel consumptions of the conventional case, which were quite different for the three approaches, as shown in Figure 4.18. Therefore, for this drive cycle, they are not much representative of the real situation.

Figure 4.21 and 4.22 illustrate the same results for the HWFET cycle.

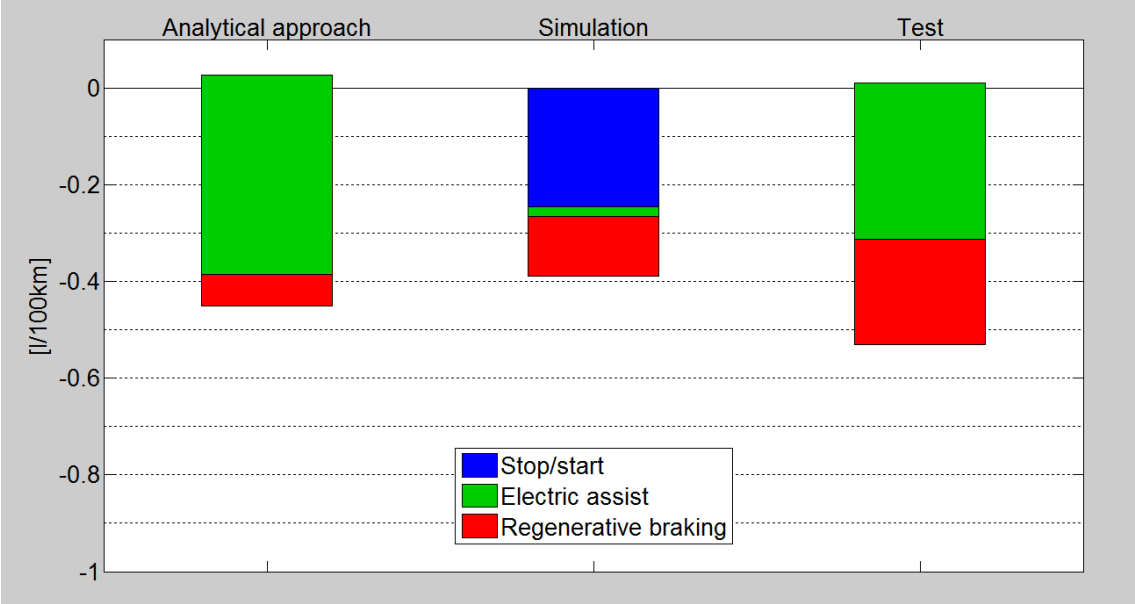

Figure 4.21 - Comparison of effect of BSG functions on fuel savings for the three approaches, on HWFET cycle, absolute values.

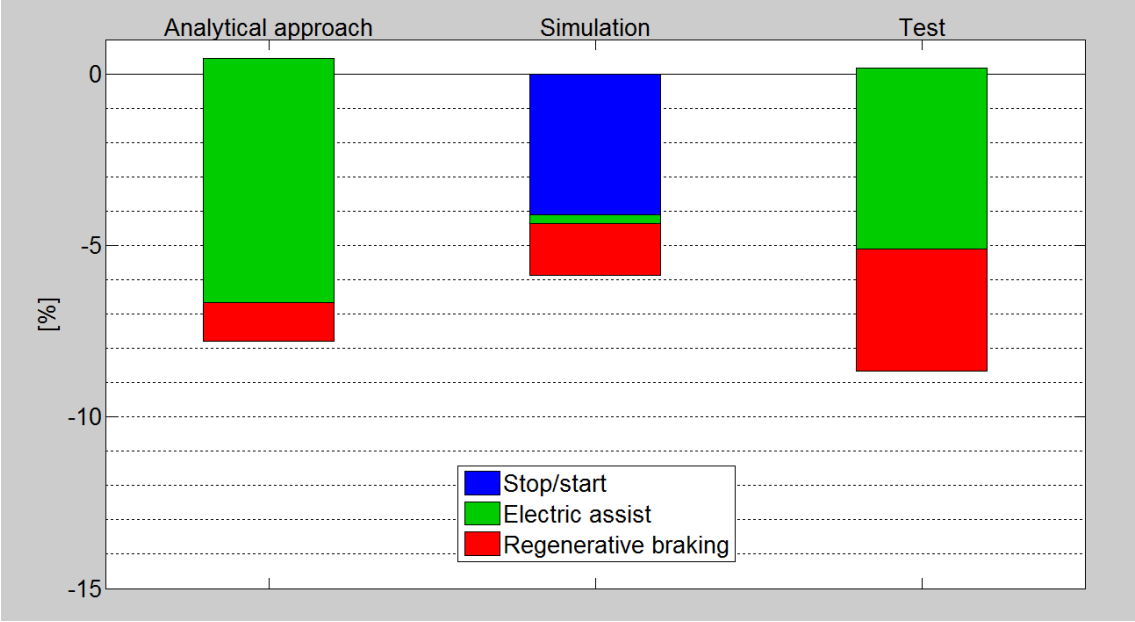

Figure 4.22 - Comparison of effect of BSG functions on fuel savings for the three approaches, on HWFET cycle, relative values.

In this comparison, while the total reduction in fuel consumption for the three approaches is closer for the UDDS comparison, the individual contributions are instead much more distant. For both the analytical approach and the test, the stop-start function reasonably increases the fuel consumption, because of the idle characteristics of this drive cycle. For the simulation instead the reduction in fuel consumption related to stop-start appears too high. In the same way, the contribution of electric assist in analytical approach and test are close, while in the simulation it appears out of range. Lastly, the fuel economy brought by regenerative braking, highly dependent on the limits and the calibrations imposed, looks dissimilar for the three approaches, increasing from the analytical to the test.

Finally, Figures 4.23 and 4.24 show the fuel consumption contributions on the NEDC cycle. Looking at the absolute values, the fuel economy associated with stop-start is very close for analytical approach and test, while for simulation it is the half of the others. In addition, the latter is lower than the corresponding value on the UDDS, indicating that something was wrong in the simulations since the NEDC has more seconds of idle time with respect to the UDDS. The contribution of regenerative braking appears instead to be homogeneous for the three approaches, as it was for the UDDS cycle. The aid provided by electric assist varies again from one approach to the other, even if in this case simulation and test results change only slightly.

The percentage values are once again distorted by the fuel consumption of the conventional case. The only point of interest is that this time the electric assist contribution for simulation and test are nearly identical.

In conclusion, it can be said that analytical approach and tests produced the closest results on the individual contributions of the BSG functions, even if the total fuel consumption values were rather different. Simulations seemed to be more inaccurate, with the results sometimes quite far from what expected. The way the fuel savings brought by stop-start are calculated in the simulations should be revised. Lastly, fuel economy due to electric assist appeared to be the most inconstant variable; more study on its modeling and simulation would be required to explain the great differences of its contribution among the different approaches.

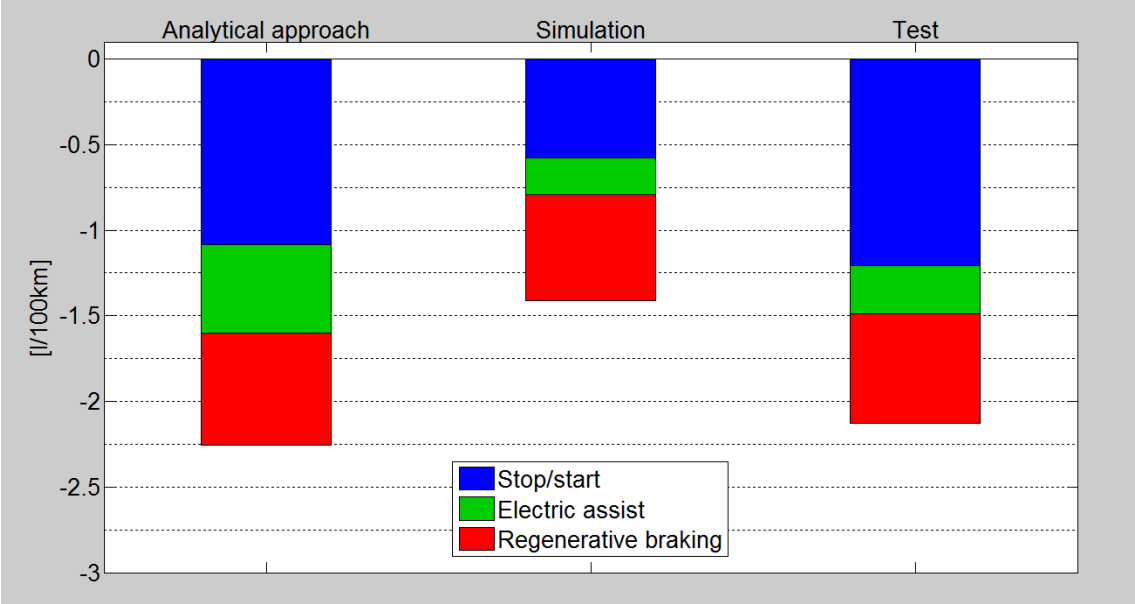

Figure 4.23 - Comparison of effect of BSG functions on fuel savings for the three approaches, on NEDC cycle, absolute values.

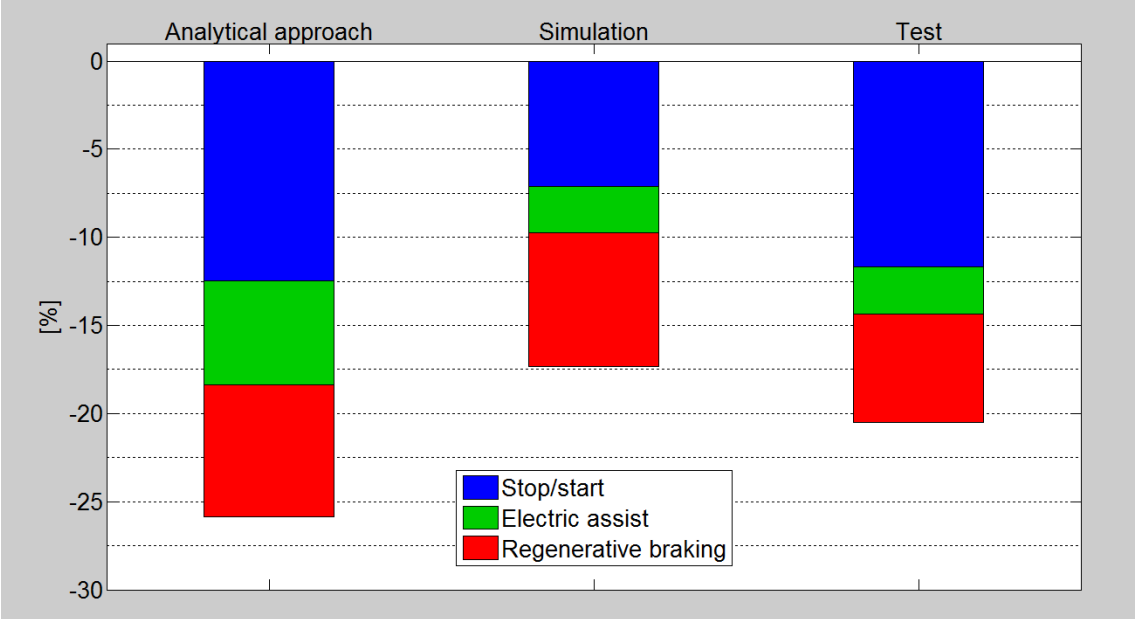

Figure 4.24 - Comparison of effect of BSG functions on fuel savings for the three approaches, on NEDC cycle, relative values.

4.2.5 Summary of the fuel consumption results

The research showed that a vehicle equipped with the BSG produces a remarkable reduction in fuel consumption with respect to a conventional vehicle. An analytical approach, simulations and experimental tests demonstrated that the main BSG features introduce fuel savings in the order of 1.5-2.2 l/100km (20-25%) on city cycle and 0.4-0.6 l/100km (8-9%) on highway cycle.

On the UDDS, most of these savings are related to the cut of fuel during idle with stop-start (about 0.9 l/100km or 10%) and to the regenerative braking (about about 0.7 l/100km or 8%). Electric assist provides indirectly some benefits on fuel consumption but lower with respect to the other two functions, since its main purpose is to improve drivability and not reduce fuel consumption. On HWFET, the overall improvements are more limited, because the characteristics of the cycle are not suitable for an efficient use of the BSG. In this case, no savings are obtained from the stop-start, while electric assist contributes for about 0.4-0.4 l/100km (5-6%) and regenerative braking for 0.1-0.2 l/100km (2-4%). NEDC shows results in between the other two cycles, since it has intermediate characteristics.

However it must be remembered that the improvements in fuel consumption are strictly dependent on system components and controls. The power capabilities of motor-generator and battery determine the amount of regenerative braking that can be obtained, which is directly linked to the fuel savings. Calibrations also play an important effect on the results: while much work is necessary to find the best controls for fuel economy, some of them cannot be implemented in a real car because of drivability issues.

4.2.6 Hints about the full hybrid vehicle

This last section provides some information about the proof-of-concept full HEV which was used for the tests. It was designed to work as a full hybrid, with a particular control strategy and the capability of running in pure electric mode, so it has a high potential in performance enhancement and fuel economy reduction, with the drawback of increased cost and complexity.

In general, parallel full hybrid vehicles are calibrated so that they run in electric mode until a threshold in terms of torque, speed or power at the wheels is exceeded.

These limits are chosen on the basis of the size of powertrain components and the performance the vehicle must achieve. Figure 4.25 illustrates what has just been explained: the area beneath the blue line includes the combinations of torque and speed at the wheels which enable the pure electric mode. This area is delimited by a maximum torque (T_{EV}), a maximum speed (n_{EV}) and a maximum power (P_{EV}).

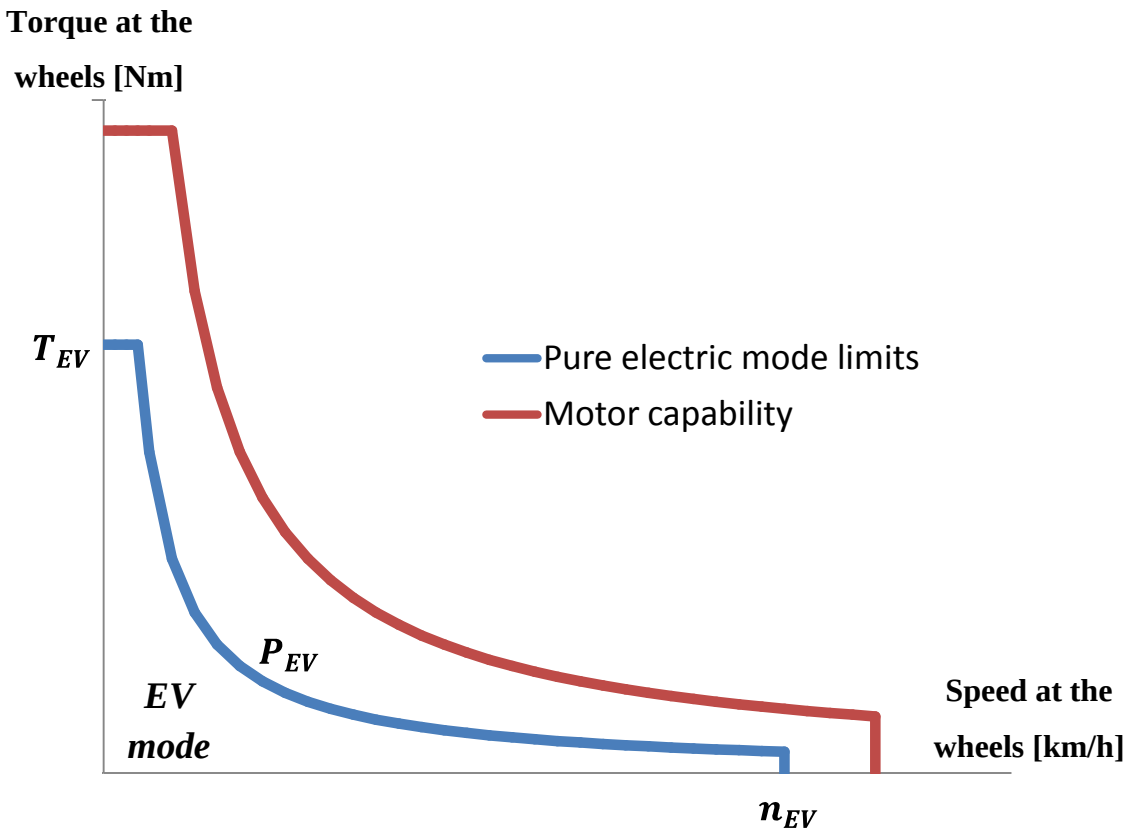

Figure 4.25 - Full HEV electric mode limits, compared to electric motor capability.

It can be noticed that even if the motor capability is higher, the limits are lower than the maximum. This happens because when a certain value of output power is exceeded, usually included between 6 and 12 kW, depending on the motor size, drive cycle and other factors, it becomes more efficient to use the engine instead of the motor. Figure 4.26 shows the fuel consumption trends when either engine or electric motor are used to propel the car (for the electric motor an "equivalent" fuel consumption is represented, calculated considering the amount of fuel required to generate the electricity to run the vehicle in electric mode). The line of the electric mode has usually a greater slope than

the engine line, at least at low output power requests, because of the electric losses occurring during motoring and generating, i.e., when fuel is used to generate the electricity for the e-drive. At the same time, the intercept with the fuel consumption axis, which corresponds to the consumption during idle, is much lower for the electric motor line than for the engine line, because lower energy losses occur in electric mode during this condition (near zero motor speed and torque).

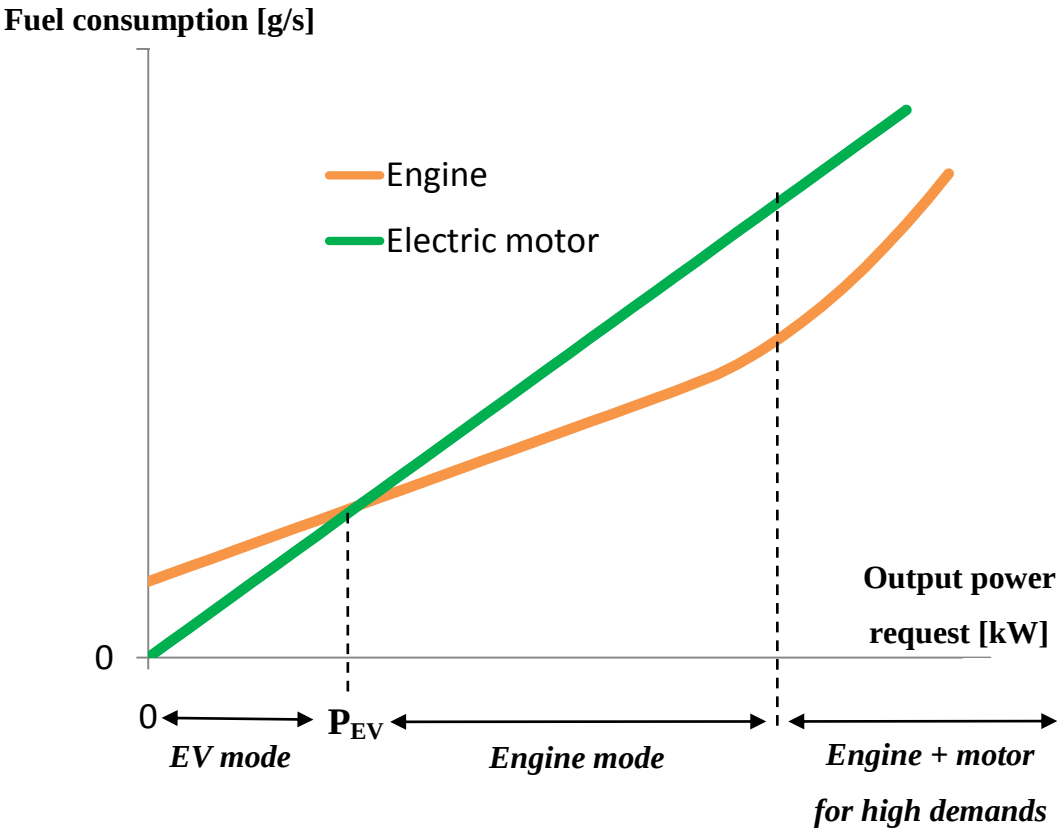

Figure 4.26 - Full HEV electric mode limits, compared to electric motor capability.

The two lines intersect at P_{EV}. After this threshold, it is more convenient to switch from electric mode to engine mode. Therefore, for low output power requests, the vehicle is run in e-mode, while for higher requests it runs as a conventional. Finally, when the power request exceeds the capability of the engine, the electric motor can be used to support the engine and improve the performance of the vehicle.

As previously mentioned, besides the threshold on the output power P_{EV}, other limits on output torque and speed are usually introduced. The limit on the torque is intended to leave a torque reserve to start the engine using the P2 motor in case P1f

torque is not sufficient, while the limit on the speed is necessary because at higher speeds the available torque would be too low, preventing good drivability.

For the considered proof-of-concept hybrid vehicle, the thresholds for electric mode are listed in Table 4.16:

Table 4.16 - Electric mode threshold for the proof-of-concept full HEV used for the tests.

EV-mode thresholds	
Power	10 kW
Speed	100 km/h
P2 torque	160 Nm

During electric drive, the engine is disengaged from the transmission by the disconnect clutch and it is off. When one of the limits is overcome, firstly the engine is started using P1f motor, then its speed is increased so that the following clutch engagement is synchronous.

Anyways, in order to have a pure electric drive, other conditions besides those just presented are checked by the hybrid controller. The most obvious is represented by the SOC: if its value is too low because of previous discharge phases, the electric mode is disabled and the engine is kept on both to propel the vehicle and to charge the battery. The SOC level should never go below 40-45% for this vehicle, in order to maximize battery life. Another condition is represented by air temperature: if it is too low, the engine is prevented to switch off in order to avoid cold restarts and to heat up the catalytic converter, in the effort of reducing pollutant emissions.

To improve the drivability, delays and hysteresis on thresholds and limits are introduced, so that too frequent switches between modes are not allowed. Moreover, the electric motor torque can be added to the engine torque when the driver suddenly requires higher power: in this way downshifts can be delayed or avoided, if the power request is limited to few seconds, further increasing drivability.

Table 4.17 shows the fuel consumption values of the vehicle tested as conventional (Case 0, analytically calculated), BSG (Case 3) and full hybrid, for UDDS and HWFET

cycles. Running the vehicle as a full hybrid brings a remarkable improvement with respect to the BSG version, especially in the UDDS cycle. Figure 4.27 presents graphically the results.

Table 4.17 - Comparison of the fuel consumption of conventional, BSG and full hybrid vehicles.

Experimental tests			
$\left[\frac{l}{100km}\right]$	**Case 0 (conventional)**	**Case 1 (Case 0 + stop-start)**	**Case 2 (Case 1 + e-assist)**
UDDS	10.82	8.64	7.20
	Abs. variation →	-2.19	-1.44
	% variation →	-20.24%	-14.22%
HWFET	6.12	5.59	5.44
	Abs. variation →	-0.54	-0.25
	% variation →	-8.66%	-4.08%

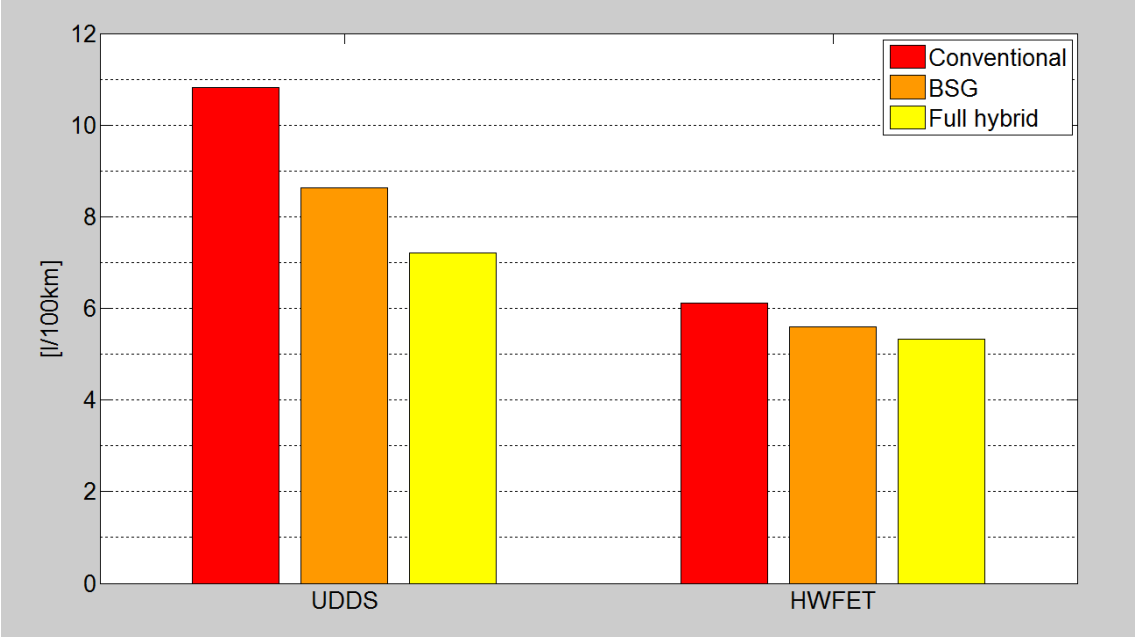

Figure 4.27 - Bar plots comparing of the fuel consumption of conventional, BSG and full hybrid vehicles.

CHAPTER 5

CONCLUSIONS AND RECOMMENDATIONS

Vehicle electrification is a growing trend that will revolutionize the current transportation system during the next decades. Among all the possible architectures and configurations, the Belt Starter Generator (BSG) represents one of the most cost-effective solutions in the vehicle hybridization process, for its characteristics of low cost and weight, easiness of implementation and reduction of fuel consumption and CO_2 emissions.

This thesis investigated in detail the BSG system. Firstly, it provided a thorough description of its features and operating principles: architectures, powertrain modifications, components and functions were illustrated, defining the main sizing criteria and the advantages and disadvantages of each configuration.

Afterwards, the dynamics of the system was modeled in Simulink to predict the performance during an engine start-up event. Models of the electric machine, belt and engine were developed and simulations were run to observe the system behavior, considering different operating conditions.

Finally, the fuel savings enabled by the BSG were quantified, adopting three separate approaches. The first one consisted in an analytical model which used energy calculations to estimate fuel consumption, needing only some general vehicle data and the drive cycle profile. Then, a more detailed model was utilized, capable of simulating the dynamics of all powertrain components; simulations were performed both to assess the effect of different vehicles and powertrains on fuel consumption and to estimate fuel savings related to each BSG functions. The last approach consisted in fuel consumption tests on a proof-of-concept full hybrid vehicle; calibration setups were developed to run the car as if it was equipped with a BSG only, and three tests were performed, corresponding to the study cases used for the previous simulations. All the obtained results were compared among each other, with the aim of validating the models, and with the fuel consumption of a conventional vehicle, in order to highlight the advantages of the system analyzed.

The main outcomes of the research are summarized in the following, and some recommendations are provided for future works starting from the results of this research.

5.1 Conclusions

Regarding the stop-start performance evaluation and modeling of the BSG, the main outcomes are reported below.

- A model for stop-start simulation was realized. It can be used to predict the performance of the system during motoring conditions: providing as input the electric machine torque, the model evaluates the speed profile of the engine. Since the logic is based on the physics of the problem, the model can simulate components different from those considered, provided that data are available.
- The effect of different engine temperatures on startup performance was investigated. Cold, ambient and warm temperature were selected and rise time to idle speed for a constant motor torque was estimated. During cold start more time is required to spin the engine up. In order to preserve drivability in such conditions, the power capabilities of the system have to be carefully selected, and a suitable control strategy has to be implemented.
- The model is able to simulate slip. A set of dynamics equations and a logic block to verify the conditions for slip occurrence were developed and implemented in Simulink.
- The information about the start-up performance allows to see the effect of electric motor torque on engine speed fluctuations. Since they are directly related to vibrations, this aspect is important for the NVH performance evaluation of the engine start-up.

Concerning the fuel consumption analysis, the main results are listed in the following.

- The research showed that a vehicle equipped with the BSG produces a remarkable reduction in fuel consumption with respect to a conventional vehicle. Analytical approach, simulations and experimental tests demonstrated that the main BSG features introduce fuel savings in the order of 1.5-2.2 l/100km (20-25%) on city cycle (UDDS) and 0.4-0.6 l/100km (8-9%) on highway cycle (HWFET). NEDC

showed results in between the other two cycles, since it has intermediate characteristics.

- BSG is more suitable for city driving, since the fuel saving comes mostly from stop-start and regenerative braking functionalities. City driving is in fact characterized by repeated stops and braking opportunities. On the contrary, highway driving have long periods of high speed with no stops and a small number of low-power brakings.
- Electric assist provides indirectly some benefits on fuel consumption, but lower with respect to the other two functions (stop-start and regenerative braking), since its main purpose is to improve drivability and not reduce fuel consumption.
- The analytical approach model proved to be a simple and powerful method for fuel consumption prediction. Being based on energy considerations, it doesn't need to evaluate the dynamics of the components, but it uses only few data and efficiency assumptions to provide information about powers and energies in play and to calculate consumption.

5.2 Recommendations

The following recommendations provide suggestions for further investigations and improvements. Regarding the modeling development, the recommendations are reported below.

- The existing model can be further improved. On the engine side, fuel introduction and firing can be implemented using the equations which were presented, or adopting different approaches; in this way a complete engine cranking can be simulated. The inertia torque of the reciprocating masses should be added as well, to correctly account for the overall inertia of the engine. The slip feature can also be improved by including equations for the determination of the belt friction capacity, on the basis of the geometry of the system and belt friction characteristics.
- New elements can be introduced to make the model more accurate. The priority would be on the tensioning system, which has a major influence on the results at very low engine speeds.

- To validate the model, tests on the start cart should be performed to obtain the engine data necessary for a correct model calibration.
- A challenging development would be the design of a control system for the motor torque, capable of driving the engine along the required speed profile and suppressing the speed oscillation. Both a closed- and open-loop controller would be required to perform these tasks.

The fuel consumption analysis can be improved in the following ways.

- The analytical approach model can be modified to obtain more accurate results: drivability constraints could be introduced to make stop-start, electric assist and regenerative braking more realistic.
- The results of the simulations should be analyzed to understand why some of them diverge so much from analytical approach and test results. Probably the simulations need to be run again reviewing the assumptions made and the data in the model.
- New calibration setups for the proof-of-concept HEV can be developed to improve its performance and fuel consumption when tested as a BSG vehicle. This may also require some hardware modifications.
- A low voltage system (< 60-65 V_{DC}) can be investigated through simulations and tests to quantify differences in terms of fuel consumption and performance with respect to the high voltage system.

REFERENCES

[1] Sousanis J.: "World Vehicle Population Tops 1 Billion Units", WardsAuto; Aug 15, 2011 (accessed Aug 1, 2012). Avalable from: http://wardsauto.com/ar/world_vehicle_population_110815.

[2] OICA, Paris, France; c2007. Production statistics (accessed Aug 2, 2010). Available from: http://oica.net/category/production-statistics/.

[3] Mi C., Masrur M.A., Gao D.W.: "Hybrid electric vehicles: principles and applications with practical perspectives". 1st ed., Chichester (UK): John Wiley & Sons, Ltd; 2011.

[4] Bentley R., Miller R., Wheeler S., Boyle G.: "UKERC Review of Evidence for Global Oil Depletion - Technical Report 7: Comparison of Global Oil Supply Forecasts"; s.l.: UK Energy Research Council; 2009.

[5] Owen N.A., Inderwildi O.R., King D.A.: "The status of conventional world oil reserves - Hype or cause for concern?"; *Energy Policy*, 2011, 38: 4743-4749.

[6] IEA: "World Energy Outlook 2010". Paris: International Energy Agency; 2010.

[7] Hughes L., Rudolph J.: "Future world oil production: growth, plateau or peak?", *Current opinion in environmental sustainability*, 2011, 3: 225-234.

[8] Webb S.: "Europe crisis, China fiscal policy risks for oil", Reuters; May 9, 2010 (accessed Aug 12, 2012). Available from: http://www.reuters.com/article/idUSTRE6482BU20100509.

[9] De Castro C, Miguel LJ, Mediavilla M: "The role of non conventional oil in the attenuation of peak oil"; *Energy Policy*, 2009, 37: 1825-1833.

[10] IEA: "World Energy Outlook 2008". Paris: International Energy Agency; 2008.

[11] EIA: "International Energy Outlook 2011". Washington: Energy Information Administration; 2011.

[12] Marland, G., Boden T.A., Andres R.J.: "Global, Regional, and National CO2 Emissions. In Trends: A Compendium of Data on Global Change"; Carbon Dioxide Information Analysis Center, Oak Ridge National Laboratory, U.S. Department of Energy, Oak Ridge, TN, U.S.A., 2007.

[13] CEC: "Inventory of California Greenhouse Gas Emissions and Sinks: 1990-1999". Sacramento: California Energy Commission; 2002.

[14] Carbon Dioxide Information Analysis Center; Oak Ridge, TN, U.S.A. (accessed Jul 28, 2012). Available from: http://cdiac.ornl.gov/.

[15] Wikipedia: "Greenhouse effect". (modified Aug 14, 2012; accessed Aug 18, 2012). Available from: http://en.wikipedia.org/wiki/Greenhouse_effect#cite_note-ipccar4syr-0.

[16] NASA; Washington, DC; GISS Surface Temperature Analysis (modified Aug 6, 2012, accessed Aug 9, 201). Available from: http://data.giss.nasa.gov/gistemp/graphs_v3/.

[17] IPCC: "Synthesis Report Summary for Policymakers, Section 5.2: Key vulnerabilities, impacts and risks - long-term perspectives", Geneva: Intergovernmental Panel on Climate Change, 2007. Available at: http://www.ipcc.ch/publications_and_data/ar4/syr/en/mains5-2.html.

[18] EPA: "Automobile emissions: an overview", U.S. Environmental Protection Agency, 1994 (accessed Aug 3, 2012). Available from: www.epa.gov/oms/consumer/05-autos.pdf.

[19] Litman T.: "Sustainable Transportation and TDM", Online TDM Encyclopedia. Victoria, BC, Canada: Victoria Transport Policy Institute, 2009 (modified Sep 1, 2011; accessed July 30, 2012). Available at: http://www.vtpi.org/tdm/tdm67.htm.

[20] Williamson S.S., Emadi A.: “Comparative assessment of hybrid electric and fuel cell vehicles based on comprehensive well-to-wheel efficiency analysis”, *IEEE Transactions on Vehicular Technology*, 2005, 54 (3): 856-862.

[21] Sanna L.: "Driving the Solution – the Plug-in hybrid Vehicle", Palo Alto (CA): Electric Power Research Institute (EPRI), 2005 (accessed Aug 12, 2012). Available from: http://mydocs.epri.com/docs/CorporateDocuments/EPRI_Journal/2005-Fall/1012885_PHEV.pdf.

[22] Archer G.: "Ricardo study finds electric and hybrid cars have a higher carbon footprint during production than conventional vehicles, but still offer a lower footprint over the full life cycle", Green Car Congress; Jun 8, 2011 (accessed Aug 17, 2012). Available from: http://www.greencarcongress.com/2011/06/lowcvp-20110608.html.

[23] Wikipedia: "Plug-in electric vehicle". (modified Aug 12, 2012; accessed Aug 14, 2012). Available from: http://en.wikipedia.org/wiki/Plug-in_electric_vehicle.

[24] IEA: "Technology Roadmap Electric and plug-in hybrid electric vehicles". Paris: International Energy Agency; 2009.

[25] Ganji B., Kouzani A.Z., Trinh H.M.: "Drive cycle analysis of the performance of hybrid electric vehicles", *Life system modeling and intelligent computing*, 2010, 434-444.

[26] ENEA: "Sistemi di propulsione elettrica ed ibrida: dalla sorgente a bordo all'attuazione meccanica". Roma: ENEA, 2009.

[27] Eshani M., Gao Y., Gay S.E., Emadi A.: "Modern Electric, Hybrid Electric, and Fuel Cell Vehicles: Fundamentals, Theory, and Design". Boca Raton (FL): CRC Press, 2005.

[28] U.S. Government source for fuel economy information website (modified Aug 15, 2012, accessed Aug 16, 2012). Available at: www.fueleconomy.org.

[29] Cai, W., "Comparison and review of electric machines for integrated starter alternator applications", *39th Industry Applications Conference, 2004*, 2004, 1: 4.

[30] Henry R., Lequesne B., Chen S., Ronning J. et al.: "Belt-Driven Starter-Generator for Future 42-Volt Systems", *SAE 2001 World Congress*, SAE Technical Paper 2001-01-0728 2001.

[31] Jayabalan R., Emadi A.: "42V Integrated Starter/Alternator Systems", *Future Transportation Technology Conference*, SAE Technical Paper 2003-01-2258, 2003.

[32] Hawkins S., Billotto F., Cottrell D., Houtman A. et al.: "Development of General Motors' eAssist Powertrain", *SAE 2012 World Congress & Exhibition*, SAE Technical Paper 2012-01-1039, 2012.

[33] Wikipedia: "Belt Alternator Starter (BAS)". (modified Jun 17, 2010; accessed Aug 2, 2012). Available from: http://wikicars.org/en/Belt_Alternator_Starter_(BAS).

[34] Tamai G., Hoang T., Taylor J., Skaggs C. et al.: "Saturn Engine Stop-Start System with an Automatic Transmission", *2001 SAE World Congress*, SAE Technical Paper 2001-01-0326, 2001.

[35] Schmidt M., Isermann R., Lenzen B., Hohenberg G.: "Potential of Regenerative Braking Using an Integrated Starter Alternator", *2000 SAE World Congress*, SAE Technical Paper 2000-01-1020, 2000.

[36] Bradfield M.: "Improving Alternator Efficiency Measurably Reduces Fuel Costs", Pendleton (IN): Delco Remy, 2008.

[37] SAE: "Bosch Automotive Handbook", 4th ed. Warrendale, PA: Society of Automotive Engineers, 1996.

[38] Schmidt M., Isermann R., Lenzen B., Hohenberg G.: "Accessories and their influence on consumption and emissions - models, simulations, measurements", *Innovative Fahrzeugantriebe*, 1998, 1418: 241-252.

[39] What-when-how: "Starter motors and circuits" (accessed Aug 4, 2012). Available from http://what-when-how.com/automobile/starter-motors-and-circuits-automobile

[40] Walters J., Krefta R., Gallegos-Lopez G., Fattic, G.: "Technology Considerations for Belt Alternator Starter Systems", *2004 SAE World Congress*, SAE Technical Paper 2004-01-0566, 2004.

[41] Walters J., Husted H., Rajashekara K.: "Comparative Study of Hybrid Powertrain Strategies", *Future Trasportation Technology Conference*, SAE Technical Paper 2001-01-2501, 2001.

[42] Leonardi F., Degner M.: "Integrated starter generator based HEVs: a comparison between low and high voltage systems", *2001 Electric Machines and Drives Conference*, pp. 622-628, 2001.

[43] Nicastri P., Huang H.: "42V PowerNet: Providing the Vehicle Electrical Power for the 21st Century", *Future Transportation Technology Conference & Exposition*, SAE Technical Paper 2000-01-3050, 2000.

[44] Barkhordarian V.: "Power MOSFET Basics", El Segundo (CA): International Rectifier (accessed Aug 19, 2012). Available at: http://www.irf.com/technical-info/appnotes/mosfet.pdf.

[45] Srinivasan V.: "Batteries for Vehicular Applications", *Physics of Sustainable Energy*, 2008, 1044: 283-296.

[46] Various authors: "Status Overview of Hybrid and Electric Vehicle technology (2007) - Final Report Phase III, Annex VII", Paris: International Energy Agency; 2007.

[47] Tamai G., Jeffers M., Lo C., Thurston C. et al.: "Development of the Hybrid System for the Saturn VUE Hybrid", *2006 SAE World Congress & Exhibition*, SAE Technical Paper 2006-01-1502, 2006.

[48] Ferrari A., Morra E., Spessa E., Ciaravino C., Vassallo A.: "Analysis of energy-efficient management of a light-duty parallel-hybrid diesel powertrain with a belt alternator starter", *10th International Conference on Engines & Vehicles*, SAE Technical Paper 2011-24-0080, 2011.

[49] Steinmaurer G., del Re L., "Optimal Energy Management for Mild Hybrid Operation of Vehicles with an Integrated Starter Generator", *2005 SAE World Congress & Exhibition*, SAE Technical Paper 2005-01-0280, 2005.

[50] Kusumi H., Yagi K., Ny Y., Abo S. et al.: "42V Power Control System for Mild Hybrid Vehicle (MHV)", *2002 SAE World Congress & Exhibition*, SAE Technical Paper 2002-01-0519, 2002.

[51] Gale A., Brigham D.: "Starter/alternator design for optimized hybrid fuel economy", *Convergence 2000 - International Congress on Transportation Electronics*, SAE Technical Paper 2000-01-C061, 2000.

[52] Canova M., Sevel K. Guezennec Y., Yurkovich S.: "Control of the start/stop of a diesel engine in a parallel HEV with a belted starter/alternator", *8th International Conference on Engines for Automobile*, SAE Technical Paper 2007-24-0076, 2007.

[53] Davis R., Lorenz R., "Engine Torque Ripple Cancellation with an Integrated Starter Alternator in a Hybrid Electric Vehicle: Implementation and Control", *IEEE Transactions on Industry Applications*, 2003, 39(6).

[54] Watson N., Janota M.: "Turbocharging the Internal Combustion Engine". New York: MacMillan Press; 1982.

[55] Chen S., Flynn P., "Development of Single Cylinder Compression Ignition Research Engine", SAE Technical Paper 650733, 1965.

[56] Patton K., Nitschke R., Heywood J., "Development and Evaluation of a Friction Model for Spark-Ignition Engines", *1986 SAE International Congress and Exposition*, SAE Technical Paper 890836, 1989.

[57] National Research Council: "Tires and passenger vehicle fuel economy - TRB special report 286", Washington: Transportation Research Board, 2006. Available from: http://onlinepubs.trb.org/onlinepubs/sr/sr286.pdf.

[58] Zhang M., "HEV Powertrain Fundamentals", in *2012 ITEC Conference*, Jun 18-20, 2012, Dearborn, MI.

[59] Wikipedia: "Driving cycle". (modified Jul 18, 2012; accessed Jul 29, 2012). Available from: http://en.wikipedia.org/wiki/Driving_cycle.

[60] Lin J., Niemeir D.A., "Regional driving characteristics, regional drive cycles", *Transport Res. Part D: Transport Environ.*, 2003, 8: 361-381.

[61] U.S. Environmental Protection Agency website (accessed Aug 19, 2012). Available at: www.epa.gov.

VITA AUCTORIS

NAME:	Stefano Baldizzone
PLACE OF BIRTH:	Torino, Italy
YEAR OF BIRTH:	1988
EDUCATION:	Liceo Scientifico Galileo Ferraris, Diploma di Maturità Scientifica, Torino, Italy, 2002 - 2007.
	Politecnico di Torino, B.Sc. in Automotive Engineering, Torino, Italy, 2007 - 2010.
	Politecnico di Torino, Master in Automotive Engineering, Torino, Italy, 2010 - 2011.
	University of Windsor, M.Sc. in Mechanical Engineering, Windsor, ON, 2011 - 2010.